Identification of the most robust and economical LS-DYNA shell element for simulation of full-scale Ship to Offshore Platform Collision (STOPC)

by

Matthew Levi Morrison

Submitted in partial fulfillment of the requirements

for the degree of Masters of Applied Science

at

Dalhousie University

Halifax, Nova Scotia,

December 2019

This Masters thesis is dedicated to the memory of my father, Loran Peppard Morrison.

Thank you for all that you have sowed.

TABLE OF CONTENTS

List of Tables vii
List of Figures viii
Abstract xiii
List of Abbreviations and Symbols xiv
Acknowledgements xxi
1. Introduction and Objective 1
2. Background / History 4
2.1 Overview 4
2.2 History of Finite Element Analysis in Collision Assessment 4
2.3 Summary of Studies by Amdahl 7
2.4 Conclusion 15
3. Available standards for collision assessment 16
3.1 Overview 16
3.2 Det Norske Veritas (DNV) 16
3.3 American Bureau of Shipping (ABS) 17
3.4 Health and Safety Executive (HSE) 17
3.5 Norsk Sokkels Konkuranseposisjon (NORSOK) 18
3.6 American Petroleum Institute (API) 18
3.7 British Standards (BS EN ISO) 19
3.8 Lloyd's Register Marine (LR) 19
3.9 Conclusion 20
4. Fundamentals / Software codes / simulation 21
4.1 Overview 21
4.2 Fundamentals of Ship Impact and Collisions 22
4.2.1 Establishing Design Loads 22
4.2.2 Conservation of Energy 23
4.2.3 Dissipation of Strain Energy 24
4.2.4 Impact Velocity 34
4.2.5 Structural Mass 36
4.2.6 Two Mass system approximation 37
4.2.7 Added Mass 42
4.2.8 Vessel Deformation and Bow types 47

4.3 Plastic Deformation in Steel 51
4.4 Response of Jacket Type Structures 54
4.4.1 Failure of tubular members 55
4.4.2 Local Denting Curves 59
4.4.3 Load Indentation Curves Validation 62
4.4.4 Braced Members 65
4.4.5 Tubular Joints 69
5. Use of FEA for STOPC assessment 71
5.1 Introduction 71
5.2 Implicit vs Explicit Solvers 74
5.2.1 Implicit Methods 74
5.2.2 Fully Explicit Solutions 76
5.3 Modeling Software 77
5.3.1 Hypermesh 77
5.3.2 LS-PREPOST 78
5.3.3 SACS 78
5.4 Analytical Software 79
5.4.1 Introduction 79
5.4.2 LS-DYNA 79
5.4.3 Abaqus FEA 82
5.4.4 SACS 83
5.4.5 Other FEA Software Packages 83
5.4.6 Post-Processing 84
5.5 Material Modeling 84
5.5.1 Overview 84
5.5.2 Stress-Strain Curve 85
5.5.3 Linear vs Non-Linear Analysis 88
5.5.4 Hardening and Softening Rules 91
5.5.5 Resultant Plasticity Material 92
5.5.6 Plastic Kinematic Material 93
5.5.7 Piecewise Linear Plasticity Material 93
5.5.8 Material Formulations 94
5.5.9 Conclusion and Recommendations 96
5.6 1D Element Formulation 97

5.7 2D Element Formulations 98
5.7.1 Overview 98
5.7.2 Hughes-Liu Shell Formulation (ELFORM 1) 98
5.7.3 Belytschko-Lin-Tsay Shell Formulation (ELFORM 2) 99
5.7.4 BCIZ triangular shell formulation (ELFORM 3) 99
5.7.5 Co-rotational $C0$, triangular shell (ELFORM 4) 100
5.7.6 Belytschko-Tsay Membrane (ELFORM 5) 101
5.7.7 S/R Hughes-Liu (ELFORM 6) 101
5.7.8 S/R co-rotational Hughes-Liu (ELFORM 7) 102
5.7.9 Belytschko-Leviathan Shell (ELFORM 8) 103
5.7.10 Fully Integrated Belytschko-Tsay membrane (ELFORM 9) 103
5.7.11 Belytschko-Wong-Chiang Formation (ELFORM 10) 103
5.7.12 Fast (co-rotational) Hughes-Liu (ELFORM 11) 104
5.7.13 Plane stress and strain formulations (ELFORM 12 and 13) 105
5.7.14 Axisymmetric solid formulations (ELFORM 14 AND 15) 105
5.7.15 Fully Integrated Shell with EAS Formulation (ELFORM 16) 105
5.7.16 Fully integrated DKT triangular shell element (ELFORM 17) 106
5.7.17 Fully integrated linear solutions (ELFORM 18, 20, 21) 106
5.7.18 8-noded Shell Formulation (ELFORM 23) 107
5.7.19 Thickness Stretch Solutions (ELFORM 25, 26, 27) 107
5.7.20 Summary of LS-DYNA Shell Elements [63] 109
5.8 3D Element Formulation 114
5.9 Meshing and Refinement 115
5.9.1 General Refinement 115
5.9.2 Adaptive Algorithms 121
5.10 Contact and Boundary Conditions 125
5.10.1 Introduction 125
5.10.2 Boundary Conditions for Truncated Offshore Structures 125
5.10.3 Pile/Soil Interaction 127
5.10.4 Boundary Conditions for Truncated Vessels 128
5.10.5 Collision Simulation and Contact 130
5.11 Comparison of Finite Element Analysis and Experimental Results 132
5.12 Summary 135
6. Simulations 138

6.1 Introduction 138
6.2 Tools and Standards 138
6.3 Stiffened Cylinder Model – Element Performance Comparison 139
6.3.1 Model Parameters and Mesh Density 139
6.3.2 Simulation Parameters 141
6.3.3 Boundary Conditions 142
6.3.4 Element and Material Formulations 142
6.3.5 Results 143
6.4 Stiffened Cylinder Model – Mesh Sensitivity Analysis 148
6.5 Investigation of noise after collision for VM stresses of explicit collision analyses ... 158
6.6 Full scale STOPC assessment of an Offshore Exploration Vessel and Vertical Monopole 159
6.6.1 Model Parameters and Mesh Density 159
6.6.2 Simulation Parameters 163
6.6.3 Boundary Conditions: 164
6.6.4 Element and Material Formulations 164
6.6.5 Contact Control Cards 165
6.6.6 Solver Control Cards 166
6.6.7 Additional Control Cards 167
6.6.8 Results 168
6.6.9 Comparison of CPU Run Times 176
7. Summary and Conclusion 184
7.1 Summary of Work Performed in this Thesis 184
7.2 Concluding Remarks 186
7.3 Recommendations for Future Analyses 188
References 190

LIST OF TABLES

Table 2-1: Various finite element models created by Jorgen Amdahl in cooperation with the Technical University of Norway 14

Table 4-1: Primary Loads considered during a STOPC event 21

Table 4-2: Equations for the calculation of energy dissipated during ship to platform collision for various platform types 32

Table 4-3: Loading on cross brace members 68

Table 6-1: Mesh Sensitivity Analysis Parameters 148

Table 6-2: Summary of MAT24 parameters used to represent vessel 164

Table 6-3: Summary of the analysis schemes performed on LSTC 120 CPU core Intel Xeon Cluster configured on LINUX 177

LIST OF FIGURES

Figure 4-1: energy dissipation during a collision event vs. Relative strength of installation and colliding vessel [19] 28

Figure 4-2 supply vessel indentation curve [19] 28

Figure 4-3 Representation of strain energy dissipation during a collision event [19] 30

Figure 4-4: Deformation of Saxon Onward resulting from bow collision [29] 34

Figure 4-5: Model for assessment of reaction force to deck [14] 37

Figure 4-6: Simplified model of a supply vessel impacting a platform [31] 38

Figure 4-7: Sideways added mass for supply vessels as a function of duration of collision [23]. 43

Figure 4-8: SPH fluid elements interacting with a fish model with an embedded proportional derivative controlled articulated skeleton [33] 46

Figure 4-9: Large ocean scene simulated with two -way coupling using the SPH method [34] ... 47

Figure 4-10: Geometry of typical bow structure [27] 48

Figure 4-11: Energy vs Deformation graph of a marine vessel experiencing a head-on collision, with and without a bulbous bow [8] 49

Figure 4-12: Bow crushing pattern resulting from head on collision [27] 50

Figure 4-13: Uniaxial stress-strain curves with Lüder's elongation paired with sketches of the appropriate surface markings [37] 53

Figure 4-14: Local deformation and yielding patters of tubular members impacted by a marine vessel [3] 57

Figure 4-15: Non-Dimensional Load indentation relationships for steel tubes [3] 57

Figure 4-16: Load displacement characteristics for tubular members [10] 59

Figure 4-17: Load indention curves for various vessel orientations [19] 60

Figure 4-18: Non-dimensional resistance local indention curves for various member sizes [41] . 63

Figure 4-19: Contact force vs. displacement curves of varoious vessel and member configurations [41] 64

Figure 4-20: Deformation modes of cross brace subjected to point load P. Note: P = denting force; b = eccentricity of load with respect to the joint span, u = resulting deformation for a given mode; Mp = full plastic moment of tubular member. [26] 67

Figure 5-1: ship to platform damage analysis [25] 72

Figure 5-2: Typical stress-strain curve of isotropic material [54] 86

Figure 5-3: $r1$ and $r2$ for deformed tubular member [57] 90

Figure 5-4: Twisted beam problem displaying overestimation of displacement by Belytschko-Lin-Tsay shell elements [61] 104

Figure 5-5: Relative cost of four noded shells available in LS-DYNA relative to Belytschko-Tsay shell [61] 113

Figure 5-6: FEA model of T-joint under impact loading (reproduced from [57]). 116

Figure 5-7: Comparison of the test and numerical results of brace punching stresses on a chord member [57] 117

Figure 5-8: Comparison of experimentally determined dissipated energy vs predicted dissipated energy 118

Figure 5-9: Bulb deformation of colliding vessel striking another vessel [5] 119

Figure 5-10: Simulation of marine vessel side collision with offshore wind turbine [57] 120

Figure 5-11: Effect of increasing mesh density for bow crushing, the variation of deformation energy vs time [31] 121

Figure 5-12: One level adaptive calculation on a square cross section beam with two faces displayed [61] 123

Figure 5-13: Model of the cross diagonal brace substructure [40] 126

Figure 5-14: Multipoint constraint with master node (M) in centre of a hollow circular cross section 127

Figure 5-15: Vessel to vessel collision with collision area finely refined [47] 134

Figure 6-1: FE Model of the stiffened cylinder 139

Figure 6-2: Schematic of the stiffened cylinder and vertical monopole 140

Figure 6-3: FE model of the vertical monopole with its boundary conditions 142

Figure 6-4: Distribution of VM stress at t=0.667s 143

Figure 6-5: Variation of von Mises Stress as a function of time in element 72554 obtained by the various element types used in the collision analysis 144

Figure 6-6: Variation of Y displacement (in the direction of the radial depth of the monopole) as a function of time of node 43089 during the collision analysis 146

Figure 6-7: Total CPU times consumed to solve the problem by the various element types 147

Figure 6-8: ELFORM -16 stiffened cylinder STOPC assessment, 1000 mm refinement, side view (+y), $t \approx 0.6s$ 149

Figure 6-9: ELFORM -16 stiffened cylinder STOPC assessment, 500 mm refinement, side view (+y), $t \approx 0.6s$ 150

Figure 6-10: ELFORM -16 stiffened cylinder STOPC assessment, 250 mm refinement, side view (+y), $t \approx 0.6s$ 150

Figure 6-11: ELFORM -16 stiffened cylinder STOPC assessment, 1000 mm refinement, isometric, $t \approx 0.6s$ 151

Figure 6-12: ELFORM -16 stiffened cylinder STOPC assessment, 500 mm refinement, isometric, $t \approx 0.6s$ 151

Figure 6-13: ELFORM -16 stiffened cylinder STOPC assessment, 250 mm refinement, isometric, $t \approx 0.6s$ 152

Figure 6-14: The specific region selected in all three mesh density models for plotting the average VM stress sampled at centroid integration points, side view (+y), $t \approx 0.25s$ 153

Figure 6-15: Stress variation of the average VM stress sampled at location shown in Figure 6-14 as a function of tune, ... 154

Figure 6-16: Y Displacement comparison of collision node 154

Figure 6-17: Variation of the average internal energy sampled at the location shown in Figure 6-14 as a function of time 155

Figure 6-18: Variation of the average internal energy sampled at the location shown in Figure 6-14 as a function of time 155

Figure 6-19: Variation of von Mises stress as a function of time in element 72554 obtained by the various time steps used in the collision analysis 158

Figure 6-20: Coarse model of the benchmark offshore research vessel used for analyses 159

Figure 6-21: Typical deck underside of offshore research vessel (global reverse isometric view) 160

Figure 6-22: Typical deck underside of offshore research vessel (magnified, reverse isometric view) 161

Figure 6-23: Refined region of the offshore research vessel model 162

Figure 6-24: Magnified view of the refined region of the offshore research vessel 162

Figure 6-25: Vessel at t=0 169

Figure 6-26: Vessel at t = 0.29s 170

Figure 6-27: Deformed vessel at t=0.485s 170

Figure 6-28: Hull elements selected for stress plotting (elements outlined by white) 171

Figure 6-29: Elements selected for stress plotting, magnified view (elements outlined in white) 171

Figure 6-30: Distribution of VM Stress plot at t=0.2894s, full scale vessel collision, ELFORM - 16, monopole hidden 172

Figure 6-31: Distribution of VM Stress plot at t=0.2946s, full scale vessel collision, ELFORM - 16, monopole hidden 172

Figure 6-32: Distribution of VM Stress plot at t=0.3011s, full scale vessel collision, ELFORM - 16, monopole hidden 173

Figure 6-33: Distribution of VM Stress plot at t=0.3116s, full scale vessel collision, ELFORM - 16, monopole hidden 173

Figure 6-34: Distribution of VM Stress plot at t=0.4002s, full scale vessel collision, ELFORM - 16, monopole hidden 174

Figure 6-35: Resultant Displacement plot at t=0.2894s, full scale vessel collision, ELFORM -16, monopole hidden 174

Figure 6-36: Resultant Displacement plot at t=0.2945s, full scale vessel collision, ELFORM -16, monopole hidden 175

Figure 6-37: Resultant Displacement plot at t=0.3116s, full scale vessel collision, ELFORM -16, monopole hidden 175

Figure 6-38: Resultant Displacement plot at t=0.4002s, full scale vessel collision, ELFORM -16, monopole hidden 176

Figure 6-39: Resultant Displacement plot at t=0.5010s, full scale vessel collision, ELFORM -16, monopole hidden 176

Figure 6-40: Variation of the VM stress of Element 19851 as a function of time in the full scale STOPC analysis 178

Figure 6-41: Variation of VM stress results as a function of time for full scale STOPC analyses performed with ELFORM 16, element 104588 179

Figure 6-42: Relative Displacement of node 19851 as a function of time for full scale STOPC analysis..... 180

Figure 6-43: Internal energy of colliding structure as a function of time for full scale STOPC analysis..... 181

Figure 6-44: Kinetic energy of colliding structure as a function of time for full scale STOPC analysis..... 181

Figure 6-45: Comparison of CPU times for various fully explicit STOPC simulations (ELFORM 1, 2, -16, and 25) and full scale STOPC simulation ran with implicit/explicit switching (ELFORM 16) 182

ABSTRACT

This thesis studies the current body of literature surrounding marine vessel to offshore structure collisions with focus toward the collision energy losses, forces, structural mechanisms at play and total resulting structural damages. The primary focus of this thesis is to determine the effectiveness, efficiency, and usability of various element formulations through full scale simulation of ship to offshore structure collisions (STOPCs). This will be performed through simulation of the collision event using various shell element formulations and comparing their results accuracy, and computer resource and CPU consumptions. It was found that element formulation 16 within LS-DYNA was the most robust element formulation available within LS-DYNA for performing full scale STOPC platform collisions. It was also determined through these studies that running full scale collision analyses using the LS-DYNA implicit-explicit solver option is far more efficient than running equivalent analysis fully explicitly.

LIST OF ABBREVIATIONS AND SYMBOLS

API	American Petroleum Institute
BCIZ	Nonconforming element of Bazeley, Cheung, Irons and Zienkeiwicz
BL	Belytschko Leviathan Shell
BS	British Standards
BT	Belytschko-Tsay Shell
BTS	Belytschko-Tsay Shell with Thickness Stretch
BTW	Belytschko-Tsay Shell with Warping stiffness
BWC	Belytschko Wong Chiang Shell
CFD	Computational fluid dynamics
CG	Center Of Gravity
CHL	Co-rotational Hughes Liu Shell
CST	Constant Stress Triangle
CPU	Computer Processing Units
DNV	Det Norske Veritas
DOF	Degree of Freedom
DWT	Deadweight Tonnage
EAS	Enhanced Assumed Strain
ELFORM	Element Formulation
FBT	Fully Integrated Belytschko Tsay
FCHL	Fast Co-rotational Hughes Liu Shell
FE	Finite Element

FEA	Finite Element Analysis
FEM	Finite Element Method
FTS	Fully Integrated Shell with Thickness Stretch
HL	Hughes Liu Shell
HSE	Health And Safety Executive
LCG	Longitudinal Center of Gravity
LR	Lloyd's Register
LSTC	Livermore Software Technology Corporation
NORSOK	Norsk Sokkels Konkuranseposisjon (International Norwegian Standards)
PC	Personal Computer
RTCL	Rice-Tracey-Cockcrift-Latham
SHL	S/R Hughes Liu Shell
SPH	Smooth Particle Hydrodynamics
S/R	Selectively Reduced Integration
STOPC	Ship To Offshore Platform Collision
VM	von Mises
α	collision angle
ε_f	failure strain
ε_g	uniform strain
ε_n	necking strain
ξ_a	displacement at collision point of supply vessel

ξ_b	net displacement from point of collision
ξ_i	displacement of offshore installation
ℓ	span of cross brace
σ	stress
σ_y	yield stress
ω_v	rotation of colliding vessel
b	eccentricity of a load with respect to the joint span
b_c	width of collision area
B_v	breadth of vessel
C_B	block coefficient
d_t	displacement of tube due to point load
d_v	displacement of colliding vessel
D_T	initial diameter of undeformed tube
D_v	draught of vessel
$D_{a\xi}$	drag coefficient
E	modulus of elasticity
E_0	initial energy of system
$E_{a,i}$	kinetic energy absorbed by offshore installation
$E_{a,v}$	kinetic energy absorbed by marine vessel
E_c	crushing energy of the colliding vessel
$E_{k,i}$	kinetic energy of the offshore installation at instance of collision
$E_{k,v}$	kinetic energy of the marine vessel at instance of collision

$E_{r,v}$	rotational energy of the marine vessel at instance of collision
$E_{s,total}$	total strain energy resulting from collision
$E_{s,i}$	strain energy of the offshore installation
$E_{s,v}$	strain energy of the colliding vessel
F	force for a given time t
F_i	topside mass of offshore installation
F_ξ	collision force between vessel and offshore installation
g	acceleration due to gravity
h_t	distance from width of collision area to end of deformation area
$H_{s(max)}$	maximum significant wave height for operation close to offshore installation
I_ξ	impulse of the collision
I_i	impulse on the offshore installation
J	mass moment of inertia of the column (including added mass)
j_a	added mass coefficient for rotational around the centre of gravity
$k_{11}, k_{22}, k_{12}, k_{21}$	stiffness coefficients
k_s	spring stiffness
l	length
l_e	element side length
L_A	accidental loads
L_D	deformation loads
L_E	environmental loads

L_L	live loads
L_P	permanent loads
m	mass
m_{ax}	added mass coefficient for surge motion
m_{ay}	added mass coefficient for sway motion
$m_{a,i}$	added mass from installation
$m_{a,w}$	added mass from water
$m_{a,total}$	total added mass
m_i	mass of offshore installation
m_v	mass of colliding vessel
M	master node
M_P	full plastic moment
P	denting force
P_c	impact at the cross brace
P(t)	impact action on offshore structure as a fuction of time
P_{u1}	ultimate lateral force before joint failure
P_{u2}	ultimate lateral force after joint failure
r_a	radius of ship mass inertia around centre of gravity
r_I	inner section radius of deformed tubular section
r_2	outer section radius of deformed tubular section
$r_{1,I}$	inner section radius around x axis
$r_{1,O}$	outer section radius around x axis

$r_{2,I}$	inner section radius around y axis
$r_{2,O}$	outer section radius around y axis
R	resistance
R_c	plastic collapse resistance in bending
R_i	load resistance of offshore installation
R_T	radius of undeformed tube
R_v	load resistance of colliding vessel
S	slave node
t	time
t_0	time when net force applied to member reaches 0 N
t_c	duration of collision
T	thickness
u	resulting deformation for a given model of cross brace
v	velocity
v_i	velocity of offshore installation
v_v	velocity of colliding vessel
$v_{v,x}$	velocity of colliding vessel
$v_{v,x}$	velocity of colliding vessel
w	vertical deformation of tubular member
w_d	dent depth
w_i	deformation of the offshore installation
w_v	deformation of the colliding vessel

w_T	vertical deformation of tube
x_v	x coordinate of colliding vessel
x_c	x coordinate of the centre of gravity of the collision point
y_c	y coordinate of the centre of gravity of the collision point
z	distance of effective pivot point to point of contact

ACKNOWLEDGEMENTS

Thank you to Dr.Farid Taheri for his consistent guidance and mentoring through my completion of this Masters thesis.

Livermore Software Technology Corporation (Ohio office) support for allowing me to run fully explicit analyses on their cluster.

My uncle, James Morrison and my mother, Frances Morrison for their encouragement.

Isla Healy, for her unwavering support.

1. INTRODUCTION AND OBJECTIVE

Ship to offshore platform collisions (STOPCs) have been identified as a major hazard to oil exploration and production offshore and can cause a catastrophic level of damage to both the vessel and platform structure. Potential consequences from STOPCs may vary from minor structural damages to major damages where the structural integrity of the platform is compromised, as well as potential production downtime, ocean pollution, and the loss of numerous human lives. In July 2005, a multipurpose support vessel lost control and collided with a platform in the Mumbai High North complex along the western coast of India, causing 22 casualties and 362 emergency rescues [1]. From 2001 to 2011, there have been a total of 26 collisions between vessels and offshore facilities taking place in the North Sea alone, with six having high hazard outcomes [2].

Tragedies such as the Mumbai High North Collision exemplify the need for a comprehensive design procedure, which is efficient and effective for adequate simulation of such a catastrophic event. Due to the ramifications of such collisions, the current body of design standards aimed at fixed oil and gas platform structures stipulates the requirement for a ship to platform impact assessments using the finite element method (FEM). In conjunction with design standards, this method allows the collision event to be addressed systemically with established loads and reactions observed through past structural failures and collisions with a far higher level of accuracy than simplifications involved when applying analytical methods. In order to achieve such an analysis in an efficient manner, an element formulation which would be feasible to use for modeling a

full-scale model of a ship yet robust enough to handle iterative contact computations effectively and efficiently, must be used.

Currently, there is not a consensus on the ideal element formulation for running a full scale STOPC analysis on a PC. This contribution this study provides to the field of STOPC analysis is identification of the most robust and efficient element-solver combination for collision assessment of a full scale marine vessel.

The purpose of this study is to determine which shell/plate element formulation best fits the aforementioned attributes in representing a marine vessel's response during a collision event, as well as highlighting the advantages/disadvantages of each formulation in terms of accuracy, robustness and computational efficiency.

In Chapter 2, background and history of use of the finite element method for assessment of STOPC platforms are presented, with specific focus on studies performed by Jorgen Amdahl.

In Chapter 3, available standards for collision assessment are briefly discussed, with specific focus on applicability toward the colliding vessel.

In Chapter 4, fundamentals of ship impacts and collisions are discussed to establish various modelling parameters requiring consideration for STOPC assessment.

In Chapter 5, various FE softwares are reviewed, implicit and explicit solvers are discussed, meshing, and various methods of material and element modelling are reviewed.

In Chapter 6, various simulations are performed to test the shell elements deemed applicable for STOPC simulations in Chapter 5. These simulations include ten STOPC simulations using a simplified stiffened cylinder model and implicit-explicit switching, a STOPC simulation using a full marine vessel using implicit-explicit switching, and four STOPC simulations using a full marine vessel and a fully explicit solver.

Chapter 7 presents a summary and concluding remarks of the thesis.

2. BACKGROUND / HISTORY

2.1 OVERVIEW

Prior to the advent of FEA, STOPCs were largely carried out using established formulas and associated charts to determine the collision energy released during the event. As early as the 1970's, computer simulation has been demonstrated to be a powerful tool as well as a limiting factor for accurate representation of ship to offshore platform collisions. During the early years, computer simulations were more focused on establishing the probability of occurrence of a particular collision event rather than the structural response of the structures involved [3]. In order to represent the actual collision event with a high degree of accuracy and customization, numerical simulations would be necessary. Over time, as computers became more effective for assessing large scale problems and accessible, there began a shift from analytical and formulaic strategies to numerical strategies and methods. This section provides various examples of how the use of FEA for modeling ship to STOPCs has advanced since the 1980's. A collision assessment performed in the 80's using the finite element method would certainly not have had included the standards, element formulations, or simulation parameters that are available today.

2.2 HISTORY OF FINITE ELEMENT ANALYSIS IN COLLISION ASSESSMENT

Numerical simulations of STOPCs had been performed as early as the 1980's, with the accuracy of results and basic tools for the generation, processing, and post-processing of these models growing more efficient and elegant over time. While the models and simulations performed in the early 1980's were very advanced at that time, it is important to note that the computers used were significantly slower than the currently available

models, and pre and post processors were limited. When these tools became available and developed more effectively in the years to follow, they still did not have the capabilities of the tools which exist today, and the cost of CPU and storage was significantly higher. Due to the lack of time-based response analysis capabilities and computational limitations, models which could accurately represent local deformation were difficult to generate and inefficient. While using a coarser model would consistently reduce computational time (given the element formulation is consistent), it would have the adverse effect of fictitiously increasing the stiffness of the structure, which would be particularly detrimental in hotspot stress areas resulting from direct contact.

Another factor to consider when interpreting and using data from early simulations is the skillset of the user who produced the study. As computer-based numerical simulation was an emerging field in the early 80's, there was a limited number of people who possessed the skillset to produce such an analysis as the existing body of knowledge for computer-based FEA simulation was minimal. Limitations also include the available data surrounding actual collision events which would have served as benchmarks for comparison purposes [4]. The type of elements used, the material model, the contact algorithm, and the mesh size must all be included with a level of detail allowing accurate representation of the collision event. Today, the tools available for the numerical simulation of collision events require a far lesser amount of user expertise while enhancing the capabilities of any qualified user with knowledge of both the software and problem parameters.

While FEA software was available in the 80's and evidence of its use for STOPCs is well documented, analytical approaches had dominated collision simulation / analysis until the early 90's [5]. Studies conducted after the mid-nineties utilized finite element codes with non-linear capability, allowing the evaluation of high quality force-deformation curves [6]. This led to a large increase to the number of FEA related publications across all structural fields. As FEA become more widespread throughout the field of collision assessment, new and more robust tools were consistently being developed and element formulations were being updated annually to reflect the ever hastening pace of technology. Computationally expensive shell element formulations began to see use as computers became more efficient. For example, modern FEA programs can accommodate time-dependent strain hardening and strain rate effects for the material properties that are considered during each time-step specified during the analysis [5]. Consequently, the results which can be produced using modern FE codes and formulations have a relatively high level of accuracy while consuming low CPU time. The progression of FEA in the field of STOPCs is evident through the studies authored by Jorgan Amdahl and presented in section 2.3.

Jorgan Amdahl has been a prominent researcher in the field of marine STOPC since the early 1980's, and has maintained a constant stream of publications on the topic, which has yet to cease. His publications provide a unique opportunity to view the gradual progression of STOPC assessment over the past 40 years; a large portion of Amdahl's work is presented chronologically in Section 2.3.

2.3 Summary of Studies by Amdahl

Jorgen Amdahl is a leading STOPC specialist who has made significant contributions to the field dating back to the late 1970's.

Amdahl performed a study in 1980 investigating STOPCs using computational methods [3]. This study, while very comprehensive, serving as a benchmark study for several to follow, did not use finite element methods and instead used analytical and probabilistic methods. These were both incorporated into a computer simulation code developed for the problem. Although there are several major contributors to the field of STOPC analysis, Amdahl has performed several notable studies over a significant period of time, which provides a clear representation of the progression of STOPC analysis as FEA programs progressed. As well.

In an early study performed by the Norwegian Institute of Technology, Amdahl and associates made use of the finite element method to address the local deformation of small scale tubular members representing cylindrical jacket elements during a ship to platform collision [7]. As finite element analysis codes were not yet adequately sophisticated to reach the level of refinement necessary to produce local deformation of tube walls with an acceptable accuracy, an additional FEA modeling program was used to account for the local deformation. The local deformation simulation was performed using IMPACT FEA code, which allowed the beam elements at the point of impact to be modified continuously to simulate the reduced plastic moment capacity [7]. IMPACT was a popular choice for the assessment of local indentation of tubular structure and was

widely used during this period [4].While this program appeared to be suitable for determining local deformation of tubular members within offshore structures, it seemed to have little capability in determining the global effects caused from collision events. IMPACT also seems to be lacking in user-friendliness, as it necessitates the use of separate programs through calculation to achieve accurate results. Such supplementary programs include:

i. A program to account for elasto-plastic material behavior for modeling response of beams
ii. A program using the yield line graphs to predict the local indentation
iii. A program for calculating reduced moment capacity due to local deformation at point of impact.

A more accurate full scale collision simulation would also take account of the effect of rotational ship motion, hydrostatic forces, and adjacent members when determining the damage done to a particular member. This study outlines the capabilities of software used in the 80's to calculate local indentation and failure modes.

The program DENTA had been developed specifically for modeling local deformations within offshore structures resulting from collisions [7]. DENTA could evaluate the ultimate load and accompanying deformations, while the post ultimate strength behavior would have to be calculated numerically. While the study had been performed in depth, all of these factors are heavily dependent on one another, and the best method would have been an explicit analysis (as explained in Section 5.5) rather than their superposition / interrelation during the process. It should also be noted that the finite element model

made use of constant stress triangles (CST's) in the refined area, which is not an optimal modeling solution. This may have been partially due to the technological limitations of the hardware used during this period as the analysis was performed using a UNIVAC 1108 computer. This computer allowed up to 262,000 words of eight ported main memory and was introduced in 1964. For comparative purposes, a modern 64 bit computer can handle $2.3x10^{18}$ words (as each word is 8 bytes).

In 1983, Amdahl published a comprehensive guide entitled "Energy Absorption in Ship Platform Impacts" which referenced a number of studies performed in the field of STOPC analysis [8]. For computational modeling of bracing elements, Amdahl once again used the finite element program IMPACT, using beams with primitive formulation (axial and bending forces only) which had been improved since his 1980 study to account for local effects. The effect of strain hardening was recognized through this analysis, and the use of spring elements was recommended to account for horizontal movement and rotation at either member end. A finite element model for a bracing structural system presented by Amdahl in this study is shown in Table 2-1 (a). The bracing system had been simulated using a total of 370 elements, which is far lower than typical global offshore structures modelled today. For finite element analysis of shells, Amdahl recommended performing a full shell analysis in which material as well as geometric nonlinearities were incorporated into the model using a program such as TUBBUC [8], which was also a commonly used program during that period [4].

In 1991 and 1993, Amdahl [9, 10] used the finite element program USFOS, which had been developed especially for the analysis of progressive offshore structure collapse. USFOS could account for large waves, elasto-plasticity, cyclic analysis in the event of storms, as well as many other critical load cases common in oceanic environments [9, 10]. A major drawback of this study was the representation of each offshore member as a single finite element. This assumption allows the mesh used when conducting a conventional linear elastic analysis to be used directly in a non-linear analysis but is more suited for the analysis of global deformations, rather than local indentation of tubular members [9]. The stiffness matrix constructed by USFOS elastic analysis accounts for large lateral deformations using Lievesly's stability functions, which are analytic functions of the axial force normalized with respect to the Euler Buckling force [9]. An algorithm was incorporated into this analysis to include numerical damping by means of time averaging, while establishing equilibrium through every time-step. This study, while far more accurate than Amdahl's earlier analyses, still required several assumptions to be made due to memory, storage, and software limitations. The study had represented the ship as a single point mass connected to the platform with the use of a non-linear spring, but had modelled the global offshore platform as stick elements, as shown in figures (b) and (e) of Table 2-1. While the simplification was deemed appropriate for the purposes of the analysis, it would be unlikely to be an acceptable assumption today, given the available modern computational power and expected accuracy of results. With such simplifications, it would be of utmost importance to accurately represent the strength of the members transmitting forces in order to provide representative acceleration of the deck, as well as the time period in which the structures are in contact [9].

In Amdahl's 2001 study, LS-DYNA was used as the computational software for the simulation of a STOPC. The results were checked against Des Norske Veritas (DNV) standards [6]. The material model used had accounted for fracture and yielding, and fracture was modelled as a decrease of the stress experienced within all elements to a small residual value. The material was represented as an isotropic elasto-plastic material using the true stress-strain curve of the material within the model represented as a piecewise function. The software and hardware capabilities also allowed strain dissipation within either structure producing a high level of accuracy. The mesh used to represent the bow structure of the colliding vessel was fairly coarse and crude, causing a possible overestimation of the crushing force [6]. This mesh model as well as the resulting stress contours on the global offshore structure model are shown in figures (c) and (f) of Table 2-1, respectively. When assessing the strain dissipation within the ship structure during the collision, a ship to member collision had been performed using a rigid cylinder to represent the offshore structure. This is now a common practice, as it allows the load contribution of the ship structure to be easily determined. The study had also investigated the variance in stresses within the structure with non-critical elements removed.

A study performed by Amdahl and Stroheim in 2013 investigated offshore platform to ice-breaking supply vessel collisions using LS-DYNA version 971-R7600 [11]. This study represented both structures using non-linear shell elements and compared the resulting collision forces to those outlined by the NORSOK-004 code. The simulation had assumed a normal collision of the supply vessel to the platform in order to maximize the eccentricity of the impact with respect to the center of gravity of the platform, which

allowed the use of a closed form solution for energy dissipation [11]. In this study, the true speed of the vessel was used to simulate the contact between the colliding and stationary structures, thus maximizing accuracy, while any added mass to the structures were represented using a simple coefficient. As is typical during STOPC assessments, the sway velocity of the platform was assumed to be negligible and set to zero. Amdahl and Stroheim had modelled approximately 1/3 of the floating production platform using shell elements which varied largely from the methods used in the 1980 models. The selected shell element was the Belytschko-Tsay shell element because of its computational efficiency. The elements had an average size of 5-10 times the plate thickness at the point of collision in order to accurately represent stresses and strains. Hourglassing control was used in order to reduce the effect in elements with low hourglassing energy. Contact algorithms were used to represent the contact surfaces which formed between the ship and offshore platform. By using a constant velocity, important material effects such as strain rate dependent hardening and dynamic modeling may have been missed. However, a reasonable time-step was used and the material response was modeled using the Rice-Tracey-Cockcrift-Latham (RTCL) damage criterion, which lessens the potential influence of strain hardening and dynamic modeling, which were ignored [12]. The 2013 study had made use of very high quality post-processing methods which allowed the modes of failure, both local and global, to be thoroughly investigated. Due to the computationally efficient software, a very refined mesh was used throughout the bow of the model as shown in (d) of Table 2-1. The use of time dependent, high quality contours allows the determination of cause of failure and consequently lowers the level of effort required to determine the changes necessary to strengthen either structure against accidental events.

In their 2014 review, Amdahl and Stroheim presented a number of case studies which investigated collision effects of vessels to offshore structures [12]. All case studies presented by Stroheim and Amdahl use non-linear finite elements and the majority of them use LS-DYNA as well as the NORSOK code. It is very evident from the studies they presented that the design standards are quite conservative in their nature and collision events should be assessed on a case by case basis. The element and material formulations used in the studies presented by Amdahl and Stroheim are incredibly high in accuracy compared to previous STOPC simulations. The material model incorporated a power law hardening model in order to accurately model plastic strain hardening in conjunction with the Rice-Trace-Cockcroft-Latham (RTCL) damage criterion [13]. This damage criterion gives a reasonable fracture prediction using automatic mesh scaling for element lengths from one to ten times plate thickness [12]. The coarse modelled areas made use of a minimum of three elements per stiffener web, and at least 5 elements modeling the region between the webs of the stiffeners. The level of refinement used throughout these studies was consistently very high throughout the models when compared to previous studies, and the contours produced were of high quality as shown in figure (g) of Table 2-1.

Table 2-1: Various finite element models created by Jorgen Amdahl in cooperation with the Technical University of Norway

1983	1993	2001	2013-2014
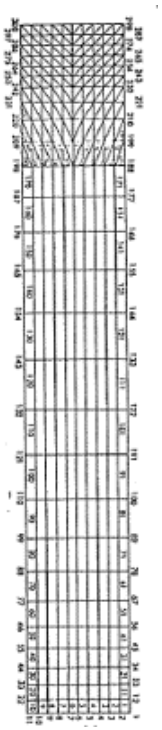 (a) finite element shell model of a bracing element (370 elements) [8]	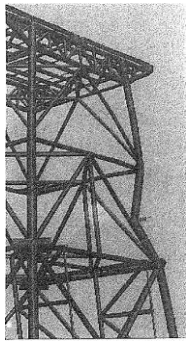 (b) point load representation of ship vessel [9]	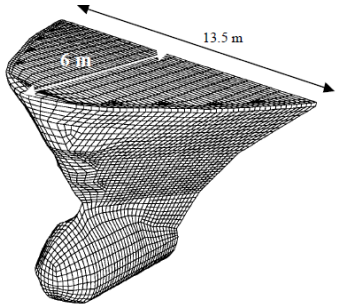 (c) fine mesh of bow and bulb and bow [6]	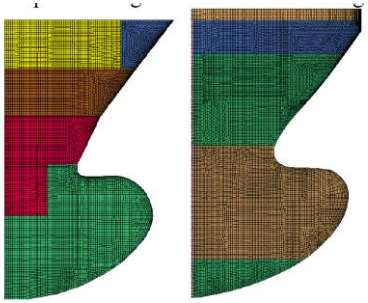 (d) mesh used for non-strengthened vessel bows from starboard side [12]
	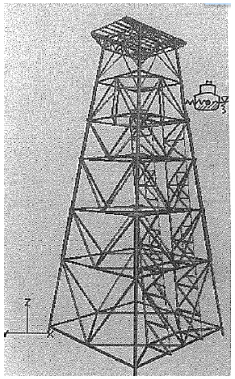 (e) full model of offshore structure [9]	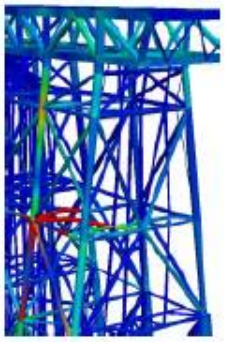 (f) stresses resulting from ship collision with full offshore structure model [6]	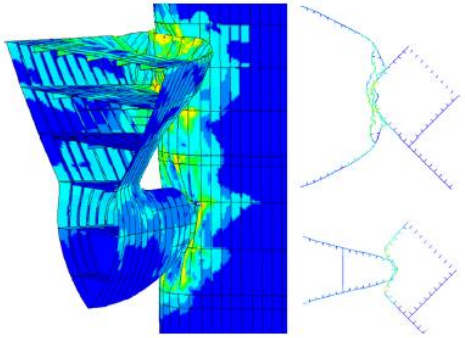 (g) simulated damage for bow and column after 51 MJ of energy has been dissipated [12]

2.4 Conclusion

Through review of analyses performed by Jorgan Amdahl and associates, it is evident that as computational power has increased over the years, both the level of refinement and the number of time-steps used in modeling collision events have consistently increased. This has in turn improved results accuracy. Recent post-processing capabilities allow the user to determine the region and mode of failure to a very high level of accuracy, allowing for more relevant results presentation with less margin of error when interpreting the results. Due to the user-friendliness of current FE programs and the relatively low level of computer programming knowledge that the user is expected to possess when conducting such an analysis, lower level of specialized expertise is required for conducting these simulations. The increased level of user accessibility to powerful FEA tools allows more researchers to partake in such studies. It has also been noted that similar to Amdahl, analyses conducted by the majority of modern STOPC assessments have utilized the LS-DYNA software suite as a primary tool for modeling, analysis, and post-processing.

3. AVAILABLE STANDARDS FOR COLLISION ASSESSMENT

3.1 Overview

The body of knowledge surrounding offshore structure design is of particular interest to energy sectors as it has a direct effect on the global cost of oil. This international interest has caused most countries involved in oil exploration to develop their own unique set of standards, which generally involve design and assessment criteria comparable to one another. While there are several standards available for offshore structure design, there are a few which have the comprehensiveness and reputation to be considered for a full scale STOPC assessment. The following standards are those provided by well-established classification organizations which provide adequate detail to effectively determine the criteria necessary for a full scale STOPC assessment both numerically and analytically. These standards will be continually referenced throughout this document and used for comparative purposes following the FEA.

3.2 Det Norske Veritas (DNV)

DNV is an international certification and classification society focusing on the technical assessment, classification, certification, and other verification and consultancy services related to the quality of ships, offshore units, and installations worldwide [14]. The DNV standard for accidental loading serves as a comprehensive guide, providing the necessary theory and computational formulae for the assessment of offshore structures subject to collision damage. The DNV standard makes heavy use of computational data achieved through numerous collision studies up to the date of publication. It is the world's largest

classification society, and has successfully classed over 13000 vessels and mobile offshore units [15].

3.3 American Bureau of Shipping (ABS)

The American Bureau of Shipping is a maritime classification society established in the USA which provides several standards for design, construction, and maintenance of offshore structures. ABS has released guidance notes on accidental load analysis and design of offshore structures in 2013. These guidance notes provide an overview of the process of identifying and assessing various accidental loads which can be experienced during STOPC events. While ABS is applicable toward assessment of an offshore structure experiencing accidental collision loads, it does not have a set of standards available for assessing of the structural integrity of the marine vessel following a collision [16].

3.4 Health and Safety Executive (HSE)

The Health and Safety Executive is a public body of the United Kingdom based out of Liverpool, which undertakes a variety of research initiatives in different marine related fields. The HSE reports on collision resistance of ship-shaped structures to side impact, identifies areas of uncertainty in the variance between established design standards, such as NORSOK and DNV [17]. It addresses the fundamentals of the formulations surrounding collision theory, but provides limited information relating to the design of offshore structures against collision and numerical simulation of the event. In addition,

HSE does not make use of studies published later than 1999, which is critical as there have been numerous related studies focusing on numerical simulation.

3.5 Norsk Sokkels Konkuranseposisjon (NORSOK)

The NORSOK standard is published by Standards Norway and is a comprehensive document which provides guidelines for steel structures design in great detail and is highly recommended for accidental collision assessment. N-003 addresses actions and action effects of offshore structures, and may be used when determining load cases during a STOPC event. N-004 focuses on the design of general steel structures, and under the ultimate limit states design, it addresses all major structural design considerations associated with tubular members. N-004 is also a valuable resource for the theorems associated with STOPC, and provides recommendations for the FEA of such events [18, 19].

3.6 American Petroleum Institute (API)

API Recommended Practice 2A-WSD (RP 2A-WSD) establishes recommended practice for planning, designing, and constructing fixed offshore platforms under the working stress design [20]. The document covers a very broad range of topics, such as planning of the offshore installation, design criteria and procedures, foundation design, drawings, fabrication and installation, inspection, surveys of the structure, and accidental loading. While API provides excellent insight and guidance over a wide range of offshore platform areas, it has limited functionality for the design of offshore platforms and numerical assessment.

3.7 British Standards (BS EN ISO)

The BSI group based in London, United Kingdom is a multinational company which provides standards across a wide array of business areas. British Standards for Fixed Offshore Structures (BSI-19902) and Floating Offshore Structures (BSI-19904-1) provide guidelines for complete offshore structure design and heavily reference other well established standards. They explain the design procedure of offshore structures with a high level of detail and provide various high quality appendices outlining the proper methodology for other design areas of offshore structures as well. While these standards are excellent references for checking the adequacy of tubular members and the overall offshore structures, they are limited in material relating directly to accidental collision of marine vessels with offshore structures.

3.8 Lloyd's Register Marine (LR)

Lloyd's Register Marine has developed guidance notes for collision risk based analysis, which heavily reference acceptable standards for collision and steel structure design, but does not discuss collision and collision theory in detail [21]. The standards which LR recognizes as being used most prominently throughout the offshore industry include API, ISO, and NORSOK. This document does not exclusively focus on STOPCs, but is well served as a reference document to be read prior to analyzing any collision event if the objective is to meet class requirements.

3.9 Conclusion

While there are a variety of codes and procedures that can be followed when determining the parameters required and the damage resulting from a collision assessment, the most comprehensive standard for the purposes of this thesis is the NORSOK. NORSOK focuses heavily on collision assessment of both ship to ship structures and STOPCs while providing guidance for criteria to be used in numerical analysis. For these reasons, it is the natural choice for the investigation of element formulations used for STOPC assessments.

4. FUNDAMENTALS / SOFTWARE CODES / SIMULATION

4.1 OVERVIEW

As durability and reliability are of utmost importance in the design and construction of any structure which affects the safety of human lives, the various design standards that govern offshore structure design and collision assessment have been written as such. Generally speaking, significant damage to the platform during a STOPC is allowable, provided that the damage does not lead to progressive collapse of the structures or prevent safe evacuation [22]. The total kinetic energy ($\text{Kinetic Energy} = \frac{1}{2}\text{mv}^2$) absorbed by the vessel and offshore installation through impact is calculated based on the basic principles of energy conservation and is one of the core principles in collision assessment. While there are several different conditions and load cases which can be applied to the offshore platforms, their components can generally be separated into the categories listed in Table 4-1 [8]:

Table 4-1: Primary Loads considered during a STOPC event

L_P	Permanent loads
L_L	Live loads
L_D	Deformation loads
L_E	Environmental loads
L_A	Accidental loads

For the purposes of determining which element formulations are optimal for the simulation of STOPC simulations, accidental loads will be the primary focus of this thesis. In the sections to follow, the various parameters governing energy absorbed by

each structure and resulting stresses/deformations will be explored with the intent of providing a comprehensive introduction to the body of knowledge surrounding STOPCs.

4.2 Fundamentals of Ship Impact and Collisions

4.2.1 Establishing Design Loads

As mentioned in section 4.1, collision loads are a major hazard to offshore structures which outweigh the severity of other loads in both magnitude and period of application. In traditional structural engineering, the loads are established by determining the worst case possible under the limit states design principle, with cataclysmic natural events being assigned a probability of occurrence and the structure designed accordingly. Similarly, the collision event with an offshore structure is characterized by the probability of occurrence and the inherent consequences of the range of vessels which may interact with the structure in conjunction with applicable design standards [3].

The design loads considered for a structure that may collide with marine vessels have been found to be far more dependent on the surrounding shipping lanes and vessels which traverse them than those documented based on previously collected data of similar structures in similar environments. The largest damage potential to an offshore structure is associated with collision with large merchant vessels; vessels which possess kinetic energy potentially so large that it would be virtually impossible to design an offshore structure to encounter the imposed loads created by such a collision [6]. For this reason, standards such as DNV establish accidental collisions to be associated with marine

vessels having a probability of collision of up to 10^{-4} per year frequency, which is a typical value across offshore design standards [23].

The design of offshore structures does not follow the traditional principles of working load or limit states designs, but instead uses the method of limit state of progressive collapse design (PLS), which allows for local failures in the form of denting, local buckling and plasticity, but does not allow failure of the platform structure [6]. As the magnitude of accidental loading far surpasses the magnitude of other loads such as environmental or live, the critical case of each loading condition is not combined into a single condition; it is only the accidental loading which includes the critical state in design. Loads applied in conjunction with accidental loading are either included far below their maximum limit or neglected altogether. Within the DNV standard, it is acceptable to use the simplification that accidental loads need not be combined with environmental loading upon the structure (note: this does not neglect any added mass which contributes to the collision event) [14]. In addition, the analysis of offshore structures subjected to accidental collision loads must consider a range of different ship collision orientations (i.e. broadside and head-on collisions).

4.2.2 Conservation of Energy

While many simplifying assumptions are often used in these assessments for the ship structure representation, adequate treatment of the relative strength between the interacting bodies is critical for impact cases with high levels of available kinetic energy [22]. In order to determine the damage that occurs between a marine vessel and offshore

platform during a collision, the traditional and widely accepted approach is to estimate the amount of energy available to cause deformation, and to determine how it is distributed amongst the involved structures [8]. The collision action is characterized by a kinetic energy, which is governed by such parameters as mass of the vessel coming into contact with the platform, the speed of the vessel at the instant of impact, and the hydrodynamic added mass associated with the colliding vessel [6].

The concern for ship collision with offshore platforms due to the high energy dissipation during the event is reflected within various design standards internationally. For instance, since 1980 the Norwegian Petroleum Directorate requires that platforms normally be designed for potential impacts by supply vessels of 5000 tons displacement, crushing with a speed of 2 m/s, yielding a kinetic energy of 14 MJ for beam impact and 11 MJ for bow or stern impact [19]. Risk analysis of planned North Sea jacket installations located close to lanes with heavy ship traffic have identified collisions with passing vessels with kinetic energy in the range of 40-50 MJ; this energy implies a vessel of 2000-3000 tons displacement travelling with a speed of 5.5-6.0 m/s [6]. Comparing these two kinetic energy values, it is evident that the accidental loading upon an offshore structure is largely a function of the shipping lanes which are within the feasible vicinity of the structure as well as the maximum size of vessels which traverse them.

4.2.3 Dissipation of Strain Energy

The principles of strain dissipation are often used to assess a STOPC in order to account for the total energy within the system before equilibrium is reached following the event.

Following the traditional approach of collision mechanics, when a constant added mass is assumed, the overall loss of kinetic energy during the collision must be absorbed by the deformation of both the ship and the platform [24]. Due to the complexity of the event, it is clearly difficult to determine how many of the external mechanics during the collision event are converted to internal energy losses.

Internal and external mechanics of both the colliding vessel and offshore structure are often considered separately as the algorithms which govern their contact are similar but not interchangeable. External mechanics refer to the global motion of the impacting bodies, which are described by such parameters as structure mass, added mass, and velocity before and after impact. Internal mechanics of the structure refer of the energy absorption within the impacting bodies through plastic strain and fracture [11]. To simplify, external mechanics refer to the parameters which cause the energy distribution, whereas internal mechanics refer to the parameters which govern how they are distributed.

For large scale collisions, a conservative assumption is that all of the energy is dissipated through elastic and plastic deformation of the structures; in actuality a portion of the energy is dissipated through elastic reactions as well as global vibrations of the structures. When assessing small scale collisions, these elastic vibrations become more significant as they account for a much larger portion of the energy involved, but as accidental collision design strictly focuses on critical conditions, the strain energy approach to the problem is

valid (7). The total energy dissipated during the collision can be represented by equation (4.1) [3]:

$$\mathrm{E}_{k,v} = \mathrm{E}_{a,v} + \mathrm{E}_{a,i} + \mathrm{E}_{r,v} \tag{4.1}$$

As it is conservative to assume no energy dissipation through rotational kinetic energy of the colliding vessel, the following simplification is often made for the purposes of analysis [14].

$$\mathrm{E}_{k,v} = \mathrm{E}_{a,v} + \mathrm{E}_{a,i} \tag{4.2}$$

where:

$\mathrm{E}_{k,v}$ = kinetic energy of the vessel at this instance of collision

$\mathrm{E}_{a,v}$ = energy absorbed by the vessel

$\mathrm{E}_{a,i}$ = energy absorbed by the offshore installation

$\mathrm{E}_{r,v}$ = rotational kinetic energy of the vessel

In most cases, the initial velocity of the platform installation is small enough in comparison to that of the vessel, so that it can be disregarded ($i.e.,\ v_i = 0$ [14])

$$\mathrm{E}_{k,i} = \frac{1}{2}\left(m_v + m_{a,w}\right)v_v^2 \tag{4.3}$$

where:

$\mathrm{E}_{k,i}$ = kinetic energy of the offshore installation at instance of collision

$m_{a,w}$ = added mass of water

m_v = mass of impacting vessel

v_v = impact velocity of the vessel

While the common assumption across all standards of design denotes minimal to zero energy dissipation through rotational kinetic energy of the vessel or vibrations of the structure, several standards suggest the use of different formulas for gross net energy dissipation through ship to platform collision depending on the type of platform used. Even in minor collisions between supply vessels and offshore structures, a considerable portion of kinetic energy can be stored as elastic energy of the ship and the platform, which is largely dependent on the mechanical properties of both [25]. The energy distribution between the two structures is dependent on a wide range of factors, and the responses of both the colliding vessel and the structure are non-linear (assuming deformation in both). This creates difficulty in justifying the use of analytical solutions as they are difficult to achieve without making several simplifying assumptions, and often overestimate the deformation of the structure being addressed.

There are a large number of empirical formulas available for the evaluation of collision responses, and while the assumptions and simplifications made for the formulas overestimate the true response of the structures, they serve as a strong indicator for design. These empirical formulas and are often used as the primary means of offshore structure accidental loading assessment during preliminary evaluation in such standards as NORSOK, DNV, and ISO. Therefore, a finite element solution to the problem is a

viable alternative to analytical methods and far more accurate, but requires full scale models to be constructed along with the use of sophisticated computational software.

With respect to the distribution of strain energy between the two structures involved in a collision, there are three distinct cases which can be used, each with a corresponding procedure. The energy dissipation distribution between the ship and offshore structure varies greatly among these three cases, as shown in Figure 4-1. The three simplified design protocols used for considering STOPCs, each with a corresponding set of assumptions, are as follows:

i. Ductile Design

ii. Strength Design

iii. Shared Energy Design

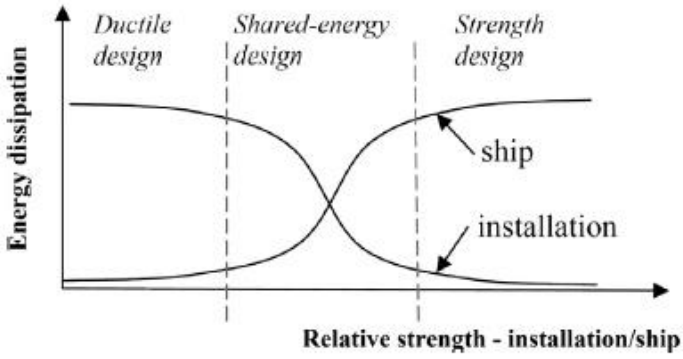

Figure 4-1: energy dissipation during a collision event vs. Relative strength of installation and colliding vessel [19]

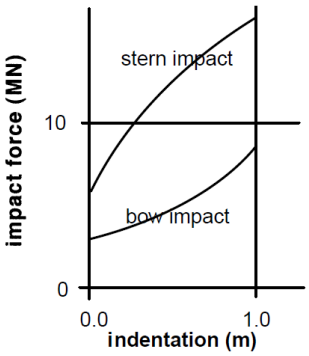

Figure 4-2 supply vessel indentation curve [19]

In the ductile design, the bow or side of the striking ship is considered to be rigid such that all of the energy is dissipated by the impacted installation. While this assumption is frequently used in practice, it results in the struck installation sustaining damage,

regardless of how well it has been strengthened [22]. This assumption is most commonly used when assessing a stern side impact rather than a bow impact due to the large increase in strain energy dissipated within the offshore structure, as shown in Figure 4-2 [26].

In strength design, the colliding vessel is considered to have a finite strength and it is assumed that the struck installation is a rigid structure, causing the colliding vessel to dissipate the majority of the strain energy. This method is valid if the struck structure has sufficient strength to resist the total crushing force imposed by the collision as well as resisting failure in local areas struck with high force intensities [22]. From a computational standpoint, strength design or ductility design is favorable over shared energy design, as they allow for one of the structures to be modelled as a completely rigid component and the other to be modelled using the actual structure's properties. Modeling structures using rigid material formulations alleviates much of the requirements for mesh quality and density, as stress and deformation will not exist in a material with infinite stiffness.

In shared energy design, both the colliding vessel as well as the struck ship/installation is considered to undergo significant deformation. The weaker structure in this scenario at any instant will deform, and consequently the analysis becomes very difficult to estimate using simple methods. Shared energy design is unfavorable from a time perspective as it necessitates finite element analysis and the solution is largely dependent on the level of computational power of the FEA program as well as the time-steps used [22].

When evaluating the structural integrity of an installation, shared-energy design and ductile design are typically used. Strength design and shared-energy design are generally used when evaluating the structural integrity of the marine vessel [14]. The energy distributed between the colliding vessel and stationary platform during the collision event may be dissipated as strain energy depending on the type of installation and purpose of the analysis being performed.

The representation of a ship to platform collision can be achieved through the use of a load deformation relationship curve as shown in Figure 4-3. The area underneath these curves can be used to determine the total strain energy dissipated during the collision through the use of the J-integral (strain energy release rate per unit fracture surface area in a material).

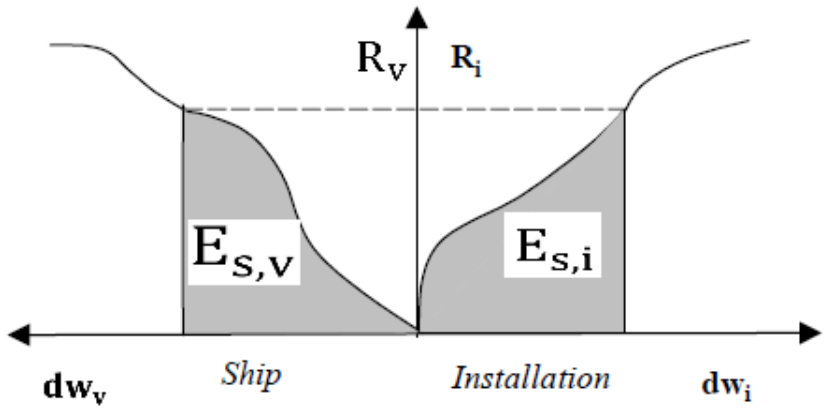

Figure 4-3 Representation of strain energy dissipation during a collision event [19]

The total strain energy dissipated during a collision event between the colliding structure and the platform structure can therefore be represented as:

$$E_{s,total} = E_{s,v} + E_{s,i} = \int_0^{W_{v,,max}} R_v dw_s + \int_0^{W_{i,max}} R_i dw_i \tag{4.4}$$

Where:

$E_{s,total}$ = total strain energy resulting from the collision event

$E_{s,v}$ = strain energy dissipated in the colliding vessel

$E_{s,i}$ = strain energy dissipated in the offshore installation

R_i = resistance of the offshore installation

R_v = resistance of the colliding vessel

$w_{i,max}$ = maximum deformation of the offshore installation

$w_{v,max}$ = maximum deformation of the colliding vessel

Shown in Table 4-2 are the formulae used within the Veritec and NORSOK standards (with similar or identical formulas used within most modern standards) for the design of offshore structures against accidental loading [23, 19]. The equations presented are for the following forms of offshore platform structures:

i. fixed offshore platform structures (i.e., platform structure is fixed directly into the ocean bottom)
ii. floating offshore platform structures (i.e., offshore oil rigs that are not attached to or resting on the ocean bottom)
iii. articulated column structures (i.e., platforms which consist of a base, a column, and a deck structure. The base is anchored to the seafloor while the column is buoyant [27].)
iv. jack-ups (i.e., offshore oil platforms where support legs are not permanently attached to seafloor, where legs can be drilled and jacked up to move to new location).

Table 4-2: Equations for the calculation of energy dissipated during ship to platform collision for various platform types

Platform Types	
Fixed	**Floating**
$\frac{1}{2}(m_v + m_{a,w})v_v^2$ (4.5)	$\frac{1}{2}(m_v + m_{a,w})v_s^2 \frac{\left(1-\frac{v_i}{v_v}\right)^2}{1+\frac{m_v}{m_i}}$ (4.6)
Articulated Column	**Jack-up***
$\frac{1}{2}(m_v + m_{a,w})v_s^2 \frac{\left(1-\frac{v_i}{v_v}\right)^2}{1+\frac{m_v * z^2}{J}}$ (4.7)	$\frac{1}{2} * m_v v_v \frac{1}{1+\frac{(m_v + m_{a,w})}{(m_i + m_{a,i})}}$ (4.8)

* Duration of collision must be significantly smaller than fundamental period of vibration

J = mass moment of inertia of the column including the added mass with respect to pivot point

z = distance from the effective pivot point to point of contact

v_i = velocity of platform

v_v = velocity of vessel

m_i= mass of installation

m_v= mass of vessel

$m_{a,i}$= added mass of installation

$m_{a,w}$= added mass of water

Various photographs of ships which have sustained collision damage have proven that complex deformation modes with several areas of energy dissipation occur during the event causing great difficulty in any large scale simplification, as shown in Figure 4-4 [28]. The four major energy dissipation mechanisms during ship collision are as follows:

i. side shell folding,
ii. deck tilting,
iii. frontal bow stretching
iv. side shell stretching.

Most ship platform collisions are a combination of these four areas, which is why the use of analytical methods is non-ideal for adequate representation of the collision event.

Figure 4-4: Deformation of Saxon Onward resulting from bow collision [29]

4.2.4 Impact Velocity

It has been proposed that a supply vessel drifting sideways in a given sea state should be the design basis accident for an offshore platform [3]. Due to the high level of kinetic energy involved in such an incident, knowledge of a reasonable and accurate velocity of the marine vessel during the collision is of utmost importance in determining the level of damage sustained by both structures. The kinetic energy during a collision event is proportional to the second power of impact velocity of the marine vessel. A steady state velocity condition is typically assumed, as wave and wind forces are assumed to be balanced by hydrodynamic resistance forces and are consequently not included.

Veritec, amongst other standards, assumes the collision velocity used for accidental collision to be related to the drifting of a supply vessel, which neglects the possibility of powered accidental collisions [23]. The impact loads from a powered collision would almost always cause a greater impact velocity of the ship to platform, but the probability of such an event occurring is considered to be negligible, and so the case is ignored [3]. The vessel will exert sway oscillations, which will be the same frequency as the waves in the region of the offshore platform. The instantaneous magnitude of the sway velocity will be normally distributed throughout the vessel, which is highly conservative, as a fully broadside collision is a very improbable event. Therefore, the velocity of the vessel can be approximated as:

$$v_v = 0.5H_{s(max)} \frac{m}{s} \tag{4.9}$$

where:

$H_{s(max)}$ = the maximum significant wave height for operation close to the platform (m)

The assumption is often made that the probability of hitting a fixed structure is proportional to the velocity of the marine vessel in question, allowing for an approximate probability distribution to be derived [3]. The assumed velocity of the vessel typically ranges from 0.5 m/s for low energy collisions to 2.0 m/s for high energy collisions. NORSOK specifies that in the case of a supply vessel impact on an offshore installation, the ship speed should not be considered below 2.0 m/s for the ALS design check [18].

4.2.5 Structural Mass

In order to accurately determine the mass of a ship to be used when determining the kinetic energy requiring dispersion if the offshore structure is the subject of the collision analysis, a review of passing ships as well as service ships should be taken into consideration alongside their relative probability. The most frequent type of collisions of ships with offshore structures are from authorized vessels which operate close to the platforms; however, involved vessels may also be an authorized vessel servicing the installations, a tanker for offshore loading in the area, or any other sort of ship which regularly passes by the vicinity of the offshore structure [3].

NORSOK specifies that in the case of a supply vessel impact on an offshore installation, the ship mass should typically not be considered less than 5000 tons [19]. It is of utmost importance to determine the size of vessels servicing the installation being assessed, as the mass may in fact be larger than the 5000 tons suggested.

During a collision event that considers the deformation of both structures, it is important to determine an accurate mass and mass distribution of each structure involved, as it directly relates to the kinetic energy and consequent strain dissipation to occur within the structures. During a finite element simulation, structural mass of the marine vessel and offshore platform should be accounted for through the density of the materials specified if the entire structures have been modelled. In the event that the structural mass does not match perfectly with what the material specifications denote, it may be appropriate to adjust the density of the material composing the structure. This will allow the structure to

achieve the correct total mass, as the weight of the entire colliding structure must be taken into account during the collision event [30]. The Two Mass System approximation can be used and is discussed further in subsection 4.2.6. as a simplified calculation to check the order of magnitude of simulated results,

4.2.6 Two Mass system approximation

In the acceleration phase which occurs during collision response, the inertia of the topside structure generates very large reaction forces. Often, as a simplified method of calculation for ductility design, it can be assumed that the offshore structure is fixed at deck level and the ship does not dissipate any of the energy from the collision, as shown in Figure 4-5 [14]. This analytical model must also be created based on the assumption that the two colliding structures can be approximated as a two-mass system using generalized masses.

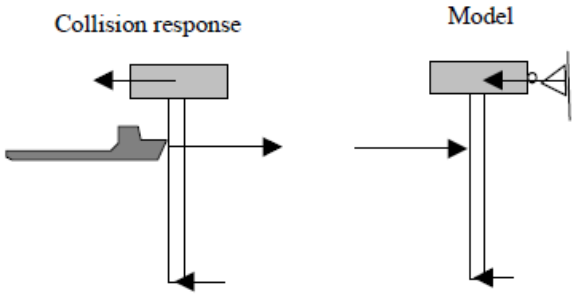

Figure 4-5: Model for assessment of reaction force to deck [14]

While this method is useful for preliminary calculations, it should not be used as a method for design, because it would only provide a rough estimation for response of the structure. To solve the issue in this simplified model, which is caused by the assumption of a completely rigid ship which dissipates no portion of the kinetic energy, Pedersen and Jensen further develop this model of a simplified theory of energy released for crushing

of structures [31]. The following derivations is provided as it outlines very well the mechanisms involved with energy dissipation during a collision event.

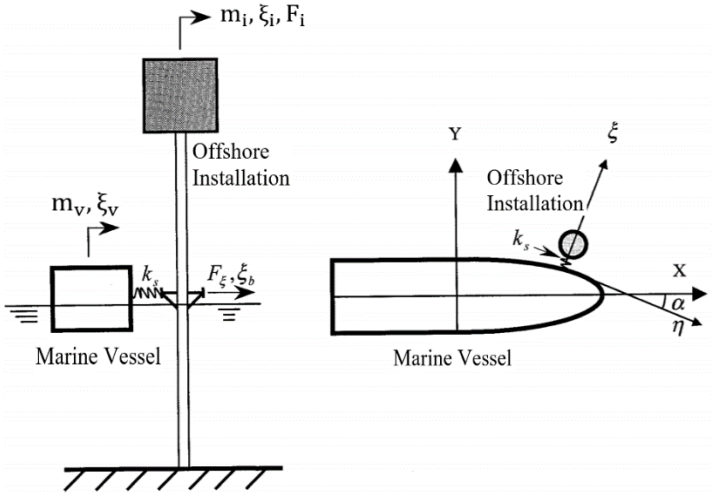

Figure 4-6: Simplified model of a supply vessel impacting a platform [31]

The following relations between force and stiffness represent the platform behavior in accordance with Figure 4-5 [31]:

$$F_\xi = k_{11}\xi_b + k_{12}\xi_i \tag{4.10}$$

$$F_i = k_{21}\xi_b + k_{22}\xi_i = -m_i\ddot{\xi}_i \tag{4.11}$$

$$t_c\sqrt{g/\,D_v}$$

Marine Vessel

where

m_i is the topside mass of the offshore installation

F_ξ is the collision force between the platform and vessel

F_i is the transmitted force acing on the generalized topside mass of the platform

ξ_b is the net displacement of the collision point

ξ_i is the displacement of the offshore topside installation

The interaction between the ship and platform can therefore be simplified by the relation [31]:

$$F_\xi = \begin{cases} k_s(\xi_v - \xi_b), & \text{for } \dot{\xi_v} - \dot{\xi}_b \geq 0 \\ 0, & \text{for } \dot{\xi_v} - \dot{\xi_v} < 0 \end{cases} \quad (4.12)$$

where

$k_{11}, k_{22}, k_{12}, k_{21}, k_s$ are stiffness coefficients derived from the structures

Pedersen and Jensen also show that at the end of a collision where $\dot{\xi}_v = \dot{\xi}_b$, the displacement ξ_i can be assumed to be negligible. Therefore, using this assumption and equations (4.10) and (4.11) [25]:

$$F_i = \frac{k_{21}}{k_{11}} F_\xi \quad (4.13)$$

From the case shown in Figure 4-6, the impact impulse of the collision between the supply vessel and platform can be expressed as [25]:

$$I_\xi = \frac{m_v}{D_{a\xi}} \left[\dot{\xi}(0) - \dot{\xi}_v\right] \quad (4.14)$$

$$D_{a\xi} = \frac{1}{1+m_{a,x}} \sin^2 \alpha + \frac{1}{1+m_{a,y}} \cos^2 \alpha + \frac{1}{1+j_v} * \frac{[y_c \sin\alpha - (x_c - x_v)\cos\alpha]^2}{R_v^2}, \quad (4.15)$$

where

R_v is the radius of ship mass inertia around the centre of gravity

x_v is the x coordinate of the centre of gravity of the striking vessel

(x_c, y_c) is the coordinate of the centre of gravity of the collision point

$m_{a,x}$ is the added mass coefficient for the surge motion (typically taken as 0.05)

$m_{a,y}$ is the added mass coefficient for the sway motion and is taken as 0.5

j_a is the added motion for the rotation around the centre of gravity

α is the collision angle as represented in Figure 4-1

$D_{a\xi}$ is a coefficient defined by the given equation

From these equations, the impact impulse on the generalized platform mass can be expressed as:

$$I_i = -m_i \dot{\xi}_i = \frac{k_{21}}{k_{11}} I_\xi \tag{4.16}$$

At the end of crushing stage, equilibrium is reached between the velocities of the supply vessel and platform at the collision point of the two structures, which allows the relation:

$$\dot{\xi}_v = -\frac{k_{12}}{k_{11}} \dot{\xi}_i \tag{4.17}$$

Presenting the topside velocity of the platform by:

$$\dot{\xi}_i = \frac{-\dot{\xi}(0)}{\frac{k_{12}}{k_{11}} + \frac{k_{11}}{k_{21}} * \frac{m_i D_{v,\xi}}{m_v}} \tag{4.18}$$

The velocities of the ship at the end of the collision can be expressed as:

$$v_{v,x} = \dot{\xi}(0)\sin\alpha - \frac{\sin\alpha}{D_{v,\xi}(1 + m_{a,x})}\left(\xi(\dot{0}) - \dot{\xi}_v\right) \tag{4.19}$$

$$v_{v,y} = \dot{\xi}(0)\cos\alpha - \frac{\cos\alpha}{D_{v,\xi}(1 + m_{a,y})}\left(\xi(\dot{0}) - \dot{\xi}_v\right) \tag{4.20}$$

$$\omega_v = \frac{y_c\sin\alpha - (x_c - x_v)\cos\alpha}{R_v^2(1 + j_a)D_{v,\xi}}\left(\xi(\dot{0}) - \dot{\xi}_v\right) \tag{4.21}$$

$$\dot{\xi}(0) - \dot{\xi}_a = \frac{\dot{\xi}(0)}{1 + \frac{k_{12}k_{21}}{k_{11}^2} * \frac{m_v}{m_i D_{v,\xi}}} \tag{4.22}$$

The energy to be absorbed by the crushing of the supply vessel and the deformation of the platform is:

$$E_c = E_0 - (E_v + E_i) \tag{4.23}$$

where: $$E_0 = \frac{1}{2}m_v[(1 + m_{a,x})\sin^2\alpha + (1 + m_{a,y})\cos^2\alpha]\dot{\xi}(0)^2 \tag{4.24}$$

$$E_p = \frac{\frac{1}{2}m_v^2\dot{\xi}(0)^2}{\left(\frac{k_{12}}{k_{11}} + \frac{k_{11}}{k_{21}}\frac{m_i D_{v,\xi}}{m_v}\right)^2} \tag{4.25}$$

$$E_v = E_0 + \frac{1}{2}m_v\dot{\xi}(0)^2\left(\frac{1}{D_{v,\xi}\left(1 + \frac{k_{12}k_{21}}{k_{11}^2}\frac{m_v}{m_v D_{v,\xi}}\right)^2} - \frac{2}{D_{v,\xi}\left(1 + \frac{k_{12}k_{21}}{k_{11}^2}\frac{m_v}{m_i D_{v,\xi}}\right)}\right) \tag{4.26}$$

Equation (4.24) represents the initial kinetic energy of the supply vessel, equation (4.25) represents the kinetic energy of the platform topside at the end of the collision, and equation (4.26) represents the kinetic energy of the supply vessel at the end of the

collision. Therefore, the total energy to be dissipated by the deformation of the ship structure during the ship to platform collision event is:

$$E_v = \frac{1}{2} k_s (\xi_v - \xi_i)^2 = \frac{F_\xi^2}{2k_s} = \frac{k_{11}}{k_{11} + k_s} (E_0 - E_v - E_i) \tag{4.27}$$

4.2.7 Added Mass

NORSOK specifies that in the case of a supply vessel impact on an offshore installation, the hydrodynamic mass can be assumed to be 40% of the ship mass for sideways impact and 10% for bow and stern impacts. This 40% value was originally developed for the collision between two ships, and is only a reasonable approximation when the duration of the impact is less than 0.5-1.0 seconds [24, 20]. For broadside ship platform collisions which exceed 1.0 s total, the added mass coefficient can approach that of the ship structure [24]. The added mass for sideway motion for typical supply vessel geometries is presented in Figure 4-7, where duration of collision is represented by t_c and the vessel breadth to draught ratio is represented by B_v/D_v [24]. It should be noted from Figure 4-7 that the maximum added mass coefficient possible is 1.0. This implies the mass added by hydrodynamic effects cannot exceed the mass of the marine vessel for design purposes under any geometry, and as the breadth to draught ratio of marine vessels increases, the potential added mass decreases. It should also be noted that these curves have been developed based on the depth and breadth of the marine vessels in question, but does not take into account the total wetted surface of the submerged portion of the vessel. For this reason, these curves should be used with caution when performing preliminary analysis of marine vessels in the vicinity of the offshore platform, as they may only provide a

reasonable approximation for determining added mass of traditional hull vessels. Marine structures such as barges and catamarans typically have non-ideal geometry for reducing drag force and subsequently added mass due to the use of large quantities of flat plating for barge structures and greater area of influence for catamarans.

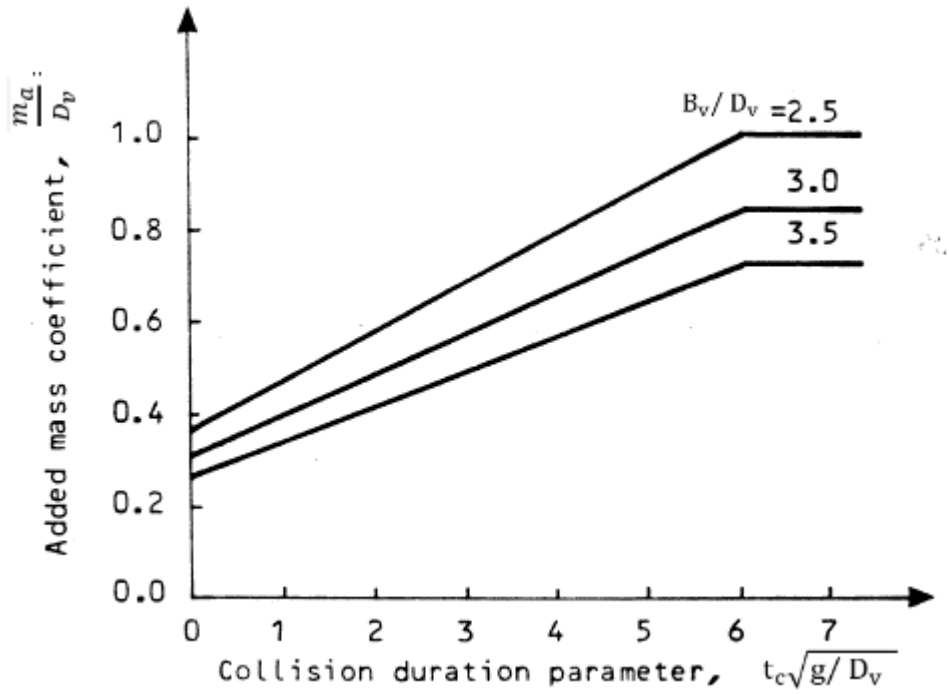

Figure 4-7: Sideways added mass for supply vessels as a function of duration of collision [23]

While Figure 4-7 is a very useful graph for sideways moving supply vessels with traditional hull shapes, it has been shown that the added mass coefficient for a STOPC is heavily dependent on the shape of the hull as well as the duration of the impact [23]. This should be taken into consideration when utilizing these curves for irregular hulls. The Veritec Standard of offshore platform design recommends the following expressions developed by Peterson and Pederson [24] for the determination of added mass in sway motion:

$$\frac{m_a}{d_v} = \begin{cases} \left(0.7 + 0.2 t_c \sqrt{\frac{g}{D_v}}\right)\left(\frac{D_v}{B_v}\right) * \frac{1}{C_B} & \text{for } t_c \sqrt{\frac{g}{D_v}} \leq 6 \\ \frac{D_v}{B_v}\frac{1.9}{C_B} & \text{for } t_c \sqrt{\frac{g}{D_v}} > 6 \end{cases} \quad (4.28)$$

where:

d_v = displacement of the vessel

m_a = added mass

g = acceleration due to gravity

t_c = duration of collision

D_v = draught of vessel

B_v = breath of vessel

C_B = block coefficient

The fluid added mass has historically been accounted for during collision analysis through increasing the mass of the ship by a percentage corresponding to its orientation during collision [32], as discussed in previous sections. This remains the method of accounting for fluid added mass throughout all modern offshore collision assessment standards but is a very crude way to represent hydrodynamic effects. If this method is implemented, the most accurate way to account for the added mass is to apply it at the wetted surface of the hull only.

Added fluid mass can be applied solely to the hull by applying concentrated mass elements over the hullform. This serves as a reasonable approximation if the impact longitudinal position is close to the longitudinal center of gravity (LCG) of the vessel [33]. More recently, there have been developments within several FEA programs, allowing for more realistic representations of fluid added mass during a collision.

The Newcastle University School of Science and Technology in collaboration with the School of Naval Architecture and Marine Engineering performed an investigation of an actual collision incident between a tanker and a bulk carrier in order to determine an appropriate means of simulation for such events [4]. This study had used the LS-DYNA code, which allows the simulation of multi-vessel dynamics in restricted water in the presence of waves, wind, and various current obstacles. This is achieved through the employment of a 4 DOF mathematical model, which reproduces the maneuvers of colliding vessels.

While not yet dominant in published STOPC assessment studies, interactive fluid-structure based simulation is a rapidly growing research area. Ideally, one day it would be applicable to the addition of fluid mass to vessel structures through the use of smooth particle hydrodynamics (SPH). These elements accurately represent the physical laws and behavior characteristics of the fluid, taking viscosity, density, and friction into consideration in order to determine the additional mass or loading that will be imposed on the deformable structure [34]. These elements have proven to be very efficient in the generation of visual representations of water induced motion and waves imposed upon

large scale structures to a high level of accuracy, as shown in Figure 4-8 and Figure 4-9 [35, 36]. They are, however, currently used predominantly for graphical display purposes or in small scale FEA models. SPH elements are quickly becoming a viable option for the representation of fluid added mass but have not seen significant usage in STOPC assessment to date. The same is true for added mass through the use of CFD (Computational Fluid Dynamics).

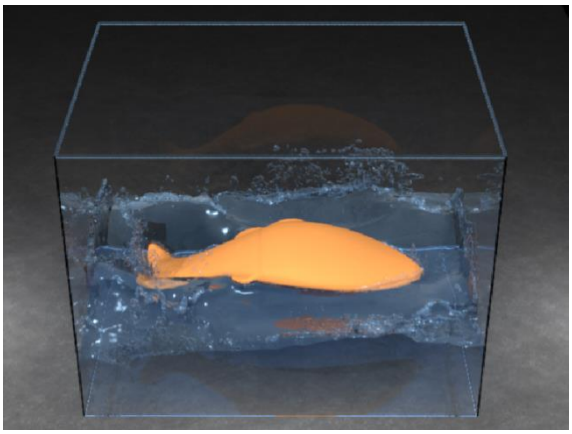

Figure 4-8: SPH fluid elements interacting with a fish model with an embedded proportional derivative controlled articulated skeleton [35]

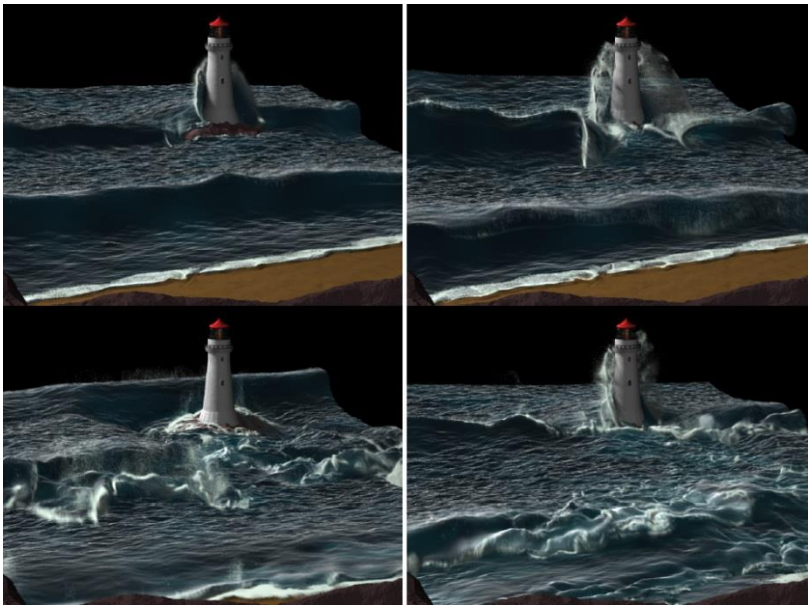

Figure 4-9: Large ocean scene simulated with two -way coupling using the SPH method [36]

4.2.8 Vessel Deformation and Bow types

The bow geometry of a given marine vessel has a major impact on the method in which deformation in both the offshore structure and vessel structure would occur during a collision event. Typically, passenger vessels and bulk carrier vessels geometry can be divided into three distinct parts: The bow, mid-parallel, and stern. The bow can be further subdivided into two distinct polygons as shown in Figure 4-10: the tetrahedral part and the remainder. In a frontal collision, damage is typically confined within the bow as the tetrahedral part is considered to be the most vulnerable part of the vessel assuming the hull form and decks are made with a constant thickness. This is because the bottom plate (typically a deck) shown in Figure 4-10 does not support the tetrahedral part of the vessel bow. The bulb is the lowest, curved portion of the bow shown in Figure 4-10:

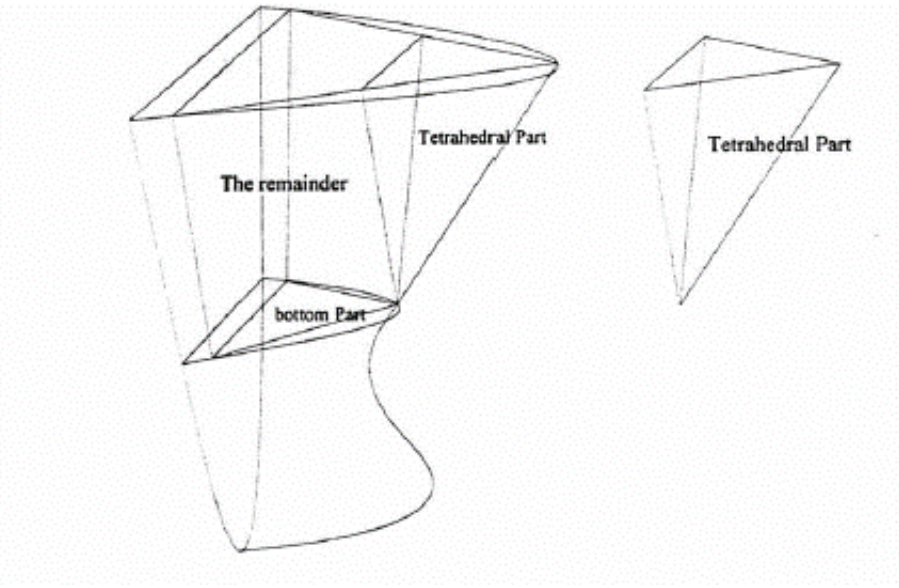

Figure 4-10: Geometry of typical bow structure [28]

The prediction of bow deformation becomes substantially more difficult to predict without detailed FEA when using a non-typical bow geometry [22]. Bulbous bows, which are common in arctic waters, have different deformation characteristics than raked bows or reinforced bows, and consequently the offshore platform must dissipate a smaller portion of the strain energy. An offshore jacket platform situated in the North Sea was analyzed for accidental vessel collision during a study conducted by the Technical University of Norway. It was found that the maximum force in the colliding vessel (assuming a linear behavior) to be less than 20 MN for a bulbous bow and less than 15 MN in the case of no bulb. The energy dissipation governed by vessel deformation was found to be at least 66 MJ for the bulbous bow and 37 MJ without the bulb. The bulbous bow had dissipated 80% more energy through deformation when compared to the non-bulbous bow. As the net energy within the collision remains the same regardless of bow

shape, any energy which is not absorbed by the bow is absorbed by the offshore platform. Consequently, ductile design is more applicable to STOPCs involving a vessel with a bulbous bow as it causes a lower amount of energy to be absorbed by the platform [6]. The immense difference in energies resulting from a head on collision with a bulbous vs a non-bulbous bowed vessel is given in Figure 4-11:

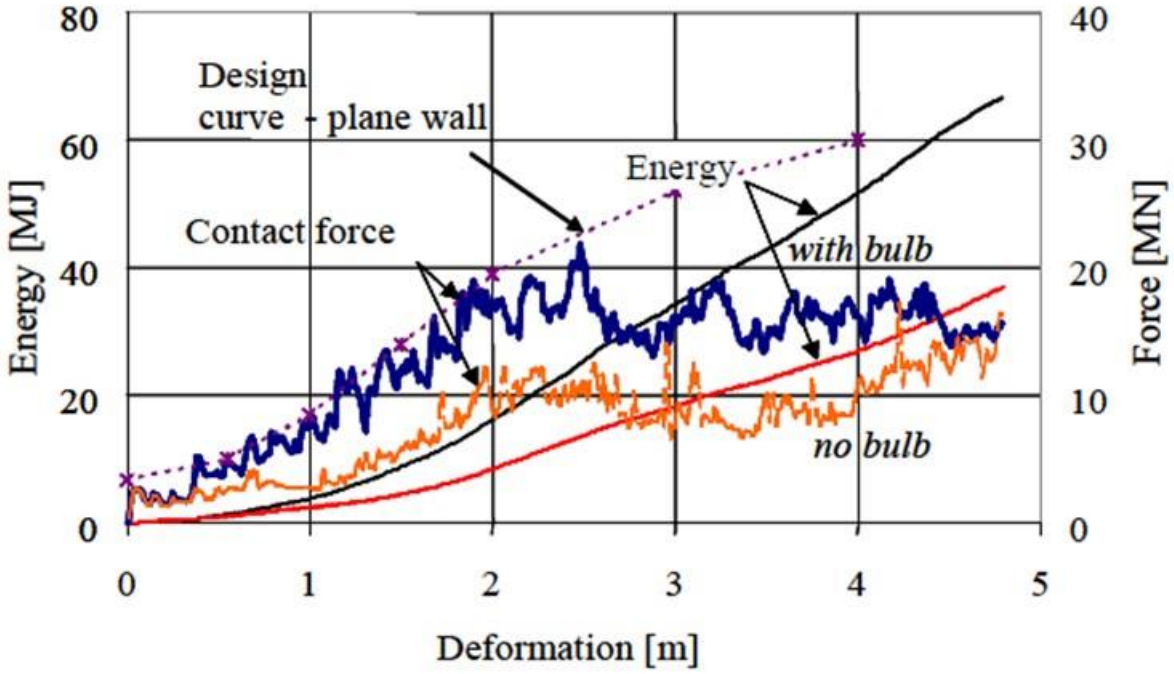

Figure 4-11: Energy vs Deformation graph of a marine vessel experiencing a head-on collision, with and without a bulbous bow [8]

A study published by MIT (Massachusetts Institute of Technology) in 2000 [28] revealed that not only do stiffened and unstiffened bows exhibit different levels of energy dissipation during a collision, but they have vastly different proportions of energy allotted to different energy dissipation modes during the collision event. It should be noted that the present NORSOK code does not cover the ice-reinforced vessel. This class of vessel

is less likely to deform because overall, it would require additional kinetic energy as ice reinforcement would stiffen the vessel structure significantly. With ice stiffened bows, it is common for energy dissipation to occur outside of the stiffened region which in turn may cause side shell bending. This would make the mean crushing force difficult to determine analytically.

When a vessel collides head on with an offshore structure, the outer hull membrane of the vessel begins to fold within itself in order to increase the bearing area of transmitted force. One of the issues with traditional and empirical methods of vessel collision evaluation is the difficulty in accounting for the rapidly developing folds which occur within the bow as shown in Figure 4-12. If a bow is assumed to fold outwardly rather than inwardly, then the crushing force predicated by the corresponding solution can be up to ten times more than the measured force [28]. This consideration raises issue with FEA study as well, as the element refinement must be quite significant in order to capture the bow folding during simulation.

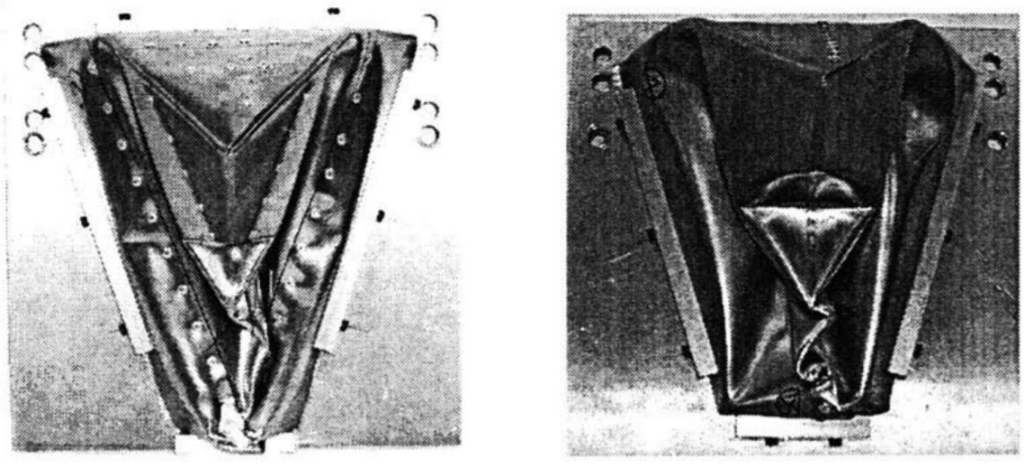

Figure 4-12: Bow crushing pattern resulting from head on collision [28]

4.3 Plastic Deformation in Steel

Plastic deformation explains the state of a material in which there is a permanent deformation or change in its shape without fracture under the action of a sustained force. The plastic region of a stress-strain curve of a material refers to the portion the curve in which there is a large quantity of strain corresponding to a small quantity of applied stress. Plastic deformation can be explained by plasticity theory, of which there are three primary approaches [37]: continuum mechanics theory, crystallographic mechanisms and twinning, and dislocation theory.

The most widely used approach to plasticity is the continuum mechanic theory, which considers yield criteria and allows predictions of the stress states which cause yielding and the corresponding strains. This theory is heavily embedded in all modern steel structure design standards, and pairs well with additional mechanical mechanisms which occur during deformation, such as strain hardening and local deformation. The second approach to plasticity theory uses the crystallographic mechanisms and twinning to explain continuum behavior. This approach is useful for the prediction of anisotropic behavior of materials but is seldom used in steel structural design. The third approach, The Dislocation theory, focuses on how slip and twinning occur and allows for an in depth explanation of strain hardening, but "its connection to Continuum theory has been difficult to bridge" [37]; Dislocation theory appears frequently in mathematical journals, its use is not common in numerical analysis of subsea pipelines or offshore structures. The Dislocation theory does, however, account for plastic deformation and isotropic hardening, and as a result is appropriate for use in the evaluation of such structures

provided it is supported by the code used for the structural assessment, and the mechanical properties of the material is very well understood.

Generally, increasing yield strengths will reduce the yield point elongation and strain hardening rate [38]. For high strength steels, the rate of strain hardening is not a constant value over the entire range of uniform plastic strain; the value is initially a high magnitude but consistently decreases after a small amount of plastic straining [38]. The three most important parameters to consider when utilizing the post-yield regime for the determination of structural integrity are:

i. Yield tensile ratio
ii. Strain hardening exponent
iii. Local elongation (Lüder's strain) and strain at ultimate tensile strength

The yield tensile ratio of a material is the ratio of the material yield strength to its ultimate tensile strength, and is often used as an indicator of the margin of safety of structures such as pipelines against failure by plastic collapse. In other words, it indicates the ability of the structure to experience plastic behavior prior to failure. It is a commonly used tool within various pipeline design guidelines such as DNV Submarine Pipeline Standard Insert or the American Pipeline Institute's specifications for line pipe.

The strain hardening exponent is a constant that describes the stress-strain behavior of the material in the work hardening region. It is well established for most steel-based materials and is critical for the accurate representation of plasticity. Strain hardening will be further discussed in Section 5.5.4

The shape of the stress-strain curve beyond yield is important in the assessment of structural integrity of such structures when applying a plastic strain approach, but it is also important to realize and consider the presence of Lüder's bands and Lüder's Plateau (yield point elongation) [38]. Lüder's bands can physically be observed in regions of plastic deformation in steel and other poly-crystalline body-centered cubic metals and within Steel, Lüder's band develops after the yield point has been exceeded, and coincide to the plastic section of the stress-strain curves shown in Figure 4-13:

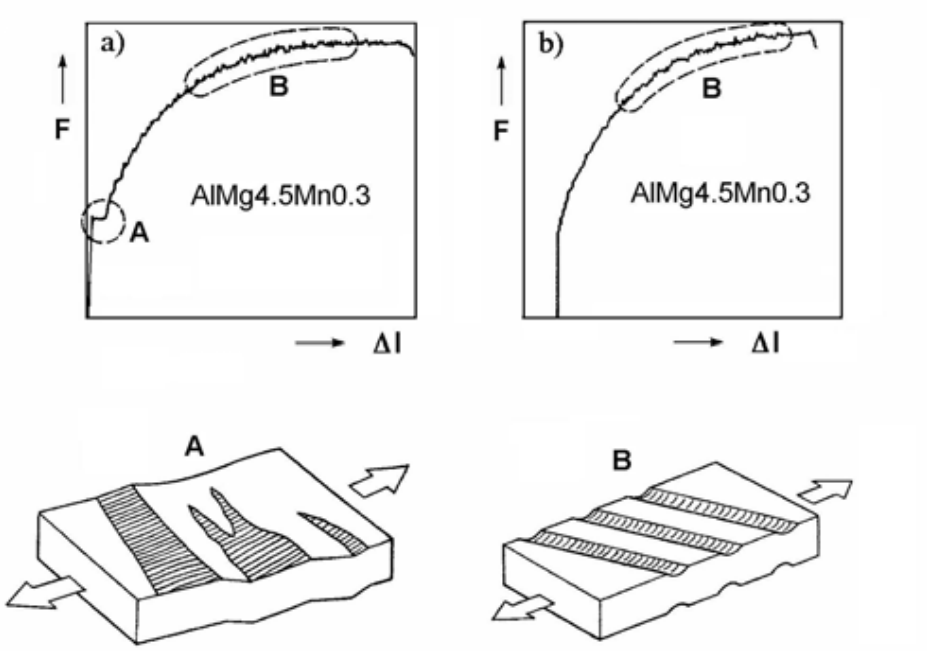

Figure 4-13: Uniaxial stress-strain curves with Lüder's elongation paired with sketches of the appropriate surface markings [39]

Lüder bands developing on the surface of metals can generally be categorized into two distinct groups:

i. Flamboyant bands

ii. Parallel bands

These two categories are attributed to specific characteristics in two separate locations of the stress-strain curve [39]. These two distinctly different forms of Lüdering are shown in Figure 4-13. Thermo-mechanical treatments such as a combination of low cold rolling reductions and annealing can reduce or completely repress the development of Lüder's bands [39]. The testing of samples for the investigation of Lüder's bands often focuses on parameters such as the upper and lower yield stress of the stress-strain curve [40], and the magnitude of the Lüder's extension [41].

4.4 Response of Jacket Type Structures

While the elements used for the formulation of the vessel structure are the primary focus of this thesis, it is also important to accurately represent the jacket structure so the energy dissipation throughout the vessel is accurate and can be properly simulated. The energy dissipated within the jacket structure during a collision event is typically split into three contributions [10]:

i. Local deformation of the tube wall at the point of impact

ii. Deformation of brace element beams

iii. Overall frame deformation

As there is considerable interaction between the modes stated above, it is very difficult to separate them in practice. It is not possible to determine an accurate general formula for

how the energy within a platform is dissipated due to the complex variety of jacket types, vessel hull types, and situations of collisions [3]. This means that in most cases, FEA would be the method of choice for achieving an accurate result of jacket structure deformation.

4.4.1 Failure of tubular members

Near the impact zone at the waterline, most offshore platforms consist mainly of tubular members. When a tubular member is subjected to a large concentrated force normal to its membrane there are two primary methods in which it can absorb energy: [24]

i. Tube will be deformed in an overall bending mode
ii. Tube will be flattened locally at load application point

The amount of energy that will be absorbed locally by tubular jacket members depends largely on the wall thickness of the tube, which are typically in the region of 20-50 mm for fixed offshore structures [3]. It has been observed that plastic deformations in compressed tubular members are not uniformly distributed throughout the structure but rather confined to narrow zones where both strain and rate of change of strain reach high magnitudes. These “hot spot” locations are referred to as hinge lines and regular pattern of wrinkles and folds within the members are formed [8]. The crumpling process of members connected to the load application point is strongly path dependent. This is because the dissipated energy is dependent on the deformation history of the entire structure. This makes FEA the most appealing method of determining the actual

deformation and stress of the structure as the option of a time dependent analysis is available within several software packages.

In the initial stages of transverse loading of a tubular member, the tube will deform locally until the applied load reaches a value at which the tube begins to yield and deflects like a beam [3]. The beam then is folded into itself in one of two different forms: one where the shell in folded with axisymmetric conditions and the other where asymmetric folds are developed. The latter mode generally occurs for thin wall tubes and is not typical of thick-walled tubes or tubes stiffened with a high number of ring stiffeners [8].

Due to the relatively high stiffness of tubular members used in offshore structures, they are able to absorb a considerable amount of energy before acting as a beam and undergoing global plastic deformation. The amount of energy absorbed before global deflection of the beam will increase farther if the ends are sufficiently restrained to represent a fixed condition rather than a pinned based on the principles of beam stiffness from classical beam theory. This is typical for members directly attached or near the platform foundation. For broadside vessel collision with vertical tubular members where the hull of the marine vessel is relatively flat, the yield lines of the tubular member can be approximated as per Figure 4-14. This allows a non-dimensional load indentation relationship to be used such as those provided in Figure 4-15.

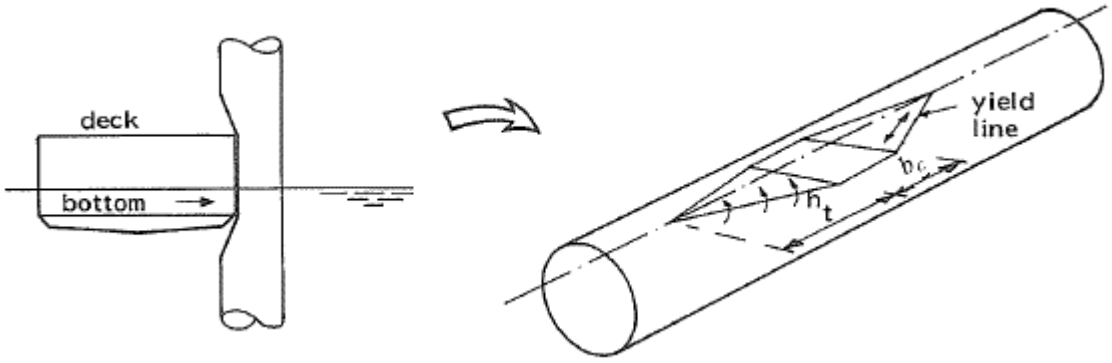

Figure 4-14: Local deformation and yielding patters of tubular members impacted by a marine vessel [3]

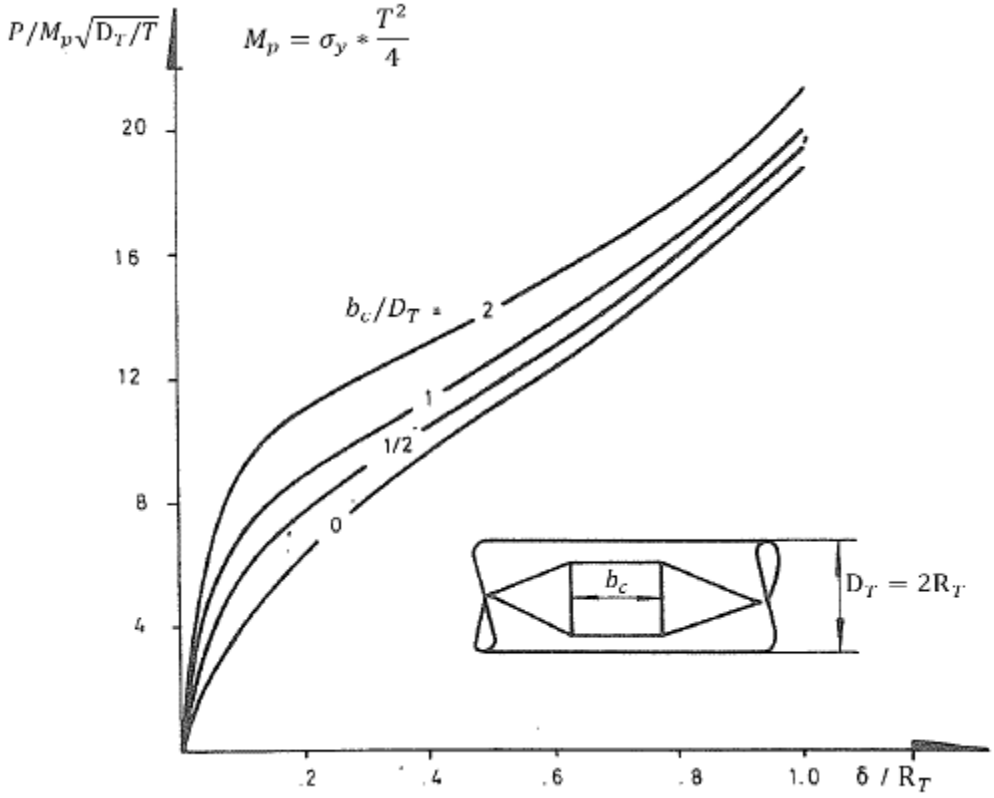

Figure 4-15: Non-Dimensional Load indentation relationships for steel tubes [3]

Many of these formulations can and should be used in conjunction with the finite element method. If assessing local deformation in tubular members only, it may be appropriate to use equivalent static loading and therefore an implicit solver. This method would only be

applicable provided the point of collision as well as the total energy dissipated energy are known and well understood and able to be simplified similarly to the functions provided in equations (4.29) [42].

where:

$$\text{Reactions of loading on tubular members} \quad P(t) = \begin{cases} \frac{2Ft}{t_0} & \text{for} \quad 0 \le t \le \frac{t_0}{2} \\ 2F\left(1 - \frac{t}{t_0}\right) & \text{for} \quad \frac{t_0}{2} \le t \le t_0 \\ 0 & \text{for} \quad t_0 < t \end{cases} \tag{4.29}$$

$t = \text{time}\ (s)$

$t_0 = \text{time when net force applied to member reaches 0 N}\ (s)$

$F = \text{force for a given time t}\ (N)$

$P(t) = \text{impact action on offshore structure as a fuction of time}$

While analytical approaches to local denting of tubular members outlined in this section can be used to approximate local deformation or reactions of loading of the offshore structure members, it is recommended to instead use fully numerical methods to determine a more accurate and comprehensive deformation and energy dissipation pattern of the collision area. This is particularly true when the vessel impacting the offshore structure has irregular geometry where these curves may not be valid. In addition, levels of refinement in the collision area should be high enough to capture all possible modes of deformation during the collision assessment.

4.4.2 Local Denting Curves

Load indentation curves primarily exist for addressing the local flattening of tubes at the load application point. These curves are typically developed with the assumption that one end of the tubular member is fixed while the other is pinned, and that three plastic hinges will develop throughout the member; one at each support and another under the applied point load [24]. The load displacements for tubular members sustaining collision damage as a function of normalized load application are as given in Figure 4-16 [10]:

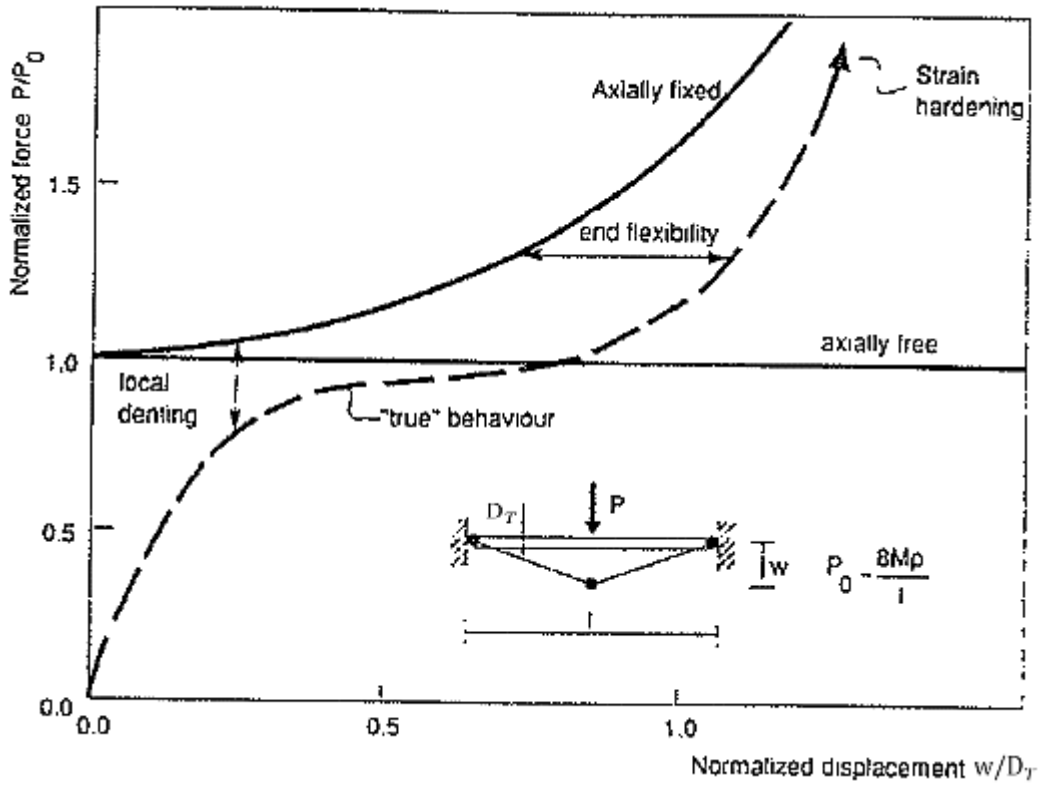

Figure 4-16: Load displacement characteristics for tubular members [10]

As these curves represent the energy absorbed by the tubular member, the total energy absorption capability can be determined through integrating the force integration curve or

measuring the area under an empirically generated curve. It should also be noted that the curves presented in Figure 4-16 have been established for ideal boundary conditions, where in practice the support of a brace will be far more flexible. Small amounts of flexibility delay the growth of member membrane forces which are essential to the dissipation of energy during a collision. As the method of force distribution throughout the member has a high impact on the development of plastic hinges, the orientation of the vessel at the time of collision will have a major effect on the indentation patterns within the offshore structure members. This is largely due to the varying stiffness throughout marine vessels. Force-deformation relationships for 5000 ton supply vessels (with stern rollers) for broad side, bow, stern end and stern corner impact are given in Figure 4-14. While it would have been very useful if a universally established column was established for STOPC assessments to better compare FEA simulation results, the author has not found any such standard.

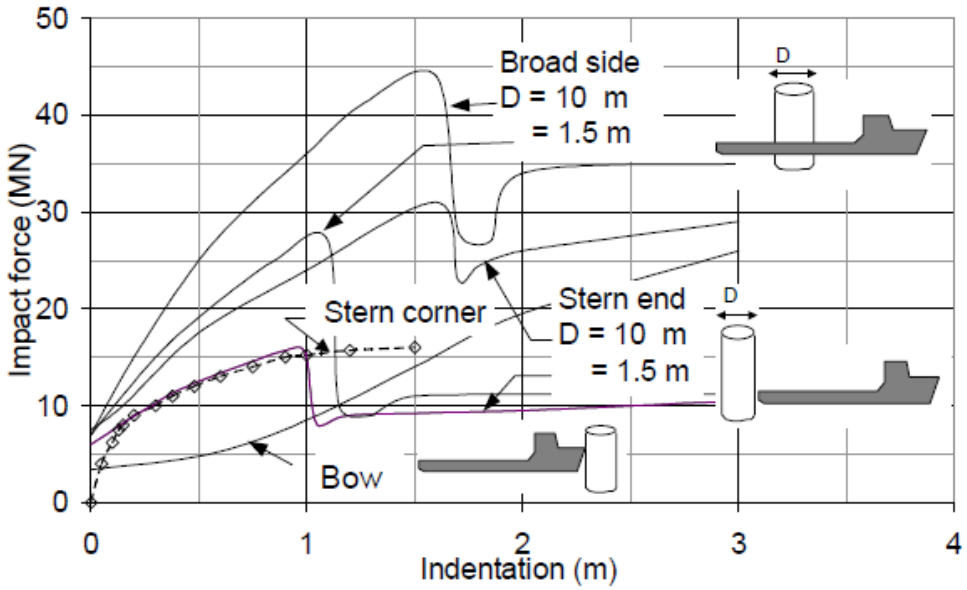

Figure 4-17: Load indention curves for various vessel orientations [19]

The curves for broad side and stern end impacts shown in Figure 4-17 are based on collisions with a rigid vertical cylindrical member (D=1.5m) and large diameter columns (D=10m). The curve shown for stern corner impact is typically used in design for large diameter column impacts and is based upon the jacket structure of a platform being rigid. The curve for bow impact is based upon collision with a rigid plane wall and is only suitable for large column impacts; it should not be used for dissimilar collision events (e.g. diagonal braces or large jacket legs at a significant angle to the vertical). For beam, stern end, and stern-corner impacts, all energy should be assumed to be dissipated by the brace. When more accurate calculations are not available, Figure 4-17 may be used for square-rounded columns [14].

When the collision force exceeds the plastic collapse load for the jacket leg, then the leg will collapse. This was taken into consideration for the development of indentation curves such as Figure 4-17 which are used as a design basis in NORSOK N-004, Appendix A [19]. Of particular note is that these curves were developed in the early 1980's, prior to the advent of advanced nonlinear finite element methods, which would have been the natural choice today [43]. It should also be noted that the NORSOK code does not take into effect wave induced rolling, which could increase the effective angle between the shipside and the leg and therefore cause a longer period with concentrated contact on the leg of the platform as well as increase the rate of contact area development between the two structures. It should be noted that the load-indentation curves developed by DNV are based on the deformation of a conventional raked bow. Many supply vessels within the

North Sea are designed with raked bows, but a variety of different bows are in service which limits the usability of these curves.

While these curves serve as preliminary design tools and provide benchmark values to compare to a full scale analysis, they emphasize the need of FEA if structure specific failure regions are to be determined, as there are such a broad spectrum of vessels, offshore structures, and member types that will affect results.

4.4.3 Load Indentation Curves Validation

Load indentation curves have long been a standard of offshore structure accidental collision design, and numerous studies have been conducted in order to validate the applicability of these curves to real collisions. This section will focus on the most recent comprehensive study validating these curves.

A study of results achieved from numerical STOPCs using NORSOK recommended procedure was performed using LS-DYNA in 2012 [43]. While this study provides a comprehensive account of various collision simulations, only the data pertinent to the validation of indention curves will be provided in this section and are as shown in Figure 4-18 and Figure 4-19 [43].

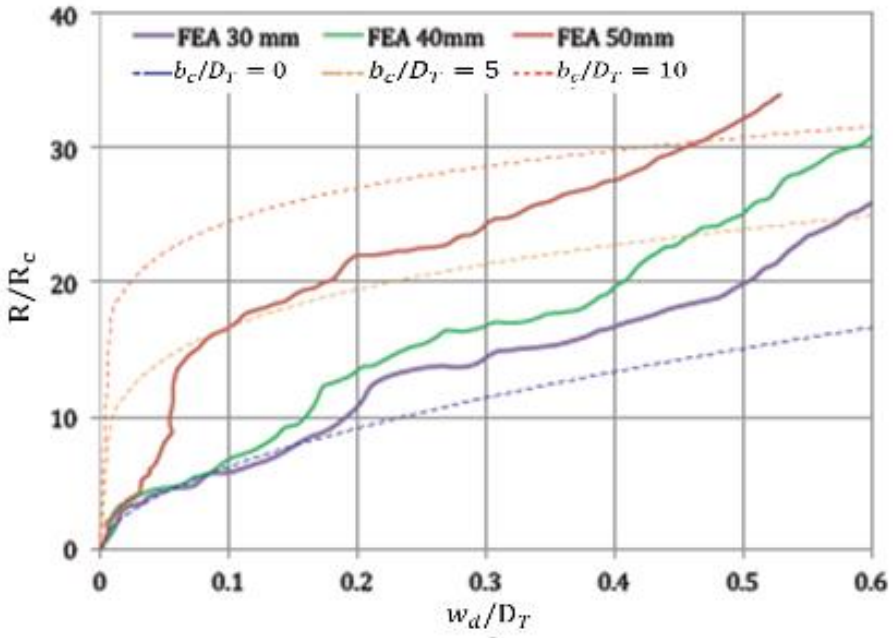

Figure 4-18: Non-dimensional resistance local indention curves for various member sizes [43]

With reference to Figure 4-18, the variables are as follows:

D_T = original tubular member diameter

R = radius of deformed area

R_c = plastic collapse resistance in bending

w_d = dent depth

b = collision width

b_c/D_T = ratio of collision width to undeformed tubular member diameter

Figure 4-18 shows that the resistance of an offshore structure leg with thickness between 30 and 50 millimeters are in agreeance with code prescribed curves. It is evident from the curves that as the denting increases, the b_c/D_T value becomes increasingly difficult to predict and cause the results to exceed values prescribed by NORSOK [43].

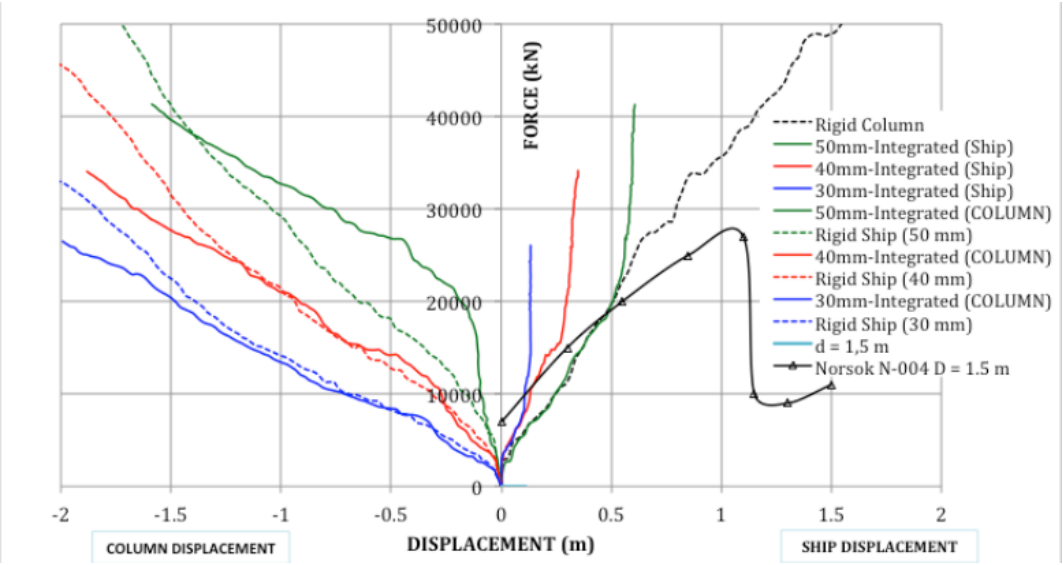

Figure 4-19: Contact force vs. displacement curves of varoious vessel and member configurations [43]

The right side of the graph in Figure 4-19 shows that the deformation within the vessel structure is far more difficult to predict using code prescribed formulae (represented by the thick solid curve) than column displacement. This is due to the high level of complexity in representing a full vessel structure compared to that of a simple vertical column. For a tubular element with wall thickness of 50 millimeters, the resistance closely resembles that of a rigid column and the leg is assumed to be strong enough to penetrate the hull of the colliding vessel. Initially, this results in a high level of energy dissipation within the colliding vessel structure, but after 0.5 millimeters of penetration, the dissipation switches to the platform leg. The left side of Figure 4-19 shows the validity of the assumption that the vessel structure is rigid for smaller size columns. The curves developed for 30 millimeter and 40 millimeter columns have good agreeance for the first 1.25 m of column displacement.

This study had concluded that the resistance of jacket legs to broad side vessel collisions should always be based on the assessment of the relative strength of both structures (shared energy design) when possible. If a very large column is used, it may be possible to assume that it is rigid for the purposes of determining vessel deformation, but as the column diameter lessens, as does the validity of this assumption. Most importantly, these studies have shown that the load curves presented in the NORSOK standard are applicable as benchmark values for STOPC analysis using modern FE software.

4.4.4 Braced Members

The energy absorption within braced members in offshore platforms is largely dependent on the geometry of the overall structure being investigated. Consequently, the empirical formulas which exist for their deformation resulting from a collision event are either largely approximated or over-estimated.

The API standard of offshore design accepts the use of the following formulas for the denting of bracing members developed by Furnes and Amdahl as well as those developed by Ellinas for deformation within braced members [3, 20, 44]

Furnes equation:

$$P_d = 15M_p \left(\frac{D_T}{T}\right)^{\frac{1}{2}} \left(\frac{w_d}{R_T}\right)^{\frac{1}{2}} \quad (4.30)$$

Amdahl's equation:

$$P_d = 40F_y T^2 \left(\frac{w_d}{D_T}\right)^{\frac{1}{2}} \quad (4.31)$$

where:

P_d = Denting Force (N)

M_p = plastic moment capacity of the tube (Nmm)

F_y = yield strength of tube materia (MPa)

D_T = Diameter of the tube (mm)

R_T = Radius of the tube (mm)

T = Wall thickness (mm)

w_d = Dent Depth (mm)

Equations (4.30), and (4.31) are applicable to both vertical and horizontal members, but are limited in that they cannot account for multiple members simultaneously [20]. This creates a built-in disadvantage to the formulae as it disallows the influence of surrounding structure to be accounted for through the calculation. The critical members during a collision event will most often be those directly impacted by the colliding vessel. In the event of a collision, maximum deformation takes place at the joint of a cross brace as shown in Figure 4-20. Therefore, these formulae have limited applicability as they have been developed for single tubular members [26].

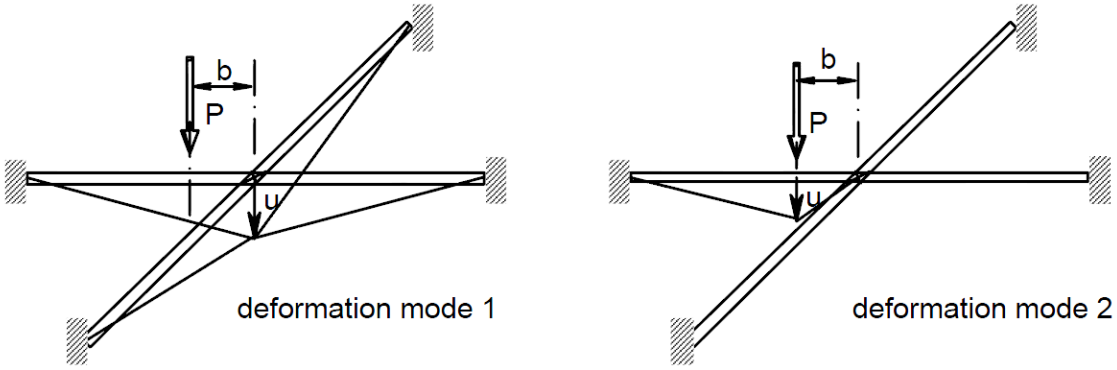

Figure 4-20: Deformation modes of cross brace subjected to point load P.
Note: P = denting force; b = eccentricity of load with respect to the joint span, u = resulting deformation for a given mode; M_p = full plastic moment of tubular member. [26]

For collision events between a ship and an offshore structure near a crossarm as shown in Figure 4-20, the HSE standard provides the formulae listed in Table 4-3 for determining the point load on a cross brace [26]:

Table 4-3: Loading on cross brace members

Case	Deformation Mode	Formula
Impact at the cross brace itself ($b = 0$)	Local (mode 1)	$P_c = \frac{16M_p}{\ell}$ (4.32)
Impact in the middle of a span $\left(b = \frac{\ell}{4}\right)$	Local (mode 1)	$P = \frac{4M_p}{\frac{\ell}{4}} = \frac{16M_p}{\ell} = P_c$ (4.33)
Impact at a distance b from the center	Local (mode 1)	$P_{u1} = \frac{2M_p}{b} + \frac{2M_p}{\frac{\ell}{2} - b}$ (4.34)
	Global (mode 2)	$P_{u2} = \frac{\frac{\ell}{2}}{\frac{\ell}{2} - b}\frac{16M_p}{\ell}$ (4.35)
Impact at a distance $b = \frac{\ell}{8}$	Global (mode 2)	$P_{u1} = P_{u2} = \frac{1664}{3\ell}$ (4.36)

Equation (4.32) through (4.36) provide loadings in accordance with the code that can then be used to determine stress, deformation, and deflection of a cross brace joint. From equations (4.32) through (4.36), the standard prescribed load governed by maximum rotation for b= ℓ/8 in the local mode is only 25% of the standard prescribed load of b=0, meaning a large increase in the impact energy absorbing capacity for b=ℓ/8. This increase will be less abrupt in physical models due to the presence of strain hardening, but should be recognized during numerical analysis [26].

4.4.5 Tubular Joints

While the deformation of a tubular member resulting from off-joint collision can generally be described by the models and equations given in sections 4.4.1 and 4.4.2, deformation within a tubular joint of intersecting members are far more complex to assess. This is largely due to the complexity of tubular joints in comparison to tubular members; while a tubular member generally has a constant cross section through the member length and behaves in a very predictable manner, tubular joints often have additional factors to consider (such as bolting details, thickness of joint, welding etc.). In addition to joint details, similar factors to evaluating braced members come into effect such as radius/thickness, eccentricity, load contribution, and angle of each member connecting to the joint. Simple formulas can be derived for a joint consisting of three in plane members where all load and member properties are known, but in the case of jacket structures a simple joint of this nature is uncommon. NORSOK presents a wide array of formulas for various joint design configurations, and investigates the different scenarios in depth in order to provide the most accurate assumption of joint reactions and design considerations [19].API standards provide a very broad minimum design capacity requirement for tubular joints which equates to 50 percent of the capacity of the incoming brace; however, within the same standard of design, the FEA method is still recommended over the traditional methods [20].

It is recommended that using FEA, the linear elastic regime of deformation be calculated using shell elements for various load cases such as axial tension, axial compression, in

plane bending and out of plane bending [8]. Of these load cases, the following should be considered throughout the analysis [26]:

i. Determine the effects of joint strength vs overall brace strength.
ii. Consider the load case that the joint is weaker than its brace.
iii. Consider the effects of the brace stubs on the structural integrity of the bracing members (as areas of the member may be weakened by bolts).

The combination of membrane forces and moments at the ends of the tubular elements determined by FEA should be checked against the empirical data of the tubular joint capacity to validate accuracy of results [8].

5. USE OF FEA FOR STOPC ASSESSMENT

5.1 INTRODUCTION

The finite element method is recommended for use in marine vessel crashworthiness due to its reliability and cost efficiency [5]. Simplified analytical approaches while helpful for the validation of FE models, require large assumptions to be frequently made with regards to the bow shape of the ship structure, the overall geometry of the offshore platform, and the influence of added mass and the fluid-structure interaction.

There are several commercial FE codes available which can accurately depict a STOPC event and process the resulting loads and deformations accordingly. Some of these FE codes include, but are not limited to: SACS, LS-DYNA, NASTRAN, ANSYS and ABAQUS. The DYNA suite of programs is particularly useful for STOPC analyses as it allows the user to specify general topography, channel configuration and environmental conditions while saving modeling and experimental time by generating multiple ship orientations and angles of collision in a batch file [4]. Finite element analysis (FEA) has a distinct advantage over analytical solutions due to the complexity and detail, which can be included in the simulation. None of the available analytical solutions can fully account for the wide array of variables present during a STOPC, and consequently they are not effective for the determination of most efficient design. Provided the mesh size and material properties of the finite element model are properly modelled, the multi-axial stress field can be considered more accurately and systematically than the comparable empirical methods, as the stresses within the structure can be very accurately depicted.

Although the finite element method is very efficient in determining the deformations and stresses present during a collision event, the allowable limits the results it achieves (such as stress and deflection, allowable simplifications, and loads used during the analysis are typically prescribed by established standards.

The complexity of the finite element simulation involves several steps from preprocessing to postprocessing and there are various methods and solutions to achieve accurate results. A process for the assessment of STOPC analysis through the use of finite element methods is as shown in Figure 5-1 [25]:

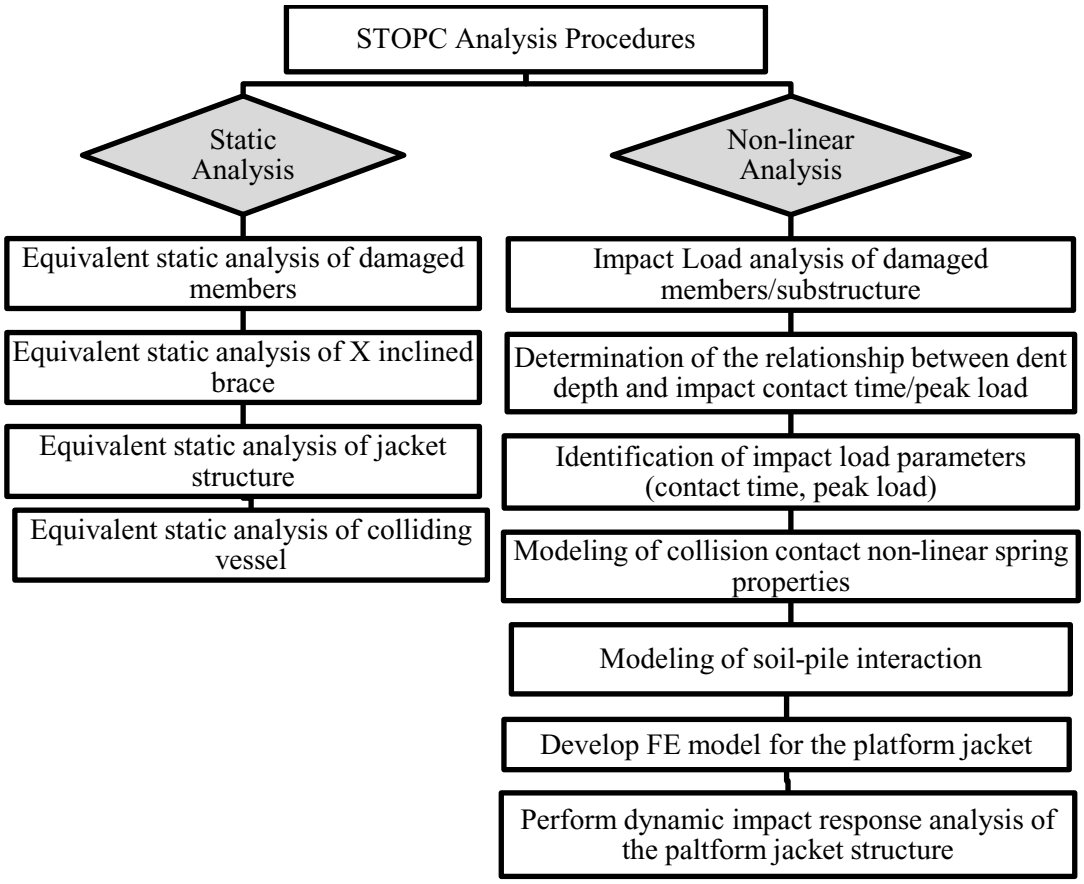

Figure 5-1: ship to platform damage analysis [25]

The procedure noted on the left side of Figure 5-1 represents the equivalent static analysis required in order to sufficiently design the structure against collision, while the procedure on the right outlines a non-linear analysis on the structure which will be discussed further in section 5.5.2. It is evident that the left and right hand side of Figure 5-1 vary largely in complexity, but that does not necessarily mean that either side is incorrect for a full scale assessment.

A balance among computational efficiency, modeling efficiency and accuracy of the simulation is necessary to achieve in order to most effectively converge on a solution without the overexertion of time, effort and resources. In all FEA, it is necessary to determine the intended purpose of the analysis before proceeding in order to determine the ideal boundary conditions, element types, and the optimal refinement of the mesh. The number of elements used should be adequately large to accurately capture the geometry and desired failure mechanisms of the colliding vessel or offshore structure, but not so large to limit computational efficiency without sacrificing quality of results [33]. The element formulations should be adequately accurate to capture the intended results of the analysis, but should not extend past the scope of the analysis for the sake of gaining nominal additional accuracy while greatly diminishing computational time (such as using solid elements in place of shells to model a ship hullform). In the sections to follow, various FE analysis parameters will be explored for the purpose of determining which grouping of features best suits a STOPC analysis.

5.2 IMPLICIT VS EXPLICIT SOLVERS

Implicit and explicit analyses are both common approaches used in numerical analysis for obtaining solutions of time dependent equations. The main difference between these two methods is the consideration given to the state of the system during any given time-step.

Standards such as NORSOK and DNV specify non-linear dynamic finite element analysis to be adequate for the assessment of collisions and collision effects, but also suggest the use of simple elastic-plastic methods with energy considerations taken into account [14, 19]. The majority of modern collision studies make use of explicit methods rather than implicit with relatively low time-steps. Both approaches will be discussed in sections 5.2.1 and 5.2.2 below.

5.2.1 Implicit Methods

Implicit methods describe numerical solutions for the determination of the state of a system by solving a differential equation involving both the current state of the system and later one. The majority of implicit methods are fundamentally derived from the Return Map Algorithm, which was developed in 1964 by Maenchen and Sacs [45], and Wilkins [46]. The Return Map Algorithm has the following fundamental steps [47]:

i. Perform a predictor step in which the entire increment of strain is used to compute trial stresses assuming elastic behavior
ii. Evaluate the yield function in terms of the trial stresses and the values of the plastic parameters obtained at the previous time increment

For the static analysis of a marine vessel or preliminary testing using equivalent dynamic loads, the implicit solver is almost always appropriate to use. Implicit methods can be used to represent the plastic deformation characteristics of steel and other granular quasi-brittle materials using multi-stage algorithms which are applicable using a variety of formulations [48]. When assessing the structural integrity of an offshore platform during a collision event, it is also possible to simplify the collision problem to a quasi-static analysis by representing the dynamic loads imposed upon the structure as equivalent static loads. A static analysis cannot, however, take residual strength of the affected members into consideration during the analysis and is consequently non-ideal for full scale collision simulation. Implicit methods also have severe limitations if the time-step it too large, particularly when applied to a collision assessment, as it does not fare well under large deformations, and is better suited when performing an analysis based on yield criteria. If the analysis of an offshore structure composed of tubular members does not take into account the cross-section reduction that occurs from local crushing, than the collision resistance will be significantly overestimated [9].

These methods use comparatively larger time-steps than explicit methods as they are conditionally stable. This is due to the creation of a system of equations for every step and the iterative nature of implicit solvers. Consequently, explicit solvers have often been the method of choice when performing STOPCs if computational time was a major factor [12, 21, 19]. Implicit analysis can also be used for a STOPC as appropriate equations have been developed for their implementation, but it may be inefficient to do so [9]. Often, simplified curves will be used in lieu of computational efficiency for implicit

analysis where the plastic region is of interest, and as computational power increases it becomes less logical to use explicit solutions.

5.2.2 Fully Explicit Solutions

Explicit methods describe numerical solutions which calculate the state of a system at a later time through solving the state of a system at the current time-step. It requires the use of smaller time-steps than implicit methods as it would only be conditionally stable, and must use a time-step heavily dependent on element size and material properties. There are fully explicit solutions which are available for the analysis of steel structures subject to plastic deformation, which include the initial strain procedure as well as the modified stiffness procedure [47]. The explicit method is non-iterative, which allows for a relatively low computational time per step [12, 21, 19]. The two main procedures that are used for explicit solutions are:

i. The Initial Strain Procedure
ii. The Modified Stiffness Procedure

The Initial Strain Procedure calculates incremental change to the state of the material with respect to time, but requires a small time-step and is computationally expensive. The Initial Strain Procedure is less accurate than other implicit alternatives, but accuracy can be improved through the use of smaller time-steps.

The Modified Stiffness Procedure is similar to the Initial Strain Procedure, but incorporates a function resembling the Newton Raphson procedure in order to calculate

the change in stiffness over time. This additional function, while allowing for a more accurate representation of the true deformation behavior of the material, increases the amount of processing power required for the analysis of a structure.

When performing FEA collision simulations, if plastic deformation is to be truly considered, then the simulation should be conducted in implicit mode. If not, then an explicit solution should be used.

5.3 MODELING SOFTWARE

5.3.1 Hypermesh

Hypermesh is a high function finite element model generation program developed by Altair Engineering for the purpose of efficient numerical model simulation. It is compatible with 24 FE software packages, some of which include LS-DYNA, NASTRAN, and ABAQUS. As the Hypermesh program has been tailored towards model generation rather than post-processing capabilities, it has very robust meshing capabilities and integrates efficient functions for the creation of high quality surfaces and mesh. A major benefit of Hypermesh is the quality of the file format conversion functions. For example, Hypermesh has the capability to convert basis mesh files from a NASTRAN .bdf or .dat file to an LS-DYNA *.k model format; it can also begin meshing geometry based formats such as *.CAD and *.IGES directly. Hypermesh offers a variety of solid meshing capabilities, such as domain specific domain methods such as SPH and CFD meshing [49].

5.3.2 LS-PREPOST

The LS-PREPOST simulator allows the user to specify general topography, channel configuration, and environmental conditions. The simulator can also be used to generate multiple ship orientation and angles of collision [4]. The main benefit of using LS-PREPOST for the modeling and simulation of the collision event is the seamless compatibility with LS-DYNA.

5.3.3 SACS

SACS is a program tailored toward offshore structure engineering developed by Engineering Dynamics and acquired by Bentley Systems in 2011 [50]. SACS is comprised of a suite of programs which provide guidance for the installation and operations, fabrication, design, and maintenance of offshore structures. It is incredibly efficient for creation of global offshore structure models due to the embedded functions focusing strictly on offshore design and load creation. The shortfall of SACS is the limited amount of studies that have been conducted using the Bentley suite of offshore structure programs due to the already established finite element analysis packages. Another disadvantage is the incompatibility of SACS file format with major model generation software, such as Hypermesh.

5.4 Analytical Software

5.4.1 Introduction

There are several commercially available FEA programs which can be used for the simulation of STOPC events. It is important to assess the code to be used prior to implementing it for the study in order to avoid forced assumptions through the analysis due to computational limitations. It is often suggested that the FEA program in question should be able to have both implicit and explicit capabilities, as well as efficient algorithms in order to converge on a solution while retaining a high degree of accuracy when assessing a fine mesh [33]. In addition, the program should either have powerful modeling capabilities, or strong compatibility with an already existent and common model file format, such as *.bdf, *.nas, or *.k. With all criteria and capabilities taken into consideration, LS-DYNA is widely acknowledged to be the most appropriate program for STOPCs [33], and accordingly will be used as the primary reference and example when explaining proper modeling and analysis techniques throughout this thesis.

5.4.2 LS-DYNA

LS-DYNA originated from the program DYNA3D developed by the Lawrence Livermore National Laboratory (LLNL) in 1976, which was capable of handling a wide range of 3D FEA problems [51]. While at the time, there were several FEA programs available, there were only a few capable of performing non-linear analysis. Originally, DYNA3D, which was an explicit solver, had a wide range of capabilities, but it was not focused on performing a wide array of problems. Instead, DYNA3D was built to create solutions to the problems at hand, and additional capabilities were added as needed. The Livermore

Software Technology Corporation (LSTC) was founded near the end of 1988, which continued the development of the program and named it LS-DYNA 3D, later shortened to LS-DYNA. This pivotal transition is apparent through several offshore structure simulations, while prior to 1990 there were very few STOPC simulations that made use of LS-DYNA. After the year 2000, it became the most prominent analysis software used for collision assessment.

While LS-DYNA has implicit analysis capabilities, its primary benefit is the robustness of its explicit solver, which allows for the free-movement of a structure without the definition of any constraints or boundary conditions. This allows for both the collision simulation and added mass from fluid-structure interaction to be easily included. This feature is beneficial for ships to offshore collisions as it allows for a much more accurate representation of the ship's motion in response to the collision without the creation of hotspot stresses incurred through the use of boundary conditions. LS-DYNA allows for specification of the initial position of each structural component, as well as an initial velocity and acceleration for each, which create simplicity in the definition of a colliding structure, as the prescription of motion to various nodal points becomes unnecessary. LS-DYNA also allows the modeling of point masses and rigid structures, which is advantageous when performing analysis using a highly simplified model. Point masses are particularly valuable for the representation of equipment on the ship structure.

The material models within LS-DYNA can be used to account for various behaviors of the material for structures involved in the collision when under dynamic loading, such as

material hardening, characteristics of stress-strain curve, and strain rate effects on yield point. It is possible within LS-DYNA to use a user-defined subroutine, which makes it ideal for the use in marine environments due to the potential large variation in temperature.

LS-DYNA has a very wide range of capabilities, such as nonlinear dynamics, rigid body dynamics, failure analysis, adaptive re-meshing, fracture mechanics and fatigue, fluid analysis (including Eularian capabilities and fluid structure analysis), smoothed particle hydrodynamics (SPH), and Fluid Structure Interaction (FSI). LS-DYNA also has a wide suite of contact algorithms allowing greater accuracy of a non-linear analysis [51]. These functionalities have made LS-DYNA the software of choice for the majority of STOPC studies performed since the 90's; some examples are:

- The University of Liege used LS-DYNA for the simulation of a collision between a ship and an offshore wind monopole [30] while the Norwegian Institute of Science and Technology used LS-DYNA to simulate collisions between marine vessels and icebergs, as well as a multitude of ship to ship collisions [22, 12, 52].

- As previously stated, Jorgen Amdahl has been involved with a multitude of STOPC studies since 1980 and has consistently published papers of great value to the STOPC field. In several of Amdahl's more recent studies, he has almost exclusively used the LS-DYNA suite of programs for the analysis of such collisions, these studies include:

i. Collision assessment of a bulbous bow impact against a semi sub platform column [12]
ii. Stern corner impact against a semi sub-platform column [12]
iii. Bulbous bow impact against a jacket leg brace [12]
iv. Beam impact against a jacket leg [12]
v. High energy ship collision with jacket legs [6]
vi. Platform vs ice-breaking supply vessel collision [11]

Overall, LS-DYNA is widely acknowledged to be a strong candidate for the simulation of collisions between marine vessels and offshore structures. The capabilities of LS-DYNA have been continuously proven to be efficient and effective when performing such analysis through the wide range of collision studies it has previously been used for. It has also been proven to be adequate for ship collisions through both comparisons to existing design standards and full scale collision experimental data [53].

5.4.3 Abaqus FEA

ABAQUS FEA (formerly ABAQUS) is a suite of software developed for finite element analysis by ABAQUS Inc. and, similarly to LS-DYNA, is heavily used in the automotive and aerospace industries [54]. Abaqus FEA has powerful contact, non-linear, implicit/explicit, and multi-body system capabilities, and while it has not been heavily used for STOPC assessments in the past, it is suitable for such an application.

5.4.4 SACS

SACS has been developed specifically for the finite element analysis of offshore structures. It gives consideration to several parameters, which would be far more difficult to account for using standard, more mainstream FEA packages. Some of SACS more unique capabilities include the setup automation of collision analysis, as well as providing some of the theory and assumptions behind the analysis techniques used within the program [55]. Non-linear pile-soil interaction is well accounted for, and the loads on offshore structures from the ocean environment are easily applied though the user interface. In addition, prominent member code checks, such as American Petroleum Institute (API), NORSOK, DNV, and British Standards, are programmed into the software package, and can be included in the input file and automatically checked once the analysis is complete.

5.4.5 Other FEA Software Packages

While the programs listed above are appropriate for collision assessment, there are several other commercially available finite element analysis software packages which can be used for a collision assessment. These options include, but are not limited to, ANSYS, NASTRAN, Sesam, Flexcom, and several more. When determining whether a software package is appropriate for STOPC assessment, the recommendations provided in section 5.4.1 should be taken into consideration (as well as all finite element analysis models and capabilities discussed within this paper).

5.4.6 Post-Processing

Most finite element programs which have analytical capabilities also have an affiliated post-processor within the suite of software provided by the parent company which allows the viewing and manipulation of results. Bentley SACS allows the results of any SACS analysis to be viewed through SACS. LS-DYNA postprocessor allows the viewing of any results generated through LS-DYNA, and most other modern FEA programs provide a means for the results to be viewed graphically provided the results have been generated using compatible software.

5.5 MATERIAL MODELING

5.5.1 Overview

The proper representation of materials is crucial during collision analysis in order to capture the response of the material within the elastoplastic region. This is the state of stress between the elastic limit of a material and ultimate strength, where material exhibits both elastic and plastic properties. It is important to consider all areas of the stress-strain curve during plastic assessment of a given structure, particularly in the plastic region and post-ultimate strength region of the curve. Often, the true stress-strain curve of the material is incorporated directly into the model to ensure proper simulation using a variety of models and methods.

There are several methods available in commercial FE programs of modeling the plastic behavior of a material. These methods have varying levels of accuracy heavily dependent on: the level of detail included in the representation of the stress-strain curve, the

mechanical behavior accounted for in the material matrix, and the failure mechanisms considered. In any collision assessment, a proper material definition is of utmost importance for proper simulation of the event as portions of the material may fail after yielding. The material definition within FEA software for linear materials generally requires density, Poisson's ratio and Young's modulus to be defined. Such a formulation is not appropriate for detailed collision simulations, as they do not consider the plastic response of the material.

The materials discussed in this section will focus on those used in conjunction with implicit modeling, as it is the more common approach to modeling steel's plasticity in a system for modern collision assessments.

5.5.2 Stress-Strain Curve

In appropriately defining a material formulation for an FE model, the stress-strain response must first be considered. A typical stress-strain curve for a steel coupon specimen is as given in Figure 5-2:

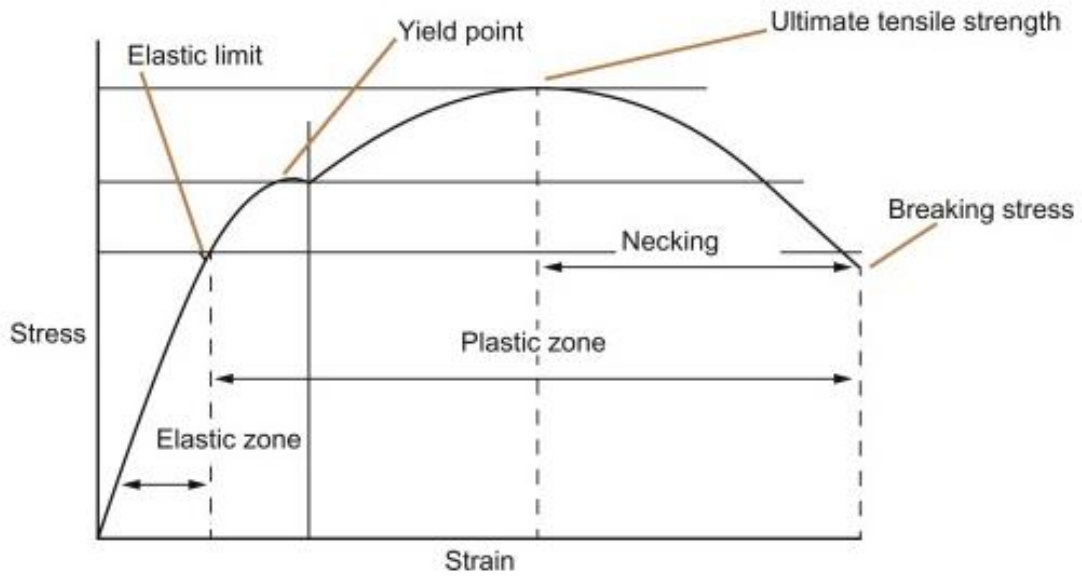

Figure 5-2: Typical stress-strain curve of isotropic material [56]

As shown in Figure 5-2, a considerable portion of the stress capacity of an isotropic material such as steel is within the elastic range, while very little strain takes place in this region. In order to construct a constitutive model for plasticity, the strain of the material is assumed to be separable into elastic and plastic regions [47]. This can be achieved using:

v. Incremental theory (typically used in an implicit analysis)

vi. Deformation theory (typically used in an explicit analysis)

As discussed in section 5.2, incremental theory involves the use of a predictor step prior to evaluating the yield function. The plastic strain will develop if and only if the elastic stress is increased beyond the yield point; the rate at which this will occur can easily be represented by incorporating a yield criterion. The simplest of these relations ignores the kinematic hardening and is independent of time or loading history [47]. This theory is largely based on the classical time-independent plasticity theory, which assumes a stress-

strain curve which is independent of the loading rate but dependent on the magnitude of loading. This ideal curve is very rarely seen in practice but allows the use of simplistic models, which can be generated at a relatively low computational cost.

At a minimum, the modeling of elastic-plastic materials should include the yield point of the material as well as the slope of the curve in the elastic perfectly plastic region; this can be achieved in its simplest form using a bilinear piecewise function defined by a graph constructed by a minimum of three points. Conversely, the most accurate material formulations would mimic precisely the stress-strain curve of the material (including local yielding achieved through mechanisms such as Lüdering) and account for plastic hardening, local yielding effects, strain rate and temperature dependency, effective plastic strain and plastic thinning.

The determination of material formulation, therefore, becomes a similar exercise to establishing mesh density, as the solution must be adequately accurate to capture the intended results of the analysis, but should not be extended to a level of detail that would consume unreasonable computational time, only producing nominal improvements to accuracy. In lieu of implementing a highly accurate stress-strain curve, corrective equations considering the relevant parameters are often implemented for FEM models to better represent the true plastic behavior of materials [57]. For the sake of computational efficiency, it is also possible to approximate material behavior using a yield plateau curve or an erosive law. An erosive law for STOPC is as given in equation (5.1) [4, 30].

$$\varepsilon_f = \varepsilon_g + \frac{\varepsilon_e T}{l_e} \quad (5.1)$$

where:

ε_f = failure strain

ε_g = uniform strain (strain associated with uniform elongation of the material)

ε_e = necking strain

T = thickness of element in consideration

l_e = element size.

While functions such as the erosive law presented in equation (5.1) are possible to program within existing FE codes, it is often unnecessary given the modern capabilities of FEA software packages. As discussed, the material definition for the steel used within both the vessel and offshore structure model should include their true stress-strain curves using the least number of points necessary. The inclusion of small local effects in the stress curve such as Lüdering is completely dependent on the intended results of the analysis. A finite element method associated to a physically based description of the behavior of steel allows the simulation of the bending process and the prediction of plastic deformation or elongation necessary to suppress the yield point elongation [58].

5.5.3 Linear vs Non-Linear Analysis

The only cases where use of linear analysis in finite element analysis is acceptable for isotropic materials are when both the following criteria are met:

i. The material will behave linearly under the applied load

ii. The geometry will behave linearly under the applied load

The first criteria addresses the need for the material considered (in most cases of vessels and offshore structures, high strength steel) to behave linearly, which is critical if a significant portion of the structure is expected to yield. Linearity allows simplicity and computational efficiency during analysis through the assumption that the stress throughout the structure would generally increase proportionally to the applied load as shown in elastic region of Figure 5-2

This assumption holds true if the purpose of the analysis is to avoid yielding and subsequent failure of the structure being analyzed, which is typical when addressing standard operational conditions and static conditions but is generally non-ideal for accidental loading. The primary use for linear analysis through a collision assessment is preliminary model simulation to ensure other parameters are working properly prior to a full simulation.

The second criterion addresses the need for a degree of rigidity when analyzing a structure if linearity is to be assumed. When the shape of a structure is assumed to change substantially through analysis, there will be a change in the stiffness matrix associated with the overall structure due to the change in the cross-section area moment of inertia of the structure. As offshore platforms are commonly constructed using hollow tubular steel members, this principle can be easily described through the assessment of a tubular member which has deformed as a result of collision.

The resistance to out of plane bending for an elliptical cross section is largely characterized by the moment of inertia of that cross section. It can be safely assumed that a tubular cross section will deform in the axis of load application (point of collision), so the failure bending mode will be dependent on the moment of inertia calculated about that axis. For an elliptical tubular cross section loaded along the y axis, the moment of inertia can be taken as:

$$I_x = \frac{\pi}{4}(r_{2,O} * r_{1,O}{}^3) - \frac{\pi}{4}(r_{2,I} * r_{1,I}{}^3) \tag{5.2}$$

where:

$r_{1,O}$ = outer section radius along the y axis

$r_{2,O}$ = outer section radius along the x axis

$r_{1,I}$ = inner section radius along the y axis

$r_{2,I}$ = inner section radius along the x axis

as shown in Figure 5-3

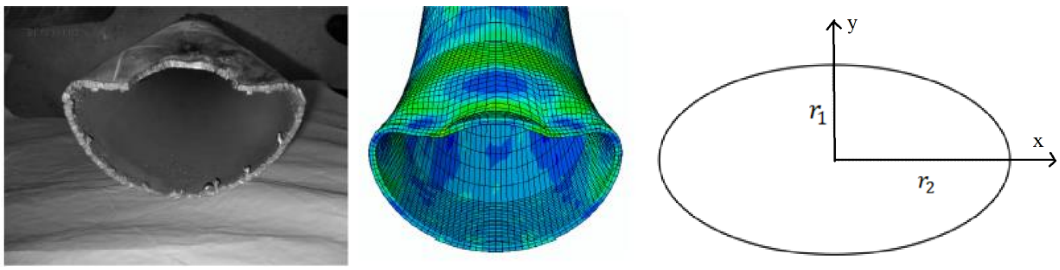

Figure 5-3: r_1 and r_2 for deformed tubular member [59]

Assuming the initially circular cross section tubular member deforms into an elliptical cross section having the same thickness and perimeter, the reduction in r_1 through denting

serves to reduce I_x exponentially. As bending stiffness is a direct function of both the elastic modulus and moment of inertia of plane area, reductions in stiffness in the direction of bending have severe effects on the overall integrity of the global structure. It is therefore necessary to perform the analysis with the change in cross sectional area of the members taken into consideration.

5.5.4 Hardening and Softening Rules

In addition to basic plasticity principles, several element formulations make use of hardening and softening rules in order to better represent the plastic region of deformation; these rules can be separated into two primary categories: isotropic hardening and kinematic hardening.

Isotropic hardening rules are based on the following principles:

i. Yield stress in tension equals yield stress in compression.
ii. As yielding progresses, the yield surfaces are uniform expansion of the original yield surface without any translation in the principal space.

Isotropic hardening uses a constant derived from rate strain rate equations to define hardening or softening of the plastic behavior of the material [47]. This derived constant (rate of plastic work) governs the size of the yield surface and is used in conjunction with the tensile stress and plastic strain functions to match the behavior of uniaxial tension or compression results. Isotropic hardening laws were first developed in 1960 [60], but are rarely used in lieu of kinematic hardening laws.

Kinematic hardening laws were introduced in the late 1950's by Prager and Ziegler [61]. This approach represents each yield surface using a linear relation allowing for the representation of detailed plastic regions.

Kinematic approaches have the advantage over Isotropic hardening in situations where components are subject to cyclic loading, as the main issues with isotropic hardening is its inability to account for the Bauschinger effect. The Bauschinger effect describes the reduction in strain hardening on the reversal of straining direction [62] and the accurate representation of long term cyclic loading.

5.5.5 Resultant Plasticity Material

Resultant plasticity material formulations are able to define elastoplastic and consider isotropic hardening while maintaining a high level of computational efficiency. This material formulation is typically used in conjunction with the Belytschko-Tsay shell or Belytschko beam element, but is not suitable for the Hughes-Liu element [63]. This type of material can also be used with Belytschko-Schwer beam, the co-triangular shell, the fully integrated shell and a variety of other element formulations [63]. While this material model is generally not as accurate as plastic kinematic materials or piecewise linear plasticity materials, it can be used in combination with high performance triangular elements in order to better simulate plasticity surfaces of yielded material [63].

5.5.6 Plastic Kinematic Material

The plastic kinematic hardening material model is a strain rate dependent elastic-plastic formulation and is suitable for modeling isotropic and kinematic hardening plasticity [64]. This material formulation is available within the majority of modern FEA programs. Plastic kinematic material formulations are ideal for simulations investigating the global behavior of a structure, but are unsuitable for the modeling of local yielding effects. This material is typically applicable to both beam and shell elements, which allows for simplicity in the generation of global structural models. It is most efficient to model all materials outside the collision region as linear elastic material, as the plastic region of the stress strain curve will not be applicable. Material within the collision region should be modelled as plastic kinematic material [63]. This is because the material outside of the high stress impact region does not reach yield stress so it will not encounter the plastic region of the stress-strain curve.

5.5.7 Piecewise Linear Plasticity Material

The use of a piecewise linear plasticity material is available within most FE programs and allows the user to define an arbitrary stress-strain curve and arbitrary strain-rate dependency. This material model is typically applicable to all forms of elements and defines the stress-strain curve using tabulated or graphical data which allows local yielding effects to be taken into consideration. The location and magnitude of any local effects would have to be well understood and documented for the material in question to implement the effects directly using the stress-strain curve. This may prove to be

unnecessary for a collision event, but should be considered as a contributing effect when comparing numerical data with measured results.

A downfall of piecewise linear plasticity models is its computational inefficiency if the curve is described by a high number of segments [63]. This material model has seen more use in recent years, and has recently been used extensively for the prediction of material failure during collisions within the automobile industry [65, 64]. While this type of material formulation requires a higher amount of computational time, it often saves time in model generation as it requires little validation for the material model development [64].

5.5.8 Material Formulations

Most FEA programs provide a wealth of solutions to material modeling with a great deal of variance in accuracy depending on the method of the analysis. LS-DYNA and ABAQUS in particular can be used to account for various behaviors of steel under dynamic loading. For simplicity purposes, only LS-DYNA material formulations will be discussed.

Within LS-DYNA, the most efficient model for modeling non-linear behavior of materials is MAT_003, which is suited to model isotropic and kinematic hardening plasticity with the option of including strain rate effects [66]. MAT_003 it is applicable to beam, shell and solid elements which increases both computational and modeling efficiency.

Several simulations using LS-DYNA have been performed assessing the collision between vessels or vessels and offshore structures, and a high percentage of these studies make use of LS-DYNA MAT_028, which allows for the definition of an elasto-plastic material. MAT_028 is available for use with the Belytschko-Tsay shell, but for such elements, isotropic hardening is only approximately modelled. For the simulation of collision of a drop hammer on steel plating, the Norwegian Public Roads Administration had used LS-DYNA MAT_123, which allowed them to define an arbitrary stress versus strain curve and strain rate dependency [66, 67, 68]. It should be noted that within collision studies, MAT_024 is also often used, which takes into account strain hardening as well as a piecewise representation of the material stress-strain curve but lacks the enhanced failure criteria available within MAT_123 [66].

It is recommended that outside the region of interest, a linear elastic material (MAT_001) or a low cost plastic kinematic material (MAT_003) be used for the representation of all steel structures represented as a non-rigid material. The implementation of more complex material models, which take the entire stress-strain curve, is computationally inefficient for areas which will remain within the elastic region. In areas where the material is expected to yield, the material should encompass the entire stress-strain curve of the material to take strain hardening effects into consideration. The use of MAT_028 or MAT_123 will allow a very accurate representation of the collision event, provided a reasonable time-step is used.

For the purpose of reducing total analysis time, it may be advantageous to first perform the analysis using a material with a low computational cost and large time-step in order to determine correctness of the model, and where high stress regions occur before making further simplifications. A more detailed model could then be performed using a smaller time-step and a more accurate material in order to achieve final results.

5.5.9 Conclusion and Recommendations

Plastic deformation is a mechanism which should be considered in all modern collision assessments as the use of plastic design methods rather than limit states greatly reduces the amount of steel required for the structure. Currently, several design standards use parameters such as the yield tensile ratio and the strain hardening exponent to describe the plastic behavior of materials, but numerical models have the capability of describing this behavior with far greater detail and accuracy and can take local deformation mechanisms into consideration.

One of the major advantages of numerical modeling over rule-based design is the consideration of local effects through iterative calculations and inclusion of the entire stress-strain curve in the model. When developing these models, it is best to use an implicit non-linear approach using the actual material's stress-strain curve while maintaining minimal curve points in order to better computational efficiency. The stress-strain curve of the material used should be accurately determined as various formulations of steel common in marine applications (AH36, DH36, Grade A, Grade B) often have slightly different curves from one another.

5.6 1D Element Formulation

The effect of the vessel-platform interaction on the distribution of damage is ideally studied through modeling both structures involved using nonlinear shell finite elements [22]. Typically, when modeling marine vessels, it is acceptable to use shell elements to represent all the major structural components such as decks, hullform, girders and bulkheads. Outside of the region of interest where the mesh is coarse, stiffeners and beams are often represented by 1D beam elements as opposed to plate elements, so to attain computational efficiency. Within the area of interest, where the mesh has been refined, beams and stiffeners are typically modelled using 2D elements in order to capture the stress distribution and deformation of the cross section.

In a global analysis, 1D elements can also be used to represent the offshore structure, but local denting, accurate strain dissipation, and reduction of bending resistance could not be taken into account. Through review of several STOPC simulations, it is gathered that the modeling of all major structural components within both the ship and offshore platform should be done using thin shell elements to represent plating and 1D elements to represent stiffener except for the region of interest. This is valid as there are unlikely to be deformation effects requiring consideration outside the region of interest. These 1D elements should be modelled with proper offsets and cross section properties if a high degree of accuracy is desired, and the inclusion of these details is a necessity when adaptive meshing algorithms are used. It is, however, common practice to use general sections throughout the model, provided they are an adequate distance away from the

collision region. Within the region of interest, the modeling of all minor and major structural components as shell structure is recommended.

5.7 2D Element Formulations

5.7.1 Overview

The selection of a 2D element formulation for a collision analysis is highly important and dependent on the software being used, the level of refinement one plans to adopt through the analysis, the objectives of the analysis, the quality of the material model and many other factors. Each shell element formulation has its advantages and disadvantages, which are to be considered during the selection process due to their large influence on result accuracy and computational efficiency. Some specific shell elements of LS-DYNA will be discussed in the following sub-sections.

5.7.2 Hughes-Liu Shell Formulation (ELFORM 1)

Hughes-Liu Shell formulation is based on degenerated continuum element formulation and bi-nodal interpolation and is consequently effective when large deformations are expected due to its accurate treatment of warped configurations. Similar to Belytschko-Tsay, one-point integration and hourglass control are used. The Hughes-Liu Shell formulation does not see as much use as Belytschko –Tsay element due to its computational cost, which increases dramatically during a non-linear analysis. While its use is currently uncommon for STOPC simulation, it should be taken into consideration through future studies when its computational time may not be an issue. LS-DYNA has a number of variations of the Hughes-Liu shell formulation (ELFORM 1, 11, 6, 7), but

ELFORM 1 is one of the most efficient of these and is recommended for use for collision analysis.

5.7.3 Belytschko-Lin-Tsay Shell Formulation (ELFORM 2)

The Belytschko-Lin-Tsay shell formulation considers 6 degrees of freedom per node, and uses single point integration with hourglass control. It is often the default element formulation of FEA software packages, and is based on the Reissner-Mindlin kinematic solution [69]. This element uses bi-linear nodal interpolation for efficiency reasons, and is not intended for use in coarse models due to potential warpage issues [69]. The Belytschko-Lin-Tsay shell element is also available in LS-DYNA and ABAQUS with five degrees of freedom in the local coordinate system. yielding six degrees of freedom globally. They have been used frequently throughout STOPCs, particularly in the works of Amdahl [22, 6, 11, 10]. Similar elements available within LS-DYNA include Belytschko-Wong-Chiang formulation (ELFORM 6), which overcomes shortcomings in warped configuration area, and Belytschko-Leviathan shell formulation (ELFORM 8), which uses physical hourglass control rather than user defined hourglass control parameters [69].

5.7.4 BCIZ triangular shell formulation (ELFORM 3)

The BCIZ triangular shell (or, Marchertas-Belytschko triangular shell element) was first developed in 1965 for the purposes of incorporating a function into triangular shell formulation which allows for both constant strain and meets constant curvature criteria of CST's [70]. Within the LS-DYNA manual, while ELFORM 3 is referred to as a BCIZ

triangular shell, it is based on the Marchertas-Belytschko shell element developed in 1974 and was the first triangular shell implemented in DYNA3D [63]. The Marchertas-Belytschko triangular shell element considers linear displacements and can treat large rotations through integrated discretized equations of motion [71]. This is performed using a central difference formula between element nodes. Within LS-DYNA, the use of this formulation is limited to triangular elements. The Marchertas-Belytschko shell requires 1417 mathematical operations which is more than twice as inefficient as the C^0 element, and its use is expected to decrease among the LS-DYNA user community due to this inefficiency [63]. In the context of collision assessments, there is not a clear advantage of using Marchertas-Belytschko formulation of the Hughes-Liu shell formulation, as if the mesh in the region of interest is of sufficient accuracy, then the use of triangular elements can be avoided altogether.

5.7.5 Co-rotational C^0, triangular shell (ELFORM 4)

A co-rotational finite element has the ability to separate the rigid body motion from the deformational motion, which makes it superior to other methods in the analysis of large displacement problems. The C^0 shell element is a computationally efficient triangular element complimentary to the Belytschko-Lin-Tsay element quadrilateral shell formulation [63]. This element requires 649 mathematical operations, while the Belytschko Lin Tsay quadrilateral shell element requires 725. This element has one point integrated triangular element formulation, and has no forms allowing hourglass control. Standard linear nodal interpolation is used to define angular and midsurface velocity as well as the element coordinates. This element formulation is limited to triangular

elements, but would not be a poor choice for collision assessment given its simplicity and computational efficiency.

5.7.6 Belytschko-Tsay Membrane (ELFORM 5)

The Belytschko Lin Tsay element formulation has a very efficient membrane element formulation, but as it cannot transfer bending moments, it is completely inapplicable to ship hulls and offshore structure modeling in the collision area [63]. Therefore, the Belytschko-Tsay membrane element formulation should not be considered for collision assessment.

5.7.7 S/R Hughes-Liu (ELFORM 6)

Similar to ELFORM 1: Hughes Liu Shell formation, the S/R Hughes-Liu element formulation is based on 5 degrees of freedom locally as well as 6 globally and makes use of bi-linear nodal interpolation. The primary difference between the Hughes Liu element used in ELFORM 6/7 and that used in ELFORM 1 is the presence of selective reduced integration to avoid most hourglass modes [69]. Selective reduced integration works to reduce issues arising from the zero energy modes, which often occur in regions where boundary conditions are applied or large point loads have been applied. As a result of this additional step, nearly four times as much data must be stored. The major benefit of selectively reduced integration is the ability to both reduce hourglassing, and prevent in plane shear locking. As in STOPC analysis, the collision load is typically applied to the vessel through contact algorithms and it is consequently unnecessary to implement this costly element formulation. The use of S/R Hughes-Liu elements (ELFORM 6) over

Hughes-Liu shell formulation (ELFORM 1) for STOPCs increases the run time significantly, but may assist in the prevention of several hourglassing modes..

5.7.8 S/R co-rotational Hughes-Liu (ELFORM 7)

The S/R co-rotational Hughes-Liu element (ELFORM 7) is similar to the S/R Hughes-Liu element (ELFORM 6) but uses a co-rotational system and reduces the total number of operations by a factor of 2 [63]. This is achieved through the following simplifications within the element formulation:

i. Strain rates are not centered
ii. Stresses are stored in the local shell system following the Belytschko-Tsay shell
iii. Jaumann rate rotation is not performed

The co-rotational system implemented within ELFORM 7 causes deformation and rigid body translation of an element to be more easily separated, which provides benefit when large deformations are expected. Although the S/R co-rotational Hughes-Liu formulation is more efficient than the S/R Hughes Liu formulation, it does not typically see use as commonly as fully integrated or single point integrated elements in STOPC analysis. If the user must make use of selectively reduced integration Hughes Liu elements due to excessive zero energy modes occurring within the model, it is recommended that ELFORM 7 be used over ELFORM 6 due to its computational efficiency and its comparatively good treatment of large deformations.

5.7.9 Belytschko-Leviathan Shell (ELFORM 8)

The Belytschko-Leviathan shell formulation is similar to the Belytschko-Wong-Chiang formulation with one-point integration. The main difference between the Belytschko-Leviathan shell and the Belytschko-Wong-Chiang formulation is that the former does not require hourglass control parameters to be set by the user. The Belytschko-Leviathan shell formulation makes use of a 7-mode projection matrix for eliminating zero energy modes, 3 rigid body and 4 drilling [63]. This is to say that the BL (Belytschko-Leviathan) shell formulation has built in hourglass controls.

5.7.10 Fully Integrated Belytschko-Tsay membrane (ELFORM 9)

The fully integrated Belytschko-Tsay membrane element has been developed using the Belytschko-Lin-Tsay shell element as an improvement on ELFORM 5 (Belytschko-Tsay membrane element). This formulation uses a 2x2 quadrature instead of a one point quadrature integration and consequently handles wrapped configurations quite well. Similar to ELFORM 5, it is incapable of transferring moment and therefore inapplicable to STOPC simulations.

5.7.11 Belytschko-Wong-Chiang Formation (ELFORM 10)

The Belytschko-Tsay element is based on a perfectly flat geometry assumption and does not consider warpage ratios when considering element results. Consequently, Belytschko Tsay shell elements may produce inaccurate results in determining stresses and displacements in heavily deformed elements. The improvements made by Belytschko, Wong, and Chiang solve the deformation problem by interpolating the element geometry

over the entire surface of the shell. The Belytschko-Wong-Chiang formation is recommended as a candidate for STOPCs, as the contact regions between the vessel and offshore structure would be subject to very large deformations and potentially high warpage ratios, regardless of the mesh refinement. The cost of using the improvements included in ELFORM 10 are not substantially more computationally expensive than the Belytschko-Lin-Tsay shells (ELFORM 2). These improvements do however produce better results for in-plane shear deformations. This is shown through the LS-DYNA theory manual using a twisted beam problem, as provided in Figure 5-4:

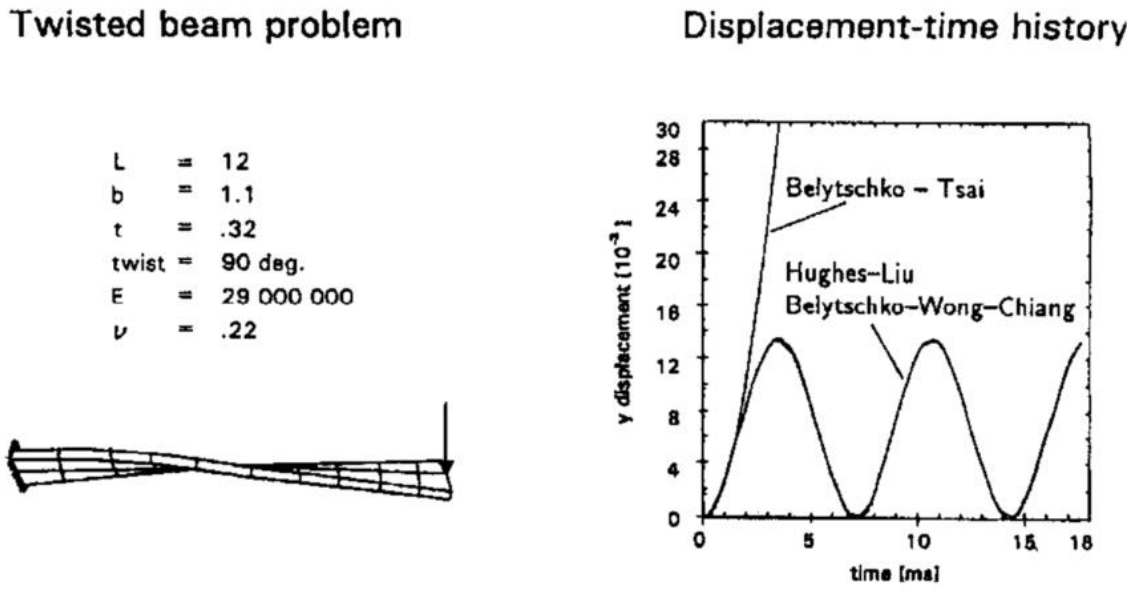

Figure 5-4: Twisted beam problem displaying overestimation of displacement by Belytschko-Lin-Tsay shell elements [63]

5.7.12 Fast (co-rotational) Hughes-Liu (ELFORM 11)

The co-rotational Hughes-Liu formulation is the same as the S/R Hughes-Liu formulation except it uses a co-rotational system. The fast- co-rotational Hughes-Liu element

formulation is very useful for large deformation problems, and are thus recommended for STOPC analysis.

5.7.13 Plane stress and strain formulations (ELFORM 12 and 13)

Plane stress element formulation (ELFORM 12) is not applicable to STOPCs as it operates under the assumption of zero stress in the Z direction. This limits most analysis to strictly 2D or slightly curved as the inability to transfer shear stresses limits applicability to complex structures undergoing collision. The plane strain element formulations (ELFORM 13) is also inapplicable to STOPCs as it operates under the assumption that there is zero strain in the z direction. Plane strain elements are more often applied to longitudinally prismatic components

5.7.14 Axisymmetric solid formulations (ELFORM 14 AND 15)

ELFORM 14 represents axisymmetric solid formulation using weighted area while ELFORM 15 represents axisymmetric solid formulation using weighted volume. Both formulations are inapplicable to STOPCs as they operate under the assumption of symmetry about the longitudinal axis

5.7.15 Fully Integrated Shell with EAS Formulation (ELFORM 16)

Fully integrated shell formulations are extremely costly from a computational standpoint, but they offer a high level of accuracy and are recommended for implicit analysis as they avoid in plane hourglassing. While the element itself is more computationally costly than the Hughes-Liu Shell and Belytschko-Lin-Tsay shell, it would allow the user to specify

an overall lower number of time-steps if using implicit analysis rather than explicit. The fully integrated shell formulation (ELFORM 16) is based on the Resissner-Mindlin kinematic assumption and performs 2x2 integration within the shell mid-plane [69]. Fully integrated shells use hourglass type 8 to add warping stiffness, which may serve to improve convergence, and is the least expensive of the 2x2 integrated elements. This element would be useful if a representative static or quasi-static analysis was to be performed when simulating the effects of the collision rather than a dynamic collision analysis, and is recommended for a full scale STOPC simulations despite being 2-3 times more CPU-intensive than the Belytschko-Lin-Tsay shell.

5.7.16 Fully integrated DKT triangular shell element (ELFORM 17)

The fully integrated DKT triangular shell element has three in plane integration points and therefore, has better bending behavior than the C^0. This element formulation is based on the discrete Kirchhoff theory, which operates under the assumption that the thickness of the plate does not change during a deformation. The Fully Integrated DKY triangular shell element is the most robust triangular shell element formulation available within LS-DYNA, and could be considered for STOPC analysis. This formulation would be particularly useful if the colliding structure was primarily CST elements.

5.7.17 Fully integrated linear solutions (ELFORM 18, 20, 21)

A discrete Kirchhoff linear triangular and quadrilateral shell element is available as a type 18 shell, while type 20 and 21 shells provide fully integrated linear strain and linear stress solutions, respectively. which is ideally used for extracting normal modes and for

static analysis [63]. For this reason, element types 18 through 21 are inapplicable to STOPC analysis and should not be considered as viable options for a contact collision analysis.

5.7.18 8-noded Shell Formulation (ELFORM 23)

This is the only 8 noded quadratic quadrilateral shell element formulation available in LS-DYNA. Higher order shell formulations can have several advantages over 4 noded quadrilateral elements. This is primarily due the higher level of accuracy 8 noded elements have over 4 noded elements through the incorporation of quadratic shape functions. This allows 8 noded interpolation to be performed, which provides a more accurate representation of element deformations and stresses than bi-linear nodal interpolation. In addition, it prevents hour-glassing under most circumstances. However, the use of this element is not compatible with contact algorithms used in this study.

5.7.19 Thickness Stretch Solutions (ELFORM 25, 26, 27)

Thickness stretch can be of considerable importance when approaching problems involving thickness strains in nonlinear shell applications. Within LS-DYNA, these are based on the Reissner-Mindlin kinematic assumption that 5 degrees of freedom in a local coordinate system yield 6 degrees of freedom globally. Element formulations allowing thickness stretch within LS-DYNA require a 3D constitutive model, use bi-linear nodal interpolation, and prevent the Poisson Locking (also known as “Volumetric Locking”) in bending modes of deformation.

If thickness stretch is to be considered through an analysis and computational efficiency is of importance, then it would be logical to use the Belytschko-Tsay formulation (ELFORM 25) due to its proven efficiency. These elements are not recommended for STOPC analysis due to the large sacrifice in computational efficiency for the marginal gain of significantly better deformation results of yielded sections and would be better suited for simulations focusing on local areas of deformation. As the focus of STOPCs are primarily the overall energy dissipation and energy transfer of the global structures, element formulations 25-27 would be of little use.

5.7.20 Summary of LS-DYNA Shell Elements [63]

ELFORM	Formulation	Comment
1	Hughes-Liu (HL) shell	• One-point in plane integration • Five through-thickness integration points • Bi-linear nodal interpolation • Good treatment of warped configurations • Hourglass control • Computationally efficient HL formulation • Computationally costly when compared to Belytschko formulation
2	Belytschko-Lin-Tsay shell	• One-point in plane integration • Five through-thickness integration points • Bi-linear nodal interpolation • Based on the Reissner-Mindlin kinematic assumptions • Most efficient element formulation • Hourglass control • Warping stiffness • Not recommended for very coarse mesh models
3	BCIZ triangular shell	• Three point in plane integration • Five through-thickness integration points • Bi-linear nodal interpolation • Co-rotational • Kirchhoff assumptions • Intended for use in conjunction with 4 noded shell elements • Roughly twice as costly as C^0 triangular shell • Not recommended for use in STOPCs over ELFORM 4 if selected, but still applicable. • Limited to triangular shell elements, unlikely to be used for STOPCs

4	Co-rotational C^0, triangular shell	• One-point in plane integration • Five through-thickness integration points • Bi-linear nodal interpolation • Co-rotational • Triangular, so very efficient for auto-meshing • Computationally efficient when compared to other triangular formulations (largely due to single point in-plane integration) • Limited to triangular shell elements, unlikely to be used for STOPCs
5	Belytschko-Tsay membrane	• One-point in plane integration • One through thickness integration point • Bi-linear nodal interpolation • For modeling fabrics. Not applicable to STOPCs
6	S/R Hughes-Liu shell	• Selective reduced integration (resulting in four in plane integration points) • Five through-thickness integration points • Bi-linear nodal interpolation • Avoids in plane hourglass modes • Bending induced hourglass modes are still possible • Computationally more costly than ELFORM 1
7	S/R co-rotational Hughes-Liu shell	• Similar to ELFORM 6, but uses a co-rotational system • More efficient than ELFORM 6 due to several simplifications
8	Belytschko-Leviathan shell	• Similar to ELFORM 10, but uses physical hourglass control. • No hourglass control parameters need to be set by user
9	Fully integrated Belytschko-Tsay membrane	• 2x2 in plane integration • One point through thickness integration • Bi-linear nodal interpolation • For modeling fabrics. Not applicable to STOPCs
10	Belytschko-Wong-Chiang shell	• Same as ELFORM 2, but avoids the shortcomings in warped configuration area through consideration of non-planar geometry

		• Costs 10% more than ELFORM 2
16	Fully integrated shell with EAS-formulation	• 2x2 in plane integration • Five point through thickness integration • Bi-linear nodal interpolation • Based on the Resissner-Mindlin kinematic assumptions • Shear correction using Bathe-Dvorkin eliminates W-mode hourglassing • Least expensive of 2x2 integrated elements • 2-3 times more expensive than Belytschko-Tsay shell • Recommended for implicit simulations
17	Fully integrated DKT, triangular shell	• Three point in plane integration points • Five point through thickness integration • Bi-linear nodal interpolation • Not recommended for primary use throughout structure as CST's are non-ideal for stress results. Applicable to STOPCs
18	Fully integrated linear DK quadrilateral/triangular shell	• For linear implicit analysis. • Intended for static analysis • Not applicable to STOPCs
20	Fully integrated linear assumed strain C0 shell	• For linear implicit analysis • Intended for static analysis • Not applicable to STOPCs
21	Fully integrated linear assumed strain C0 shell	• For linear implicit analysis. • Intended for static analysis • Not applicable to STOPCs
23	8-node quadratic quadrilateral shell	• Quadratic shape functions • Better intra-element interpolation
25	Belytschko-Tsay shell with thickness stretch	• One-point in plane integration • Five point through thickness integration

		• Bi-linear nodal interpolation • Co-rotational Lagrangean formulation • Based on the Reissner-Mindlin kinematic assumption • Thickness stretch requires 3d constitutive model • Hourglass control
26	Fully integrated shell (EAS formulation) with thickness stretch	• Four-point in plane integration • Five point through thickness integration • Based on the Reissner-Mindlin kinematic assumption • 2x2 integration • Bathe-Dvorkin transverse shear correction • Additional feature of linear strain through thickness to avoid “Poisson Locking” • Similar to ELFORM 16, but with added thickness stretch
27	C0 shell with thickness stretch	• Same as co-rotational triangular shell • Only applies to triangular shells

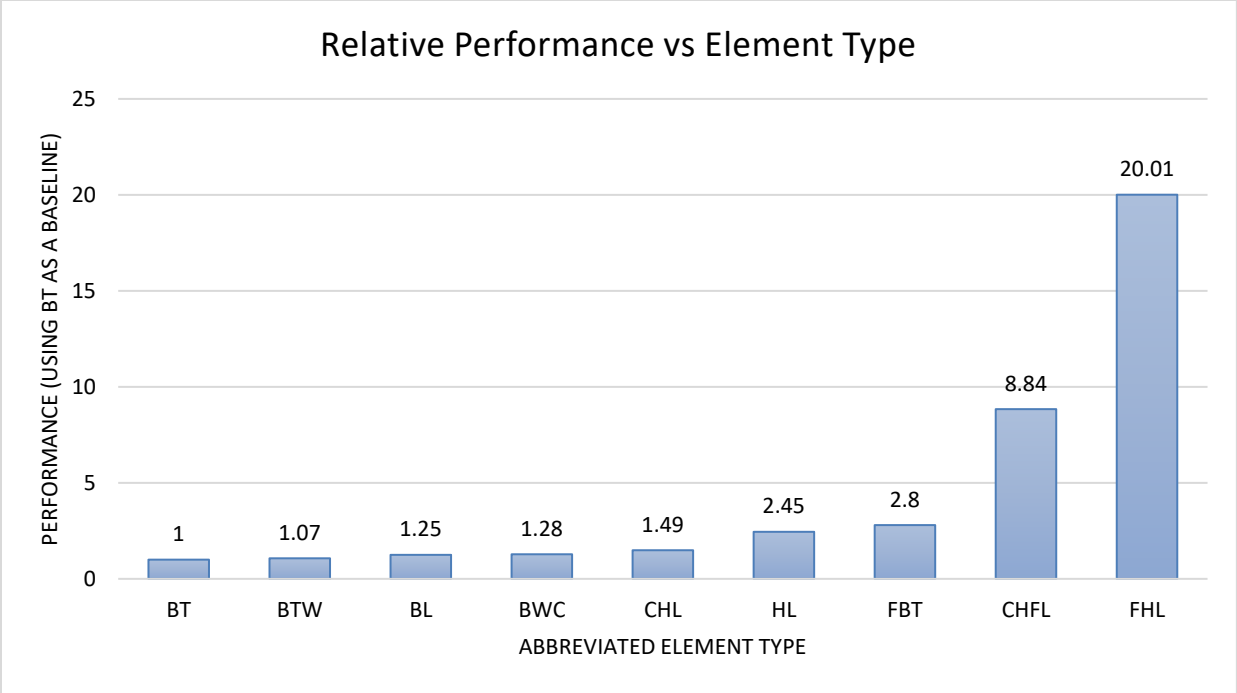

Figure 5-5: Relative cost of four noded shells available in LS-DYNA relative to Belytschko-Tsay shell [63]

The following abbreviations are used in Figure 5-5

BT = Belytschko – Tsay Shell (ELFORM 2)

BTW=Belytschko Tsay Shell with warping stiffness taken from Belytschko Wong Chiang shell (ELFORM 2, but with option 1 selected within BWC card)

BL = Belytschko Leviathan shell (ELFORM 8)

BWC = Belytschko Wong Chiang shell (ELFORM 10)

CHL = Corotational Hughes Liu Shell (ELFORM 7)

HL = Hughes Liu Shell (ELFORM 1)

FBT = Fully integrated Belytschko – Tsay Membrane (ELFORM 9)

CFHL = Corotational Fully integrated Hughes Liu shell

FHL = Fully integrated Hughes Liu shell (ELFORM 16)

5.8 3D Element Formulation

In general, solid elements are typically not used for the simulation of a STOPC. Solid elements can, however, be used to represent large base plating beneath major equipment, or the equipment itself if a uniform mass distribution is desired. If solid elements are to be used for thick base plating structure or in engine locations, it is recommended a simple four node tetrahedron be used [72].

In addition, it is recommended that LS-DYNA solid ELFORM 1 be used as it assumes a constant stress throughout the solid element for computational efficiency if solid components are not the focus of the analysis [73]. As shell formulation is rightfully selected as the element of choice in the collision area for STOPC, detailed modeling techniques and theory of solid material/element formulations will not be discussed in this document.

Solid elements are not typically used for STOPC analysis due to both the amount of computational power required for analyzing solid element structure vs equivalent shell element structure, and the inaccuracies they often provide when used to analyze thin shells. Through thickness stiffness of thin shells are comparatively much greater than their flexural stiffness; consequently, solid elements often experience numerical issues and produce and inaccurate results.

5.9 Meshing and Refinement

5.9.1 General Refinement

The number of elements used within any FE model is highly dependent on the discretion and experience of the individual performing the analysis, but should be minimized while maintaining the required accuracy of results in order to reduce computational time wherever possible. The results achieved from the analysis are largely dependent on the accuracy of the model, and the refinement required are thus denoted by what results the model is intended to achieve. Most STOPC assessments seek to determine the global kinetic energy transfer among the structures involved in a collision event, which allows most of the structure to be modelled with coarse mesh. Studies concerned with local deformation or highly accurate kinetic energy transfer simulations during a collision event should use a high level of refinement in all areas that are expected to yield.

The location of collision is consistently refined during STOPC studies, as the failure modes in this region (such as crushing and indentation), largely influence the global failure modes of the structure. As the distribution of kinetic energy dissipated within the offshore platform and marine vessel during a STOPC are largely dependent on their rigidity and crushing response, it is crucial to ensure the refinement in these regions is adequate. Collision studies have refined regions near the collision area as coarse as five times the unrefined area, to as fine as a mesh with element size approaching the thickness of the plating (note: using the latter method will denote greater refinement levels for broadside collision than bow collision due to plate thicknesses) [74, 12].

Tubular joints within offshore structures are often a point of failure due to mechanisms such as punching when a proportionally small bracing member connects to a large chord member, or under dynamic behaviors, during a collision event. As a result, these joints are often a point of interest during collision events and are refined if high punching stresses are anticipated. Similar recommendations have been used for the assessment of cross-brace joints, where punching failure is less of a concern at the point of collision and all other connection locations [42]. In a study performed by Qu et al. [59], they made use of the finite element method to simulate the dynamic behavior of a steel tubular T-joint sing ABAQUS 6.10, as shown in Figure 5-6.

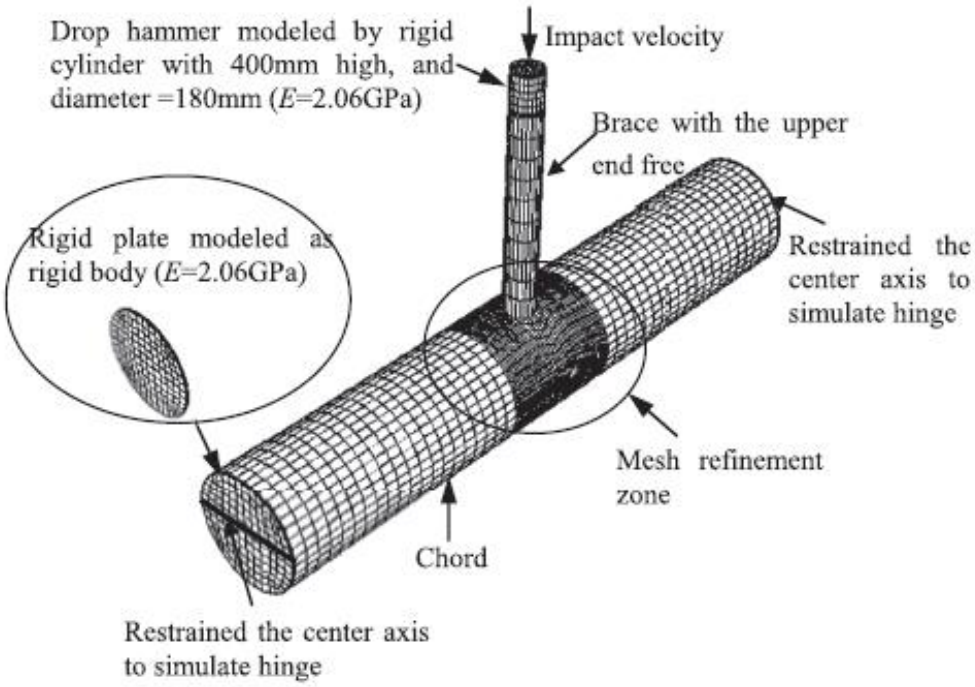

Figure 5-6: FEA model of T-joint under impact loading (reproduced from [59]).

It should be noted that the "rigid plate" in this case was not in fact modelled rigidly as it had a modulus of elasticity of 2.06 GPa. (It is noted that a modulus of elasticity of 2.06

GPa is in fact incredibly low, and is likely a typo by the author. The elasticity of the rigid material is far more likely to be 2.6TPa). To make the plate truly rigid, it would be advantageous to use a rigid material formulation or a significantly higher modulus of elasticity. A fictitious cross section was modelled within each member in order to truncate the actual members and apply the boundary conditions. The results of this study are shown in Figure 5-7 :

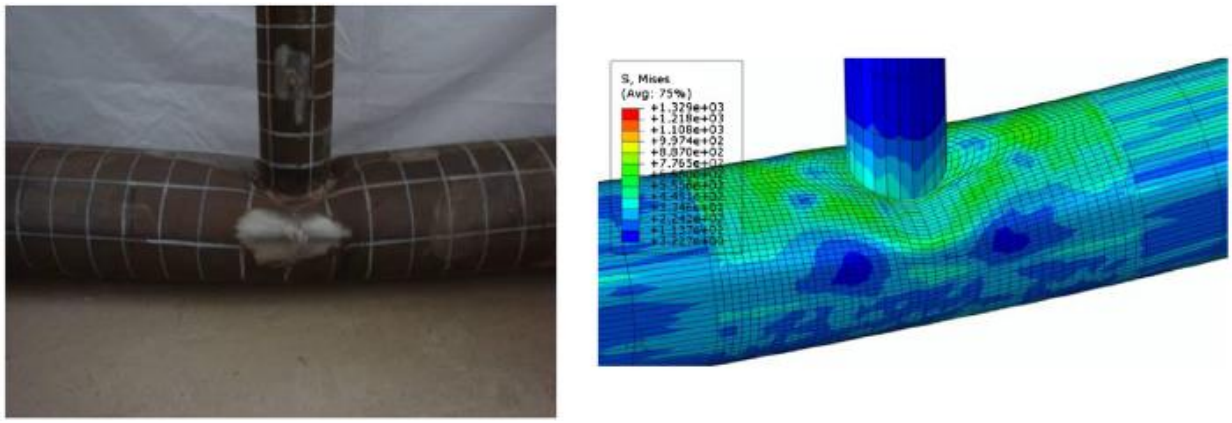

Figure 5-7: Comparison of the test and numerical results of brace punching stresses on a chord member [59]

The chord has been refined at the connection point in order to accurately determine the deformation in that area. The brace has been modelled with high aspect ratio elements in order to save computational power, as the element length in the plane of the load application (which in this case is strictly axial) does not have a significant impact on the quality of results achieved due to the coplanar property of element rows. During this study, experiments were conducted in order to compare the results with those generated numerically, and time history curves of strain were subsequently generated. A comparison of the results is as shown in Figure 5-8.

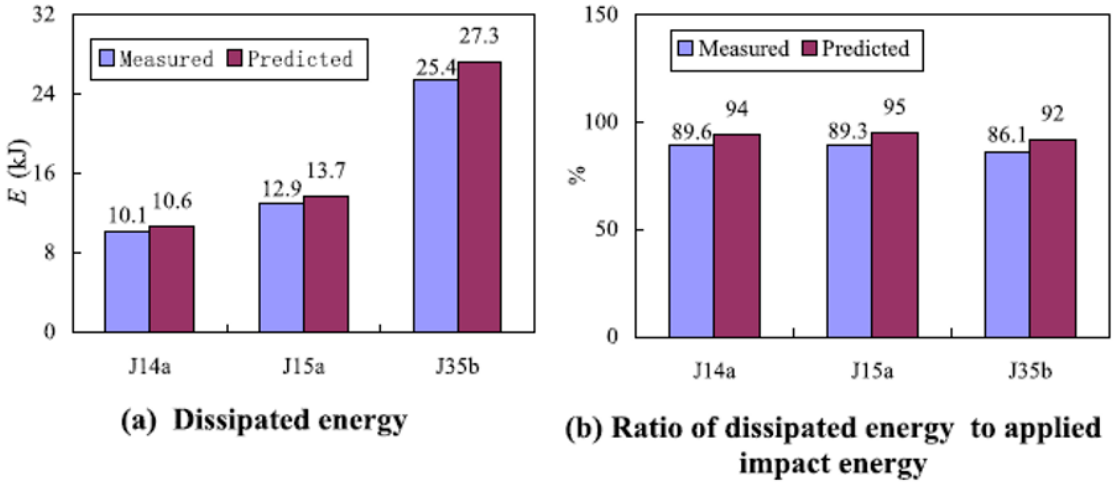

Figure 5-8: Comparison of experimentally determined dissipated energy vs predicted dissipated energy

Overall, this experiment provides a useful comparison in the similarity and margins of error in the simulated energy dissipation results. The authors had stated a major advantage of using FEA software to experimental results is the amplified deformation plots(true deformation with a scaling factor applied for visualization) available in the post processing programs, which allow for a comprehensive animation outlining the mode of failure [59]. In cases where the primary purpose of the study is to determine the local deformation effects of the tubular members, the tubular members with the greatest local deformation can be modelled using high density shell elements, while the structure outside of the region of interest can be modelled using pipe elements [42].

During collisions, areas which will dissipate the largest portion of energy, and therefore undergo the highest deformation, will require the greatest refinement. Figure 5-9 shows an FEA model of a hull simulated to undergo large deformation due to a collision event:

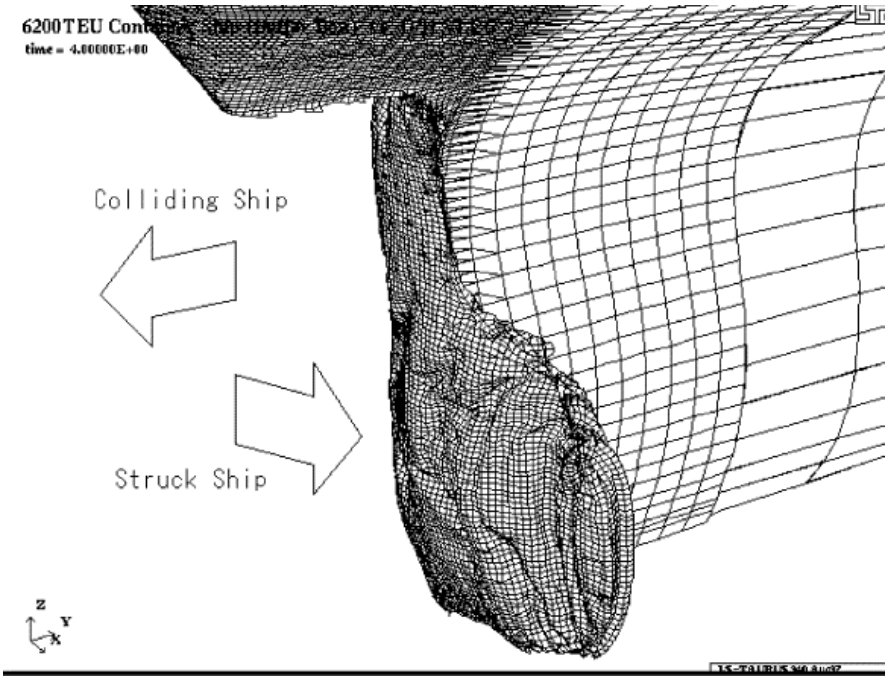

Figure 5-9: Bulb deformation of colliding vessel striking another vessel [5]

Figure 5-9 shows the bulb of a marine vessel subjected to a high level of damage from an accidental collision with another vessel as shown by the out of plane deformation of the bulb [5]. This bulb and bow of the colliding vessel have been modelled with very high levels of refinement in order to accurately capture this deformation, with the mesh gradually reducing in both size and quality outside of the area of interest.

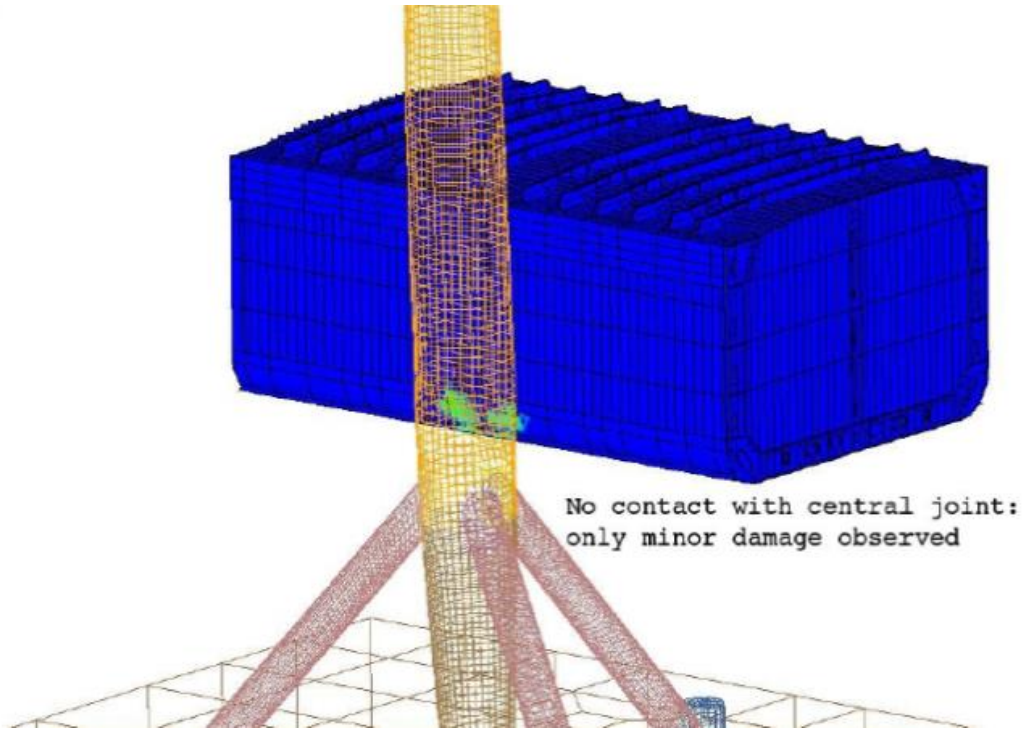

Figure 5-10: Simulation of marine vessel side collision with offshore wind turbine [59]

The deformation of the colliding structure is also strongly considered in the broadside collision shown in Figure 5-10, where the elements are long and narrow in the vertical direction as the deformation will inevitably be around the vertical axis of the monopole [67]. Mesh simplifications such as this are crucial in reducing the overall computation time of a collision event, and should be used wherever possible.

Figure 5-11 shows the effect of increasing mesh density for bow crushing deformation energy vs time for different mesh densities in the area of interest during a collision event [33]. The blue line (labelled “mesh”) represents the original refinement throughout the structure while the pink line (labelled “mesh4”) represents a level of refinement four times greater than the original mesh.

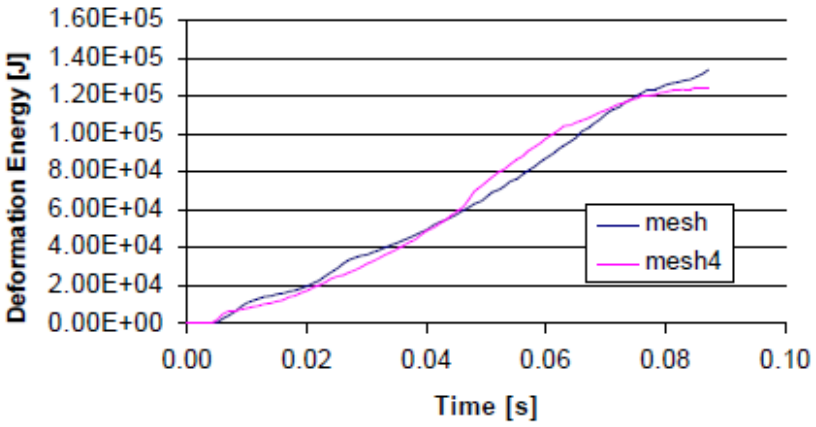

Figure 5-11: Effect of increasing mesh density for bow crushing, the variation of deformation energy vs time [33]

Figure 5-11 shows the marginal effect increasing mesh density would have once an adequately refined mesh has already been achieved. A balance between mesh density and computational time because the computational time required by the FEA program to process the model can be allocated to deal with more advantageous issues, such as an opting for a shorter time-step, or selection of a more sophisticated failure criteria. The mesh should only be as fine as necessary to provide accurate results within a reasonable margin of error established prior to the analysis.

5.9.2 Adaptive Algorithms

Adaptive meshing is the mechanism where a region of mesh is refined based on a pre-specified, user-defined criterion to increase accuracy of results. It is a particularly advantageous tool when a region of mesh has significantly higher stresses than the rest of the FE model, which is a common occurrence in collision simulations. Adaptive

strategies are now a common practice in FEA, as it can eliminate the need to manually refine a region of the model, thus saving time in the models creation.

The two necessary components of an adaptive meshing procedure are (a) a tool for determining conformity to an established criterion at which the adaptive mesh algorithm would commence, and (b) an algorithm to define a spatial discretization [75]. With reference to (a), the primary criterion, which would be of interest in a STOPC would be deformation. However, stresses, strains, or nodal displacements would each be an acceptable criterion from which to trigger the adaptive algorithm. With reference to (b), there are various algorithms available for adaptive solutions which include R-adaptivity, P-adaptivity and H-adaptivity.

R-adaptivity is based on the relocation of nodes by maintaining a consistent degree of freedom and element connectivity, thus, rendering an overall low computational cost in comparison to other algorithms [76]. While R-adaptively is commonly used for FEA, it is typically used in models with solid elements and rarely for models with shell elements [51].

P-adaptivity does not change the density of a mesh, but instead changes the degree of the interpolating polynomials used for element formulation [75]. It should be noted that P-adaptive methods are not available within LS-DYNA [63].

H-adaptive strategies allow for a shift in both the connectivity of elements and total DOF while maintaining a consistent polynomial degree of shape functions [76]. LS-DYNA makes use of an h-adaptive method for the automatic refinement of shell elements [63]. An example of this is as shown in Figure 5-12:

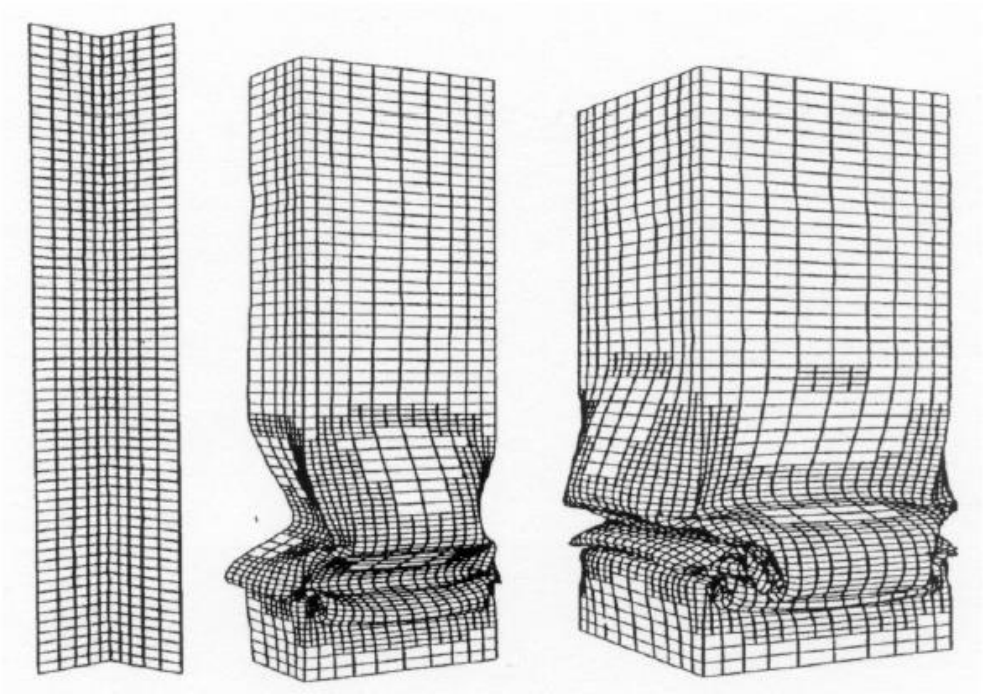

Figure 5-12: One level adaptive calculation on a square cross section beam with two faces displayed [63]

While there are several methods for h-adaptivity (as the method of refinement and criteria for doing so can be largely varied), LS-DYNA uses algorithms developed by Belytschko, Wong, and Plaskacz in 1989 [63]. This is employed within LS-DYNA through the control card *CONTROL_ADAPTIVE, which activates the adaptive meshing [51]. This adaptivity control card allows specification of a time interval between adaptive refinements, level of refinement per time-step, adaptive algorithm used when refining surrounding area, criteria by which the refinement gets activated, and various error prevention keywords.

The h-adaptivity algorithm within LS-DYNA can be used for a variety of non-linear analyses with high degrees of accuracy [75]. A minor disadvantage of the h-adaptivity algorithm used by LS-DYNA is its allowance for unconnected edges between original nodes during refinement (as shown in Figure 5-12). This is to say that if a shell element is split into four due to high stresses, but the adjacent element(s) are not, then there will be unequivalenced edges along the sides of the split element. This can cause fictitious out of plane deformation at the unattached nodes, but provided it occurs outside the area of interest, then it will have little effect on the stresses or displacements found in the area of interest. In addition, the adaptivity algorithm used by LS-DYNA does not convert 1D elements to 2D elements, although if the marine vessel beam/stiffener/girder was initially modelled using 2D shells then it would be accordingly refined.

No adaptive meshing has been used in any of the STOPC studies referenced in this thesis which may be due to the increased computational cost of its implementation. An example of how the incorporation of adaptive meshing would be beneficial in a STOPC if a sole coarse model of a marine vessel model was to be used for a collision with an offshore structure at various angles in 10 degree increments to simulate the resulting array of incremental deformations. When using the traditional localized refinement scheme, it may be necessary to locally refine specific areas of both the offshore platform and the vessel for each heading (direction of vessel with respect to collision object). This is because the vessel will contact the offshore structure at different angles and locations as heading changes. With adaptive meshing, however, the heading and consequent loading

parameters would have to be adjusted, but no localized area would require manual refinement. The use of adaptive meshing algorithms should be explored when performing STOPC assessment as an alternative to manually re-meshing the high deformation areas in both structures. While it has not been used for the simulations presented within this thesis, adaptive meshing should remain a consideration for future studies of STOPC assessment.

5.10 Contact and Boundary Conditions

5.10.1 Introduction

The boundary conditions implemented during a collision event are largely dependent on the portion of structure considered at the location of contact, the extent of the model present (three hold vs full vessel), as well as the purpose of the analysis. The types of boundary conditions used through vessel to fixed offshore structure collision events can generally be separated into two different groups: boundary conditions representing pile/soil interaction, and boundary conditions representing a portion of either structure.

5.10.2 Boundary Conditions for Truncated Offshore Structures

In order to save on both model generation and CPU times, it is advantageous to model only the portion of the structures that will be involved in the collision, and the surrounding structure that is likely to deform. When performing studies on the impact of tubular members, it would be tedious to model the entire structure, so it is a common practice to model a single tubular member in the impact area.

A study performed by Zhenjiang University in collaboration with Nanyang University presents a non-linear dynamic analysis procedure for the determination of impact action based on damaged components, and evaluates the overall damage effects on the platform structure [42]. Like several others, this study had opted to model a portion of the offshore structure and had only considered the members directly affected by the collision in a realistic manner. Small portions of the chords of the braces were connected to the member at which the loading was applied, and the boundary conditions were applied to the ends of the chord instead of the brace. The truncated members included within the model all have boundary conditions applied at their truncated end. This model is shown in Figure 5-13.

Figure 5-13: Model of the cross diagonal brace substructure [42]

This provides a much more accurate representation of the restraints applied to the structure than applying the idealized boundary conditions to the ends of the brace or chord member being impacted such as that shown in Figure 5-6, as it incorporates the displacement contribution of the adjacent structure [59]. If shell elements are used for the

simulation of a collision event causing local indentation of tubular members, the truncated members should include fictitious transverse plate at the point of truncation so the boundary condition could be applied to the center of the plate. This minimizes the fictitious membrane forces that would otherwise develop along the length of the member [59]. Another method of achieving a similar effect would be to use multipoint constraints to connect all nodes around the circumference (Slave nodes, S) of the truncated tubular member to a master node (M) placed in the center of the tube, as shown in Figure 5-14:

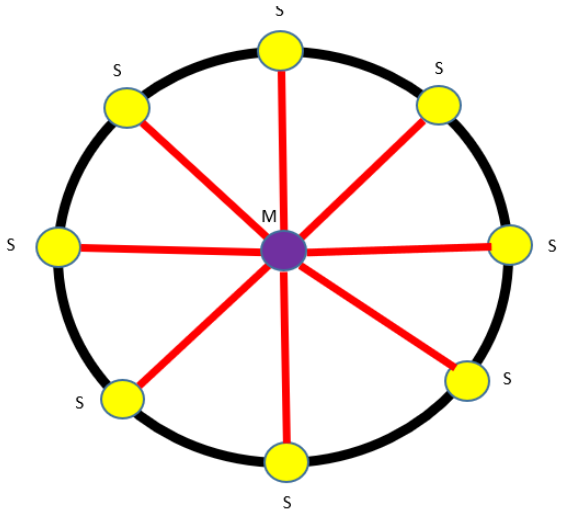

Figure 5-14: Multipoint constraint with master node (M) in centre of a hollow circular cross section

5.10.3 Pile/Soil Interaction

The boundary conditions imposed at the base of a fixed offshore platform due to the pile/soil interaction is a direct function of the stiffness of the soil, as well as the depth at which the pile is buried. This is rarely used in collision simulation studies, but should be considered for models where the full fixed offshore platform is being considered.

In several STOPC models, where the global response of the offshore structure is not the primary focus of the analysis, the soil to pile interaction would be simulated using rigid boundary conditions at the location where the structure first comes into contact with the soil. This approach would have little influence on local indentation of tubular members or global deformation of the colliding vessel. However, it is non-ideal for predicting the global response of the offshore structure, as instilling infinitely stiff boundary conditions at the mudline could cause fictitious local failure where the structure interfaces with the soil [30].

The alternative to applying rigid boundary conditions at the mudline is the use of non-linear springs to simulate the pile/soil interaction [42]. These non-linear constraints should represent three translational and three rotational spring elements corresponding to the central node of bottom cross sections of the jacket of the pile members [30].

5.10.4 Boundary Conditions for Truncated Vessels

For the sake of computational and modeling efficiency, it is a common practice to only model the striking portion of the vessel, truncate the portion which is not expected to undergo large deformations, and represent the truncated portion through the use of boundary conditions, rigid links, or rigid geometry. The rest of the vessel is often represented with either a coarse mesh, or the overall weight / energy is adjusted to represent that of the entire vessel. When this is done, the hydrostatic and hydrodynamic forces, structural mass and additional fluid mass from the truncated portion of the vessel must be adequately translated to the modelled portion of the vessel in order for the

simulation to have any level of accuracy. This method of truncation is a standard practice for marine vessel collision assessments.

A study performed by Dalhoff and Biehl [67] investigated the collision of a double tanker, a single hull tanker, a container ship and a bulk carrier with an offshore wind turbines. LS-DYNA was used for constructing the non-linear static and quasi-static collision models, which allowed for-user supplied subroutines be implemented within the code. Within this study, one to two holds of the vessels were modelled using finite elements, while the rest of the vessel was modelled as a rigid body connected to these holds at the outer nodes. This allowed the influence of the wind and waves imposed upon the vessel to be more accurately represented as their forces would have acted upon the true geometry of the marine vessel rather than be represented through equivalent loading [67]. This was done by applying rule loading to the entire vessel, which was therefore transferred through the structure and accurately represented in the area of interest. By modeling the entire vessel with approximate masses matching that of a stability booklet (a ship specific document detailing the mass, moment of inertia, and draft details), the total mass of the vessel is accounted for during the collision and the inertia is dissipated accordingly.

Head on collision assessments performed by Amdahl frequently truncated the vessel aft of the critical region in order to increase computational efficiency [10, 6, 12]. This method of truncation is appropriate, provided the boundary conditions are sufficiently far

from the point of impact to minimize any contribution they may have towards the stiffness of the structure [52].

5.10.5 Collision Simulation and Contact

When performing an analysis of a STOPC, it is critical that an appropriate contact algorithm be used in order to properly simulate the collision event. There are a variety of contact algorithms available within LS-DYNA and ABAQUS, but very few are applicable for accidental loading collision assessment if yielding material and partial failure is expected to occur and both colliding bodies are unattached initially.

Typically, multiple contact algorithms are used simultaneously to simulate the contact incurred through the collision. Firstly, contact must be specified between the vessel and the offshore structure. This structure to structure interaction can be simulated using the LS-DYNA contact card **CONTACT_AUTOMATIC_SURFACE_TO_SURFACE,* using a friction coefficient of 0.3 for dry steel to steel contact [22, 77, 78]. Secondly, the interaction among various surfaces of the vessel and/or offshore structure must be accounted for to properly model the interaction in deformation of various components correctly. This can be specified using the LS-DYNA contact card **CONTACT_SINGLE_SURFACE* or *CONTACT_AUTOMATIC_SINGLE_SURFACE* using a friction coefficient of 0.3 [51, 12, 78]. The inclusion of a self-contact algorithm is fundamental when performing any local analysis with high fidelity mesh to properly simulate the effects of crumpling. Tie contact algorithms may also be appropriate when simulating point impacts for local indentation or punching of a tubular member [59].

If a contact surface is specified after the marine vessel and structure are appropriately modelled, the specification of an initial vessel velocity will eliminate the need to calculate any additional vessel to structure forces, which would have been required otherwise [42, 30]. This is advantageous in both reducing modeling time, and producing more accurate results as the representative forces derived from relevant FE codes and design standards can be superseded by a detailed representation of both structures [18]. Capturing the true deformation of both structures would be far more achievable and accurate using a contact method of analysis due to the elimination of gross approximations.

Additional considerations when considering contact models would be taking advantage of the recent development of more robust formulations available in FE software packages that are not yet prevalent in collision simulations. These include “mortar contact” and “friction penalty algorithms”. Friction penalty algorithms relate to frictional forces incurred during the collision due to the sliding of one surface over the other. This algorithm makes use of a Coulomb formulation and uses the equivalent of an elastic plastic spring. This is performed by [63]:

i. computing the yield force as a function of the friction coefficient
ii. computing the incremental movement of the slave node
iii. updating the interface force to a trial value
iv. rechecking the yield condition and then
v. scaling the trial force in accordance with the calculation [63].

This method has the disadvantage of producing stresses exceeding what a given material can handle, which is handled in LS-DYNA with an additional operation. Due to the number of steps involved with such an algorithm, it is assumed that this process would be computationally inefficient. The advantage of this formulation is that it is quite robust and can avoid a wide variety of potential issues typical in collision analysis.

While this will not be the dominant mechanism taking place during a STOPC event and is not typical, its inclusion should be considered. Mortar contact is a segment to segment penalty base algorithm implemented in LS-DYNA that is far more robust than the available equivalent formulations. This function is particularly useful when considering elements of a higher order than simple shell elements and is available for implicit and explicit analysis solutions. No evidence was found by the author of its use in previous collision assessments, which is likely due to the high computational effort required by this method.

5.11 Comparison of Finite Element Analysis and Experimental Results

While finite element analysis of STOPCs is becoming more and more accurate as the years pass, there remain large differences between experimental and computed results due to the large number of variables associated with an accidental collision event. One of the major difficulties with acquiring data for such events is the magnitude of cost associated with performing full scale ocean collision tests and the scarcity of existing data associated with collision events. While the collision event can be represented

through FEA, it is likely that parameters governing the collision simulation will become more accurate as more collision event data becomes available.

The Association for Structural Improvement of Shipbuilding Industry and the Netherlands Foundation for the Coordination of Maritime Research conducted a series of full-scale tests for vessel to vessel collision [53]. The tests were conducted in a harbor basin in the Netherlands and were compared to LS-DYNA FEA results. Parameters measured during the collision include:

i. The penetration of the bow of the striking marine vessel into the side of the stricken vessel.
ii. The contact force between the striking vessel and the struck vessel.
iii. The strains during the collision event.
iv. Rigid body motions of both vessels.

The first experiment simulated the marine vessel collision without the influence of water and restricted movement to the horizontal plane. In order to reduce computation time, only a small part of the struck marine vessel was modelled in detail using shell and beam elements as the deformable structure, as shown in Figure 5-15. The remaining marine vessel was modelled as an undeformable rigid body, which, as mentioned in section 5.10.4, is very non-typical modeling technique for collision simulations. The purpose of the first step of the experiment was to determine the time dependent collision force.

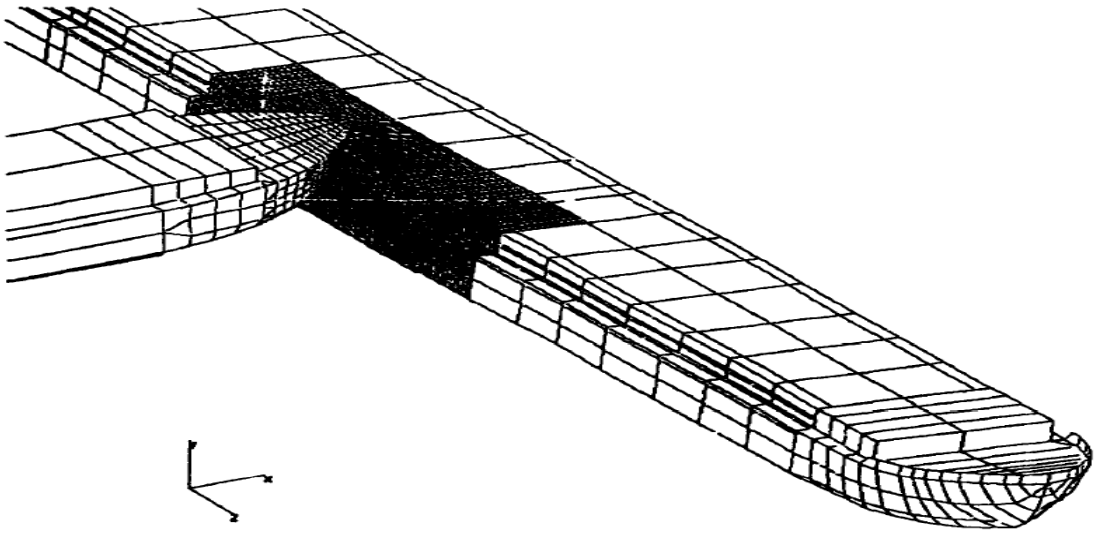

Figure 5-15: Vessel to vessel collision with collision area finely refined [53]

In step two, the water reaction force was determined using a two dimensional transient symmetric model of water and a 1 m vessel cross section. The MSC/PISCES code was used to determine the resistance force of the water acting laterally on the struck vessel per unit length as a function of colliding ship velocity [53].

The final step of the simulation performed in this experiment was simply a repetition of the first step, but with a more complete model, and using the fluid added reaction forces computed in step 2. The contribution of the surrounding fluid was accounted for using a series of dampers attached to the non-collision side of the struck vessel, which have characteristics based on the results calculated in step 2. By multiplying the resistance force per unit length by the total length of the vessel, the total resistance force could be determined, which allowed the dampers to take the acceleration of water surrounding the vessel into consideration. These dampers were modelled as spring elements in order to prevent any stiffness contribution they may impose upon the structure. This method of

simulation provided collision forces 30-70 percent higher than the measured maxima, which was largely due to the assumed rigidity of the colliding vessels.

While this study was focused on a vessel to vessel collision, the margin of error between the simulated and experimental results should still be of particular interest when considering a STOPC. The parameters used during an accidental collision assessment use the upper limits of every loading present in the analysis, such as marine vessel size, velocity, added mass of fluid, and motion of the offshore structure when collision occurs. This will inevitably cause an overestimation of the collision forces imposed upon the structure during an actual accidental collision. In addition, if the shared energy approach is not used through the analysis, and instead one of the structures is assumed to be rigid, therefore dissipating a greater proportion of the strain, then the results will be even more conservative. From these experiments, it can be concluded that the FEM provides results which typically overestimate those which would result from a real world collision.

5.12 SUMMARY

Since the first marine STOPC studies performed in the early 1980's, there have been significant developments in the commercially available finite element analysis packages appropriate for such analysis. LS-DYNA is the most prominent software used for marine STOPC assessments, but many modern FE software packages have the capabilities to perform such analysis with a similar degree of accuracy. The collision assessment FE codes must consistently be used through the process of simulation, analysis and post-processing, as they govern the appropriate parameters required for establishment of

loading and permissible stress levels. While major accidental loading design standards have always suggested limitations for the allowable stress and deformation of offshore structures, they are beginning to include recommendations for proper simulation and methodology associated with the finite element analysis of collision events. Shown below are areas of improvement that ought to be considered within the design standards and FEA software packages:

1. Currently, the design standards focus largely on the establishment of loads to be assigned to the colliding structures, but typically do not discuss the boundary conditions accounting for pile/soil interaction, or when truncating tubular members for local deformation assessment.
2. Design standards assign an arbitrary value for the fluid added mass based on the mass of the marine vessel. This is a very inaccurate method of assessment as the fluid added mass is more dependent on the vessel geometry than the mass of the vessel itself. This issue should be resolved.
3. Computational fluid dynamic analytical software are typically separate from finite element analysis packages, but are unavailable through most FEA program suites. In order to accurately simulate fluid loads on both structures, it would be ideal to have this feature built into the programs.
4. While most FEA programs have a very strong base for structural representation, the inclusion of fluid SPC (single point constraint) elements is not present within all program suites; moreover, it appears to be limited to some of the FE vendors. SPC elements are a quickly developing tool that may be advantageous to utilize

for modeling inner fluid tanks or external fluid interaction with the hosting structures during such assessments.

5. Often, even modern studies neglect the sway motion of the offshore structure prior to collision. While this will not affect members deformation significantly during a collision event in comparison to that experienced from the collision, it should still be taken into consideration when there is significant sway or offshore structure mass. If the total energy contribution provided by sway of the offshore platform is shown to be negligible in comparison to that provided by the colliding vessel for a given collision event, then the decision to neglect the sway velocity would be far more justifiable.

6. SIMULATIONS

6.1 INTRODUCTION

Using established collision standards of design and worst-case loading scenarios, multiple full scale STOPC simulations have been performed using the finite element method. Various shell element formulations have been explored through the analyses and the accuracy of their results and simulation times have been compared. Three sets of analyses were performed to determine which element formulation would be ideal for full scale STOPC assessments and are presented in sections 6.3 and 6.5:

1. Simplified STOPC assessment using a stiffened cylinder and a vertical monopole
2. Full scale STOPC assessment using a research vessel and a vertical monopole using implicit/explicit switching
3. Fully explicit STOPC assessment using a research vessel and a vertical monopole to compare results to those found in step 2

6.2 TOOLS AND STANDARDS

While there are various standards available for the assessment of STOPCs (as listed in section 3), NORSOK has been the primary standard used through this section due to the high volume of collision assessments performed under its guidance.

ALTAIR Hypermesh has been used as the primary means of model development and manipulation due to the wide array of modeling tools it has available. LS-DYNA has been chosen for the simulation of the collision events due to its exceptional handling of collision-based contact problems and nonlinear solution efficiency as discussed in section

5.4.2. LS-PREPOST has been chosen to postprocess the results achieved through the analyses due to its seamless compatibility with LS-DYNA. All analyses referenced in section 6.3, section 6.4 and sections 6.6.1 through 6.6.8 have been performed using a 64 bit 8 CPU HP EliteBook 8570w with 16384 MB RAM configured on WINDOWS, while the analyses performed in section 6.6.9 has been performed using a 120 CPU core Intel Xeon Cluster configured on LINUX platform.

6.3 Stiffened Cylinder Model – Element Performance Comparison

6.3.1 Model Parameters and Mesh Density

A preliminary collision assessment was performed between a stiffened cylinder model and a vertical column to establish the optimal simulation parameters and determine which elements were suitable for a full scale STOPC using implicit / explicit switching. The stiffened cylinder model used for this assessment was modelled as being 25 mm thick, an 85 m length, and a 40 m diameter as shown in Figure 6-1:

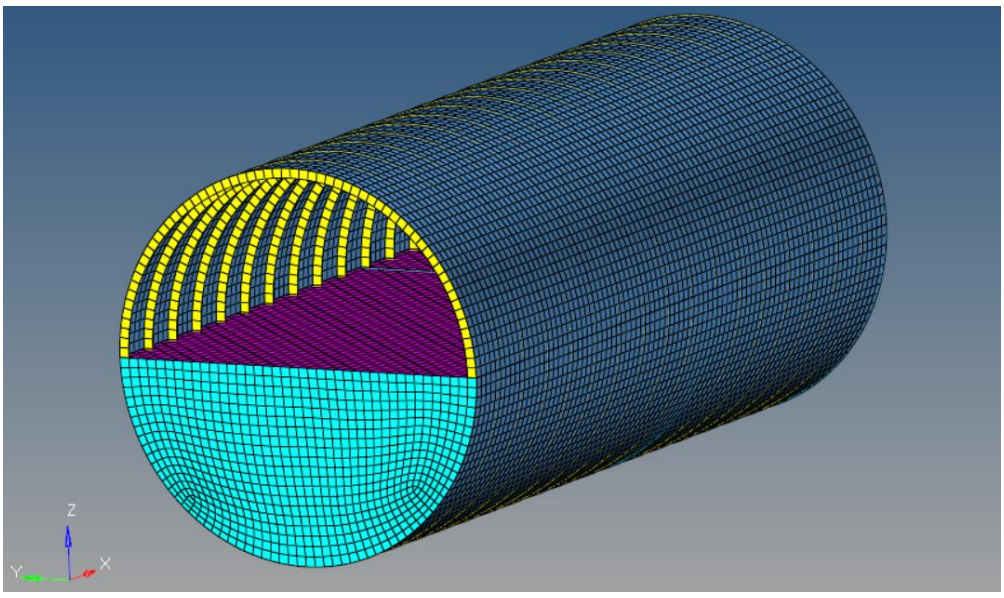

Figure 6-1: FE Model of the stiffened cylinder

A mesh density with an average element size of 1000 mm was used to construct the model for simplicity, and all materials modelled as AH36 steel. The stiffened cylinder model was transversely stiffened by 1000 mm deep, 25 mm thick flatbar circumferential stiffeners spaced longitudinally at 5000 mm interval. The model was also stiffened by a 25 mm thick deck bisecting the cylinder. 25 mm thick watertight bulkheads extending from the bottom of the cylinder to the deck are located at both ends as well as 35 m from either end. This model was produced to approximate a simple model of a full scale marine vessel with framed and watertight bulkheads.

The vertical column model used for this analysis is as shown alongside the stiffened cylinder in Figure 6-2:

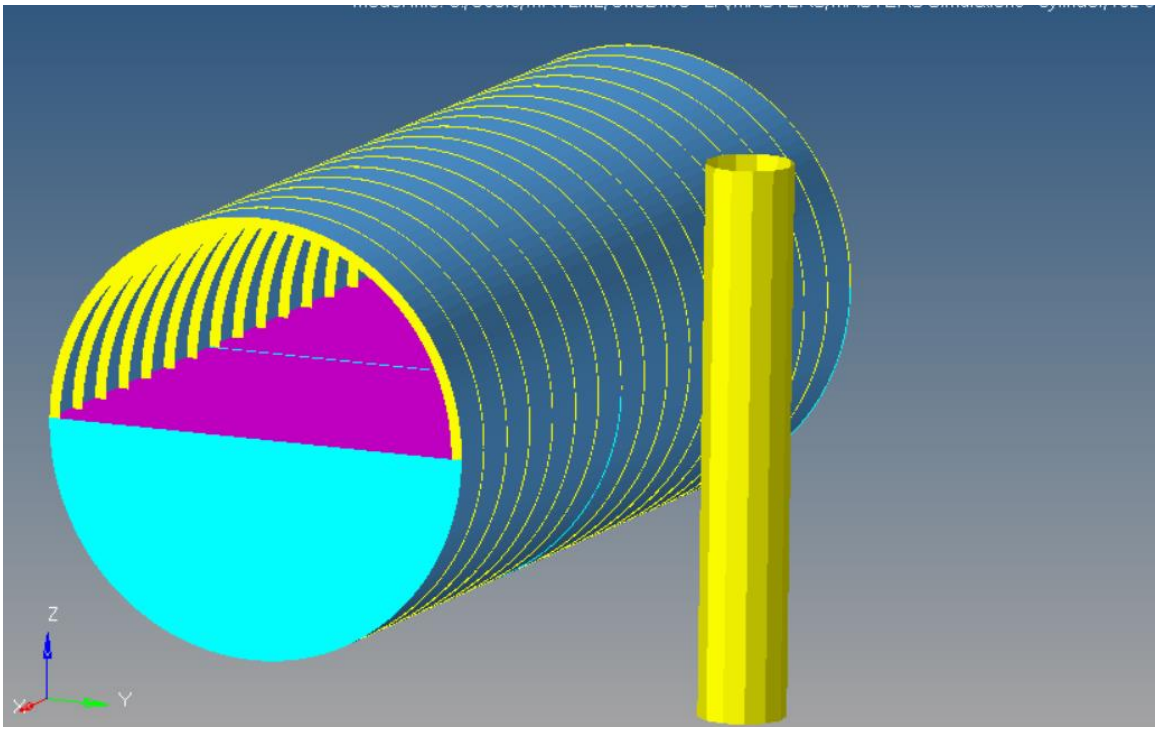

Figure 6-2: Schematic of the stiffened cylinder and vertical monopole

The wall thickness of the vertical monopole modelled has a 100 mm thick HSS to allow the maximum energy dissipation through deformation to occur within the stiffened cylinder.

6.3.2 Simulation Parameters

The stiffened cylinder was simulated to approach the vertical monopole broadside at a velocity of 7.1 m/s (in the direction of the radial depth of the monopole). This velocity was chosen using NORSOK standards of maximum broadside collision speed of a marine vessel with a stationary object in the North Sea. While mass has been included, vertical acceleration due to gravity was not considered for simplicity purposes. The Newark time integration Gamma constant of 0.6 and Beta of 0.38 were used. Initial simulations showed great inefficiency in using fully explicit analyses parameters. Consequently, automatic implicit to explicit switching was used to maintain the accuracy provided by the explicit solver while allowing timesteps that were not involved in the collision to be simulated implicitly. An initial time step of 0.01 s was used for the implicit portion of the analysis, but was automatically adjusted depending on the level of deformation taking place for any given time step. Automatic surface to surface mortar contact was used due to its robustness and proven efficiency. Adaptive mesh refinement algorithms were not used during these analyses, as this would cause difficulty in directly comparing element formulations across models; this is because the adaptive meshing may not produce the same resultant mesh throughout each model.

6.3.3 Boundary Conditions

The stiffened cylinder model was not constrained, as it was intended to represent a full marine vessel. Pinned constraints were used at all nodes at the top and bottom of the monopole section, as shown in red in Figure 6-3:

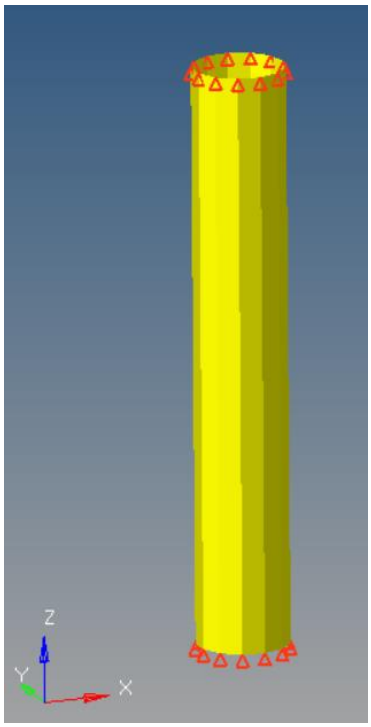

Figure 6-3: FE model of the vertical monopole with its boundary conditions

6.3.4 Element and Material Formulations

As per recommendations noted in Section 5.7, collision assessments have been performed using LS-DYNA shell element formulations of {1,2,6,7,8,10,11,16,23,25,26} to simulate various components of the stiffened cylinder model. Triangular plate element formulations were not investigated as part of this assessment, as they are not recommended as a primary element formulation for a collision assessment. To simplify the analysis, the vertical monopole has been represented using ELFORM 1 in all models.

For simplicity and efficiency purposes, a simple plastic yielding material model (MAT 3) has been used, which requires materials yield strength but does not take the overall stress-strain curve into consideration. A conservative yield strength of 350 MPa was selected for the analyses. In a full scale energy dissipation collision assessment, it is recommended to accurately represent the material stress-strain curve.

6.3.5 Results

The VM stress results at t=0.667s for simulation 1 (i.e., element ELFORM 1 was used to model the stiffened cylinder) are as shown in Figure 6-4:

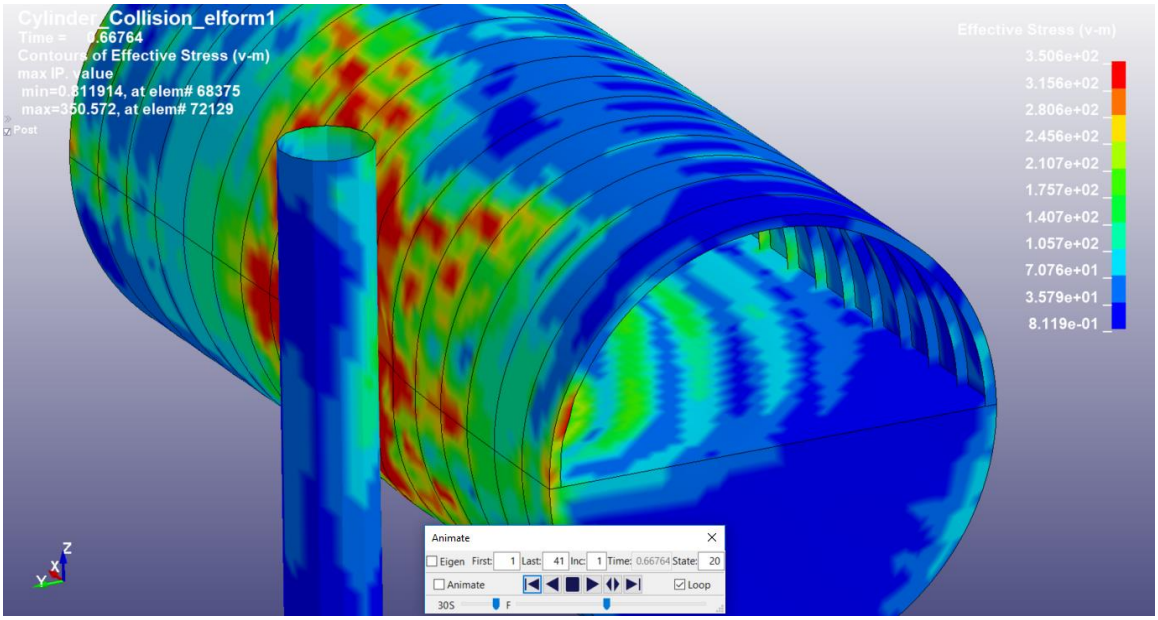

Figure 6-4: Distribution of VM stress at t=0.667s

While all element formulations produced a similar stress and yielding pattern within the stiffened cylinder model, there was a high level of inconsistency in stress magnitudes once an element had yielded. Element 72554, which is located on the external stiffened

cylinder shell near the collision point, was chosen for comparison across the simulations. The von Mises stress history of element 72554 for the 10 of the 11 selected element formulations are shown in Figure 6-5:

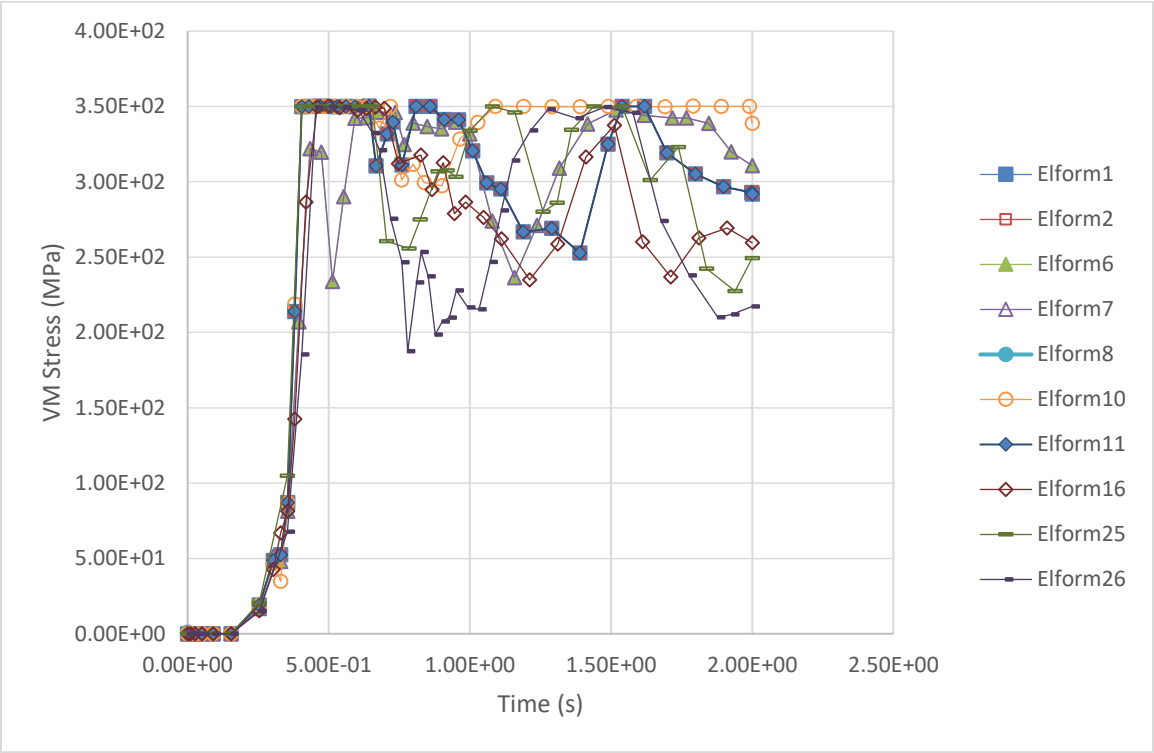

Figure 6-5: Variation of von Mises Stress as a function of time in element 72554 obtained by the various element types used in the collision analysis

Results from element formulation 23 (8-noded shell formulation) were excluded from Figure 6.5 and all following graphs of results. Due to an incompatibility in LS-DYNA between ELFORM 23 and mortar contact, simple surface to surface contact had to be specified when running ELFORM 23. While the analysis ran to completion, time history graphs of element behavior in the collision area showed maximum stresses of roughly 100 MPa before yield before immediately decreasing in stress. Furthermore, only one data point in the VM stress plot for Element 72554 showed stresses reaching 250 MPa

(whereas other analyses exhibited VM stress results with multiple sequential data points at yield during the collision event, as shown in Figure 6-5). For this reason, element formulation 23 cannot be considered for STOPC analysis.

Among the remaining 10 formulations (presented in Figure 6-5), there is a high level of consistency among the predicted von Mises stress in element 72554 before the material starts yielding, after which the results differ greatly. The margin of error may be reduced if a finer mesh is used to model the collision area, or probably if the actual material stress-strain curve of the material was incorporated in the analysis. A more robust material model and a finer mesh density in the area of interest will be used in modeling the full STOPC.

As the collision occurs solely in the Y direction (in the direction of the radial depth of the monopole, see Figure 6-4) the Y displacement of node 43089, which is located on the surface of the stiffened cylinder at the location of collision, was traced or monitored through all simulations, which are illustrated in Figure 6-6:

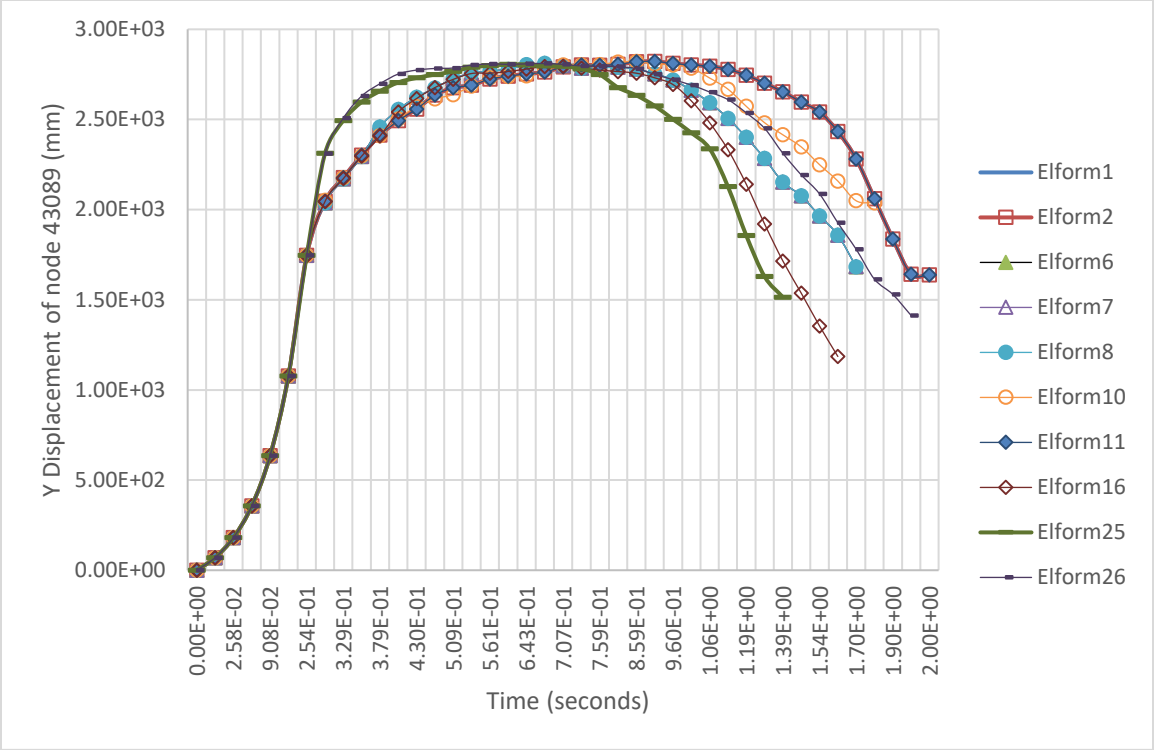

Figure 6-6: Variation of Y displacement (in the direction of the radial depth of the monopole) as a function of time of node 43089 during the collision analysis

Prior to the collision (t<0.25s), all the curves produced by the element formulations are identical. Once the two structures come into contact, ELFORM 25 and ELFORM 26 produce similar results, but different to the results produced by the other element formulations tested. This is likely due to the fact that ELFORMS 25 and 26 account for the through-thickness stretching in their formulations. The results of other element formulations are in very close agreement until t=0.75s, at which stage they begin to diverge from one another. The solution CPU in seconds associated with each element formulation are provided in Figure 6-7:

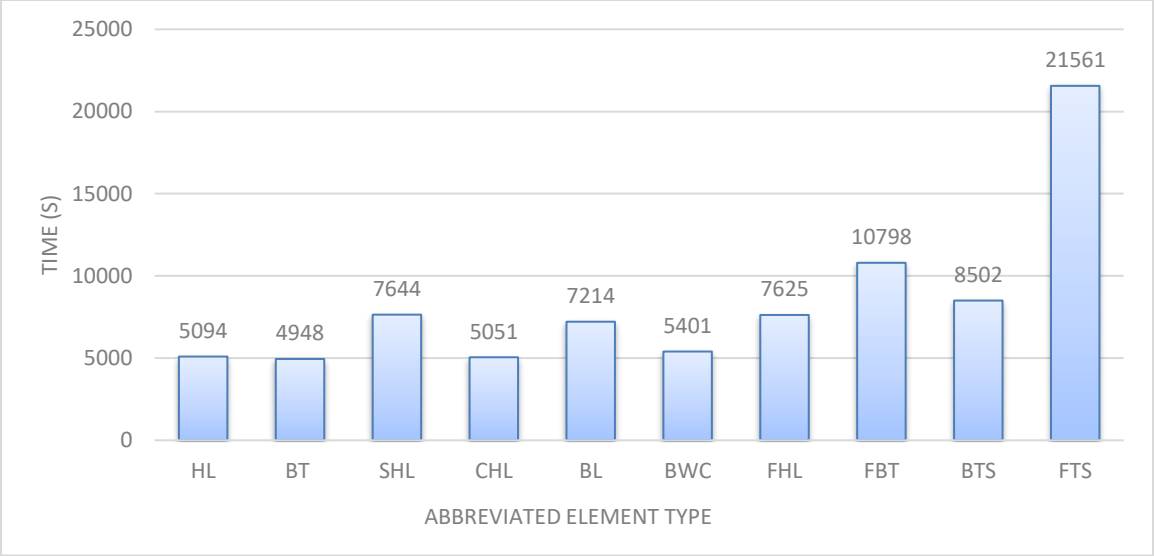

Figure 6-7: Total CPU times consumed to solve the problem by the various element types

HL = Hughes Liu Shell (ELFORM 1)

BT = Belytschko − Tsay Shell (ELFORM 2)

SHL = S/R Hughes Liu Shell (ELFORM 6)

CHL = Corotational Hughes Liu Shell (ELFORM 7)

BL = Belytschko Leviathan shell (ELFORM 8)

BWC = Belytschko Wong Chiang shell (ELFORM 10)

FCHL = Fast Co − Rotational Hughes Liu (ELFORM 11)

FHL = Fully integrated Hughes Liu shell (ELFORM 16)

BTS = Belytschko − Tsay Shell with thickness stretch (ELFORM 25)

FTS = Fully Integrated Shellwith thickness stretch (ELFORM 26)

The variations in solution times amongst various element formulations are fairly significant, with the most costly element (FTS) being over four times more expensive than the least costly element (BT). This is to be expected due to the less sophisticated

element formulations, and will be compared to the full ship simulation study to determine whether the differences in solution time are scalable. As a full scale ship collision is far more complex then the stiffened cylinder model, this study serves as a useful guide for element formulations available for STOPC with coarse or simplified models but only as an indication as to which may be available for full scale STOPC.

6.4 Stiffened Cylinder Model – Mesh Sensitivity Analysis

As the analyses performed in section 6.3 were primarily to determine the efficiency of the various element formulations available in LS-DYNA for collision analyses, an additional study has been performed to determine the sensitivity of mesh size in the collision area of a full scale STOPC simulation. This study was performed using four FE models of varying refinement using ELFORM -16 by incorporating the explicit-implicit switching option and the parameters discussed in section 6.3.2. While the same geometry/structure was used through all analyses, the level of mesh refinements used for constructing the four models are as presented in Table 6-1:

Table 6-1: Mesh Sensitivity Analysis Parameters

Model ID	Element Size (mm)	Total number of elements
1	1000	16260
2	500	72816
3	250	292124
4	125	1168496

While the models in Table 4-3 had all been created and initiated within LS-DYNA, the 125 mm model could not be analyzed due to storage and computational power constraints of the 8 CPU HP EliteBook 8570w with 16384 MB RAM. Distribution of the von Mises stress produced by each model at t = 0.60 mm, where the stress patterns are most comparable, have been provided in Figure 6-8 through Figure 6-13:

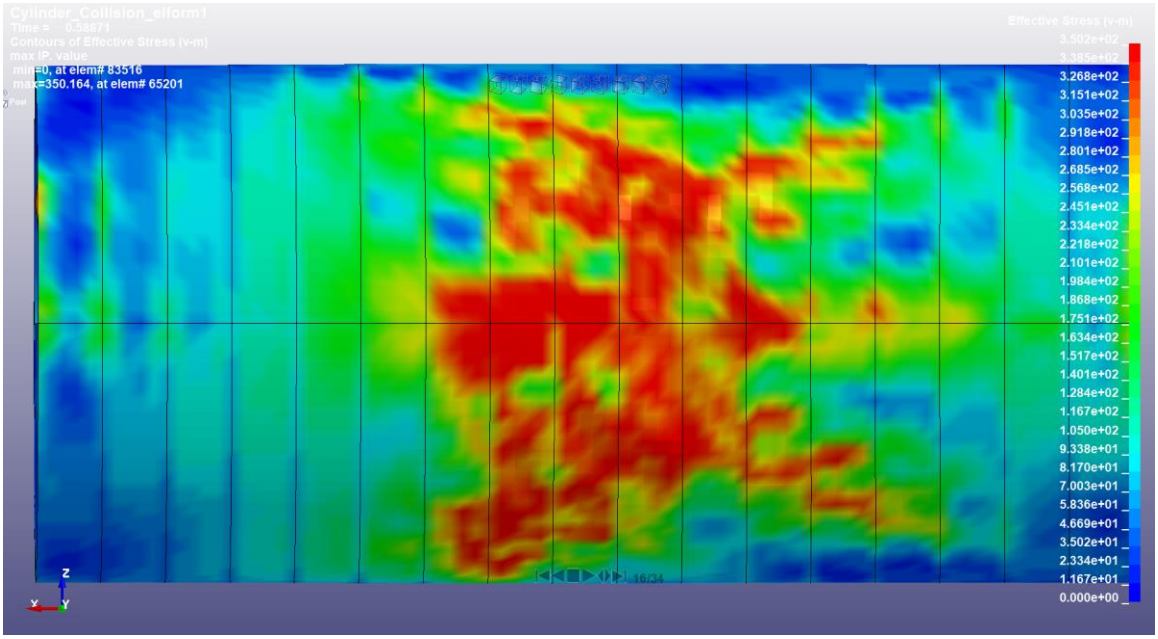

Figure 6-8: ELFORM -16 stiffened cylinder STOPC assessment, 1000 mm refinement, side view (+y), $t \approx 0.6s$

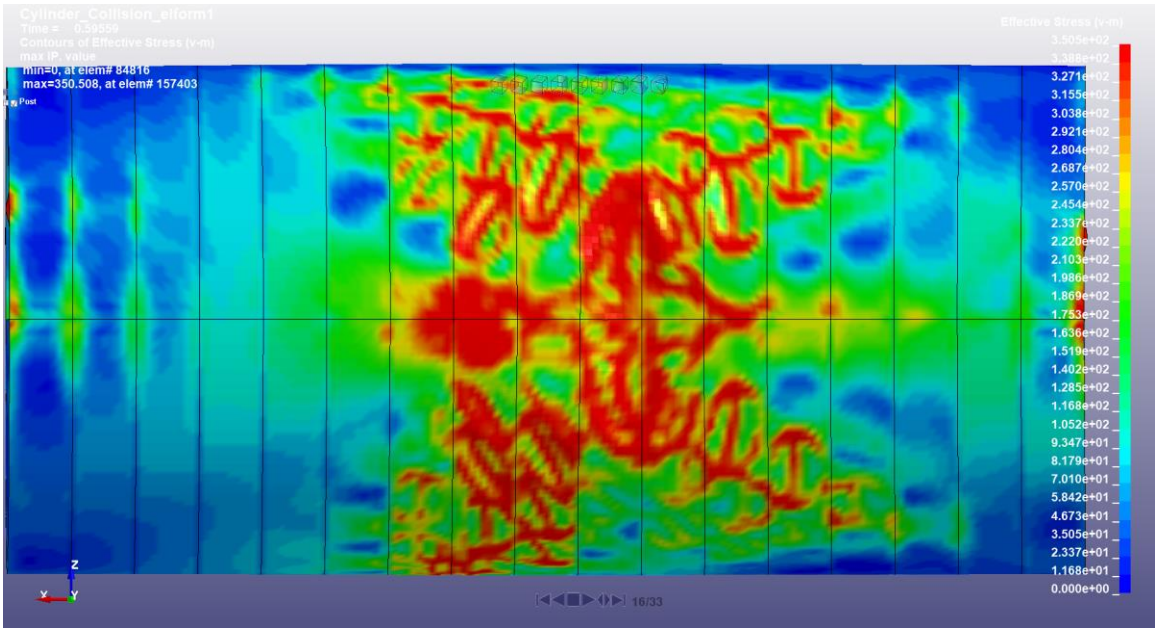

Figure 6-9: ELFORM -16 stiffened cylinder STOPC assessment, 500 mm refinement, side view (+y), $t \approx 0.6s$

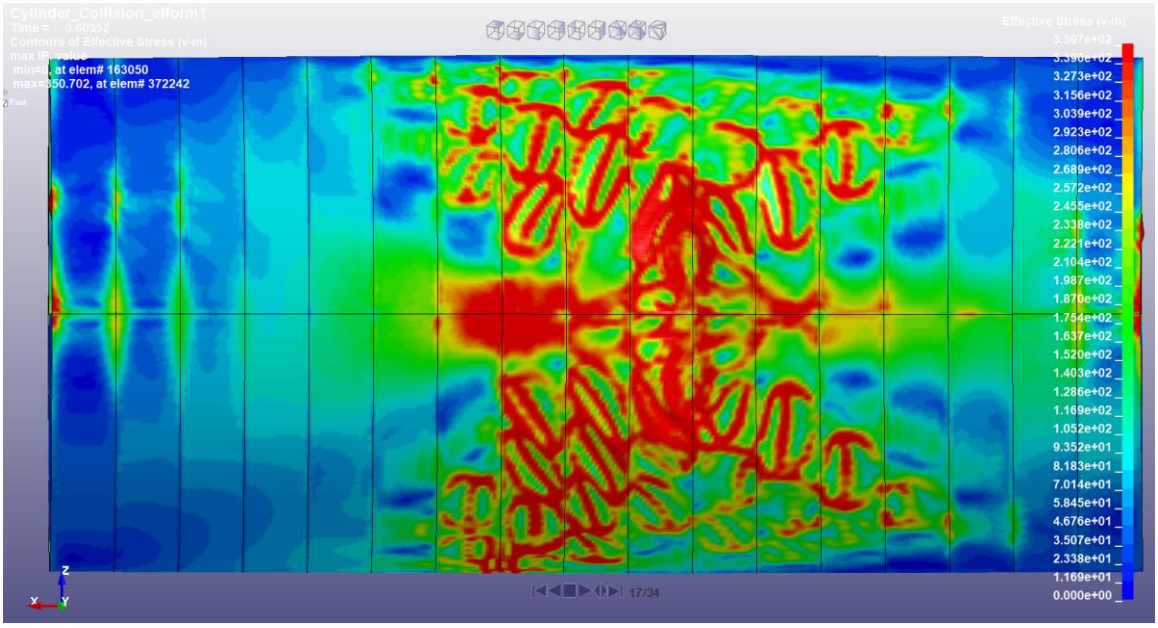

Figure 6-10: ELFORM -16 stiffened cylinder STOPC assessment, 250 mm refinement, side view (+y), $t \approx 0.6s$

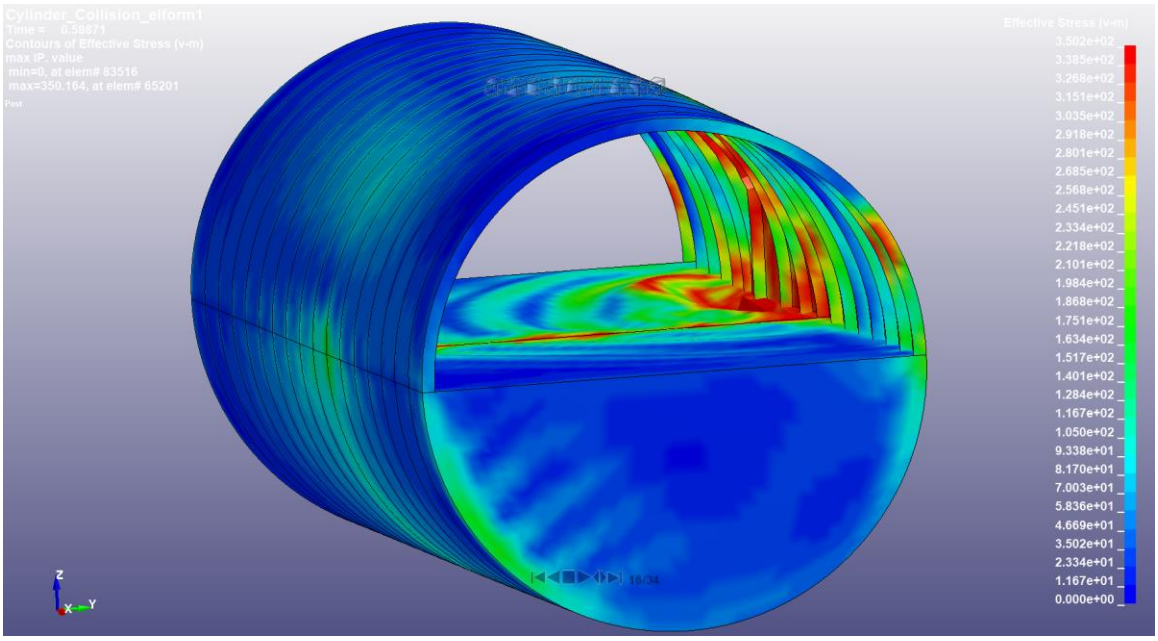

Figure 6-11: ELFORM -16 stiffened cylinder STOPC assessment, 1000 mm refinement, isometric, $t \approx 0.6s$

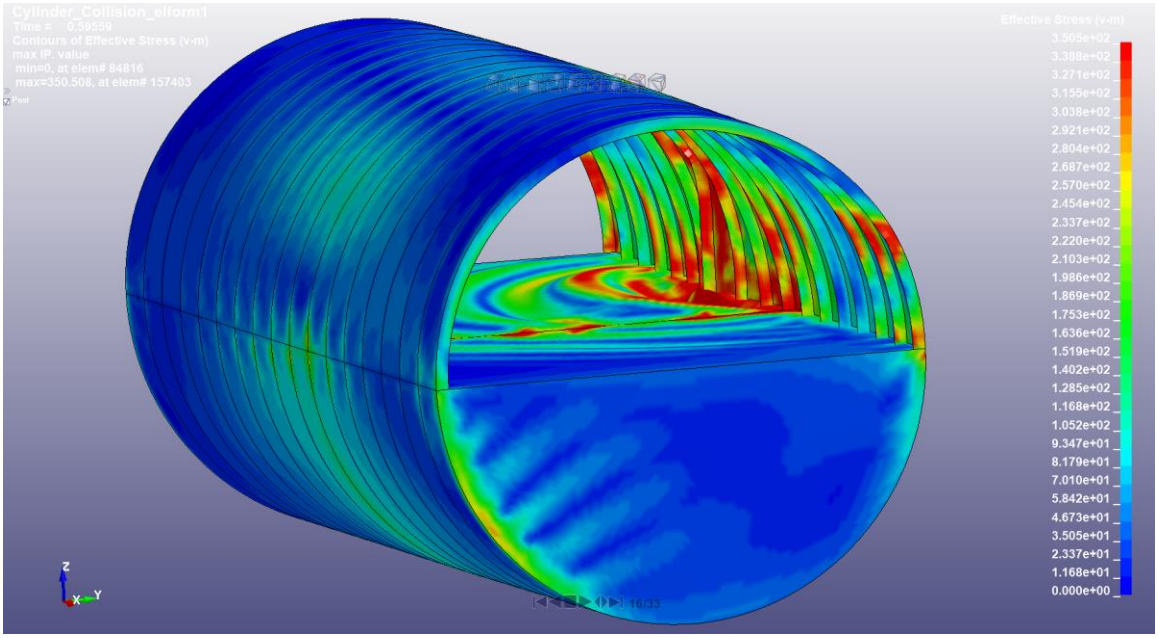

Figure 6-12: ELFORM -16 stiffened cylinder STOPC assessment, 500 mm refinement, isometric, $t \approx 0.6s$

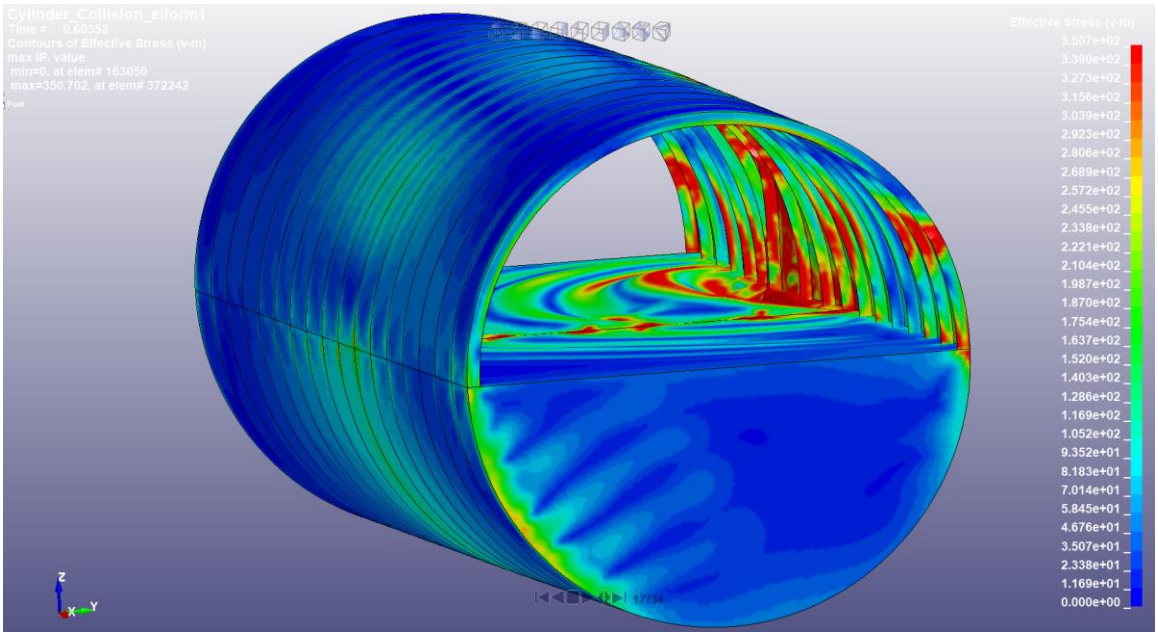

Figure 6-13: ELFORM -16 stiffened cylinder STOPC assessment, 250 mm refinement, isometric, $t \approx 0.6s$

As seen in the figures above, there is a significant difference in the stress pattern between the 1000 mm and 500 mm models. The 500 mm model produces more detailed stress patterns, capturing the warping of the steel plating between the transverse stiffeners clearly. Visually, there does not appear to be any significant difference in the VM stress patterns produced by the 500 mm and 250 mm models. The 250 mm model produced pattern has higher resolution in the yielded areas, but overall, it exhibits the same pattern and behaviour as that of the 500 mm model.

To further understand the differences in the VM stress patterns between the models in the collision area, the stress pattern sampled at elements centre integration point at the same specific region of each model is illustrated in Figure 6-14 and the stress comparisons between these cases are plotted in Figure 6-15. Moreover, the average values of the VM calculated within the small regions identified by the square (noted on each region) are

plotted in Figure 6-15. Furthermore, the radial displacement at that location obtained from each model is illustrated in Figure 6-16, followed by the plots of the kinetic and internal energies in Figure 6-17 and Figure 6-18.

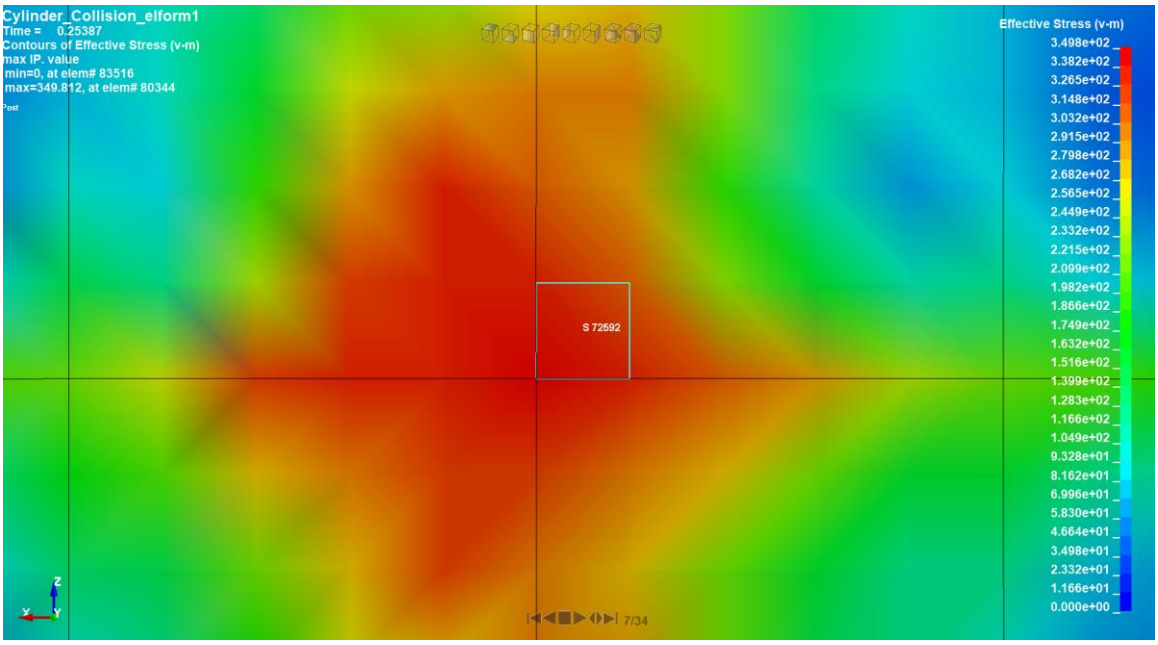

Figure 6-14: The specific region selected in all three mesh density models for plotting the average VM stress sampled at centroid integration points, side view (+y), $t \approx 0.25s$

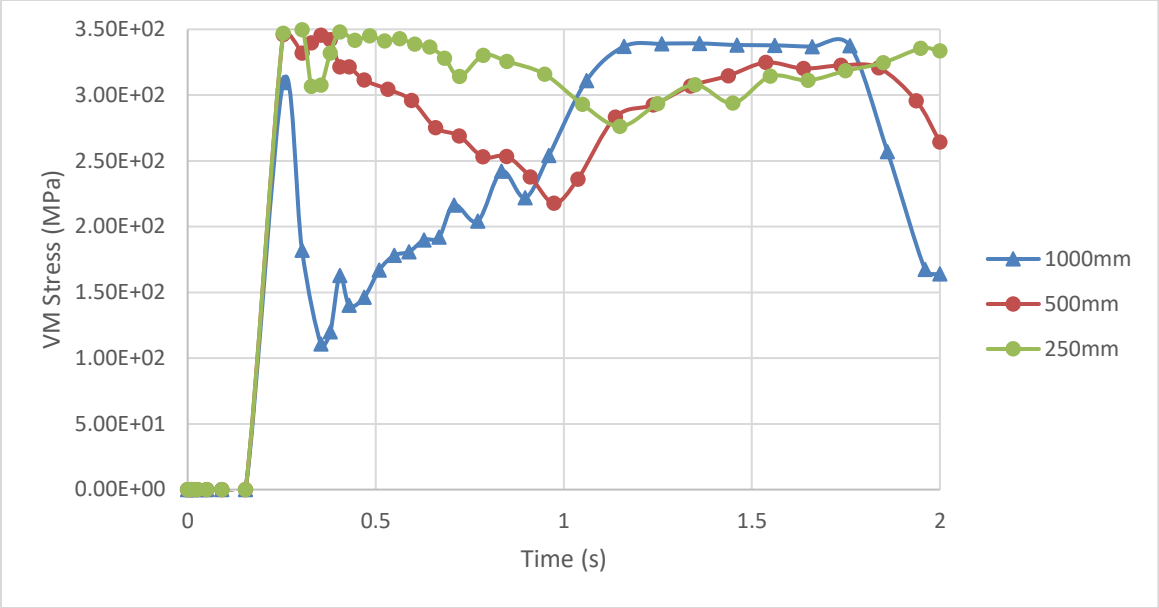

Figure 6-15: Stress variation of the average VM stress sampled at location shown in Figure 6-14 as a function of tune,

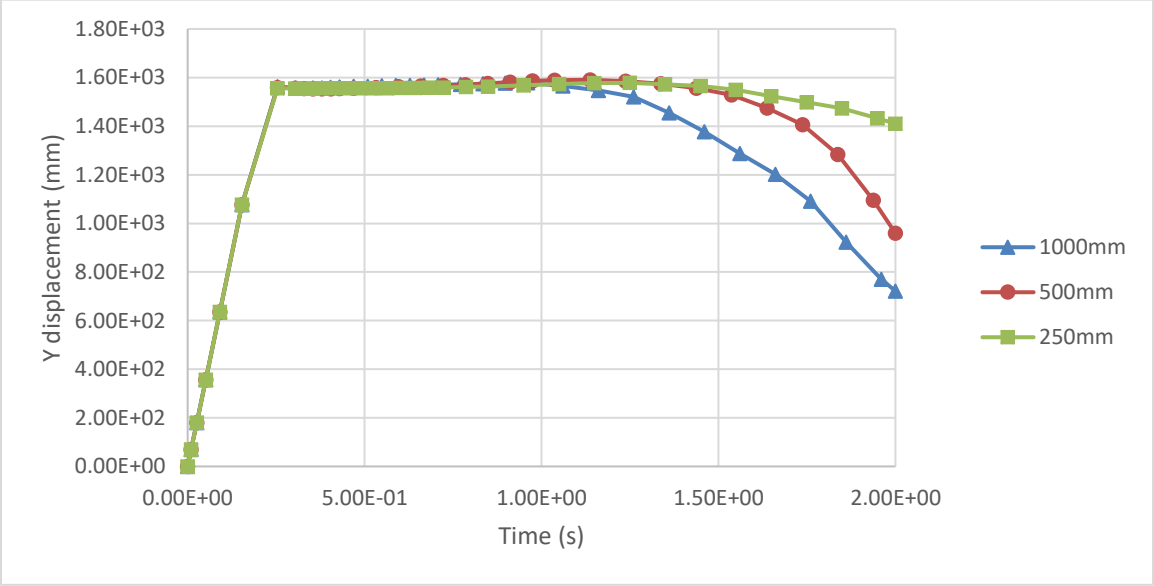

Figure 6-16: Y Displacement comparison of collision node

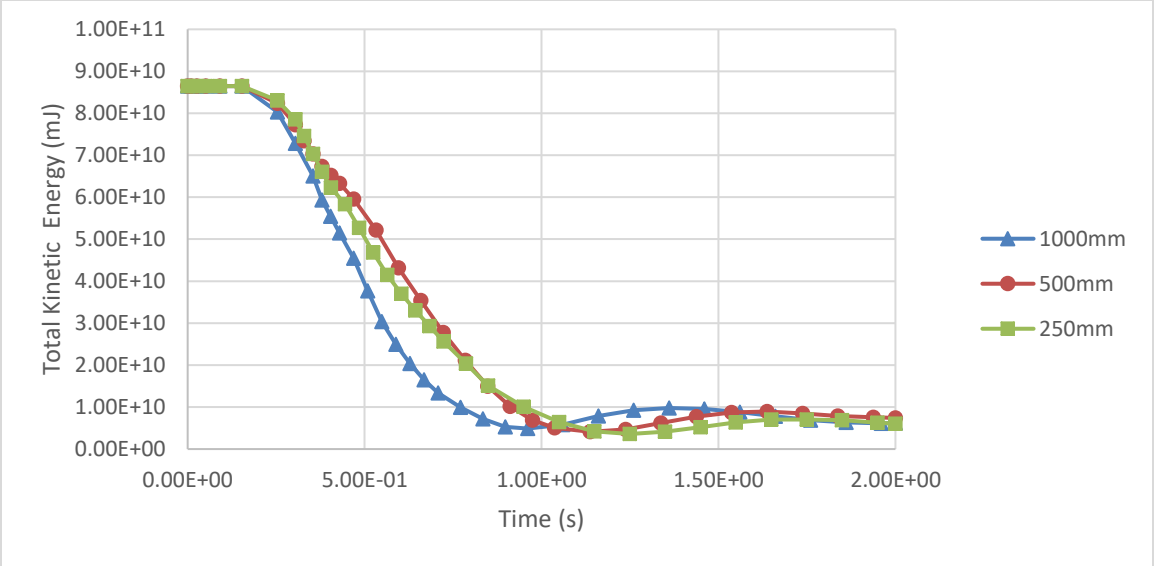

Figure 6-17: Variation of the average internal energy sampled at the location shown in Figure 6-14 as a function of time

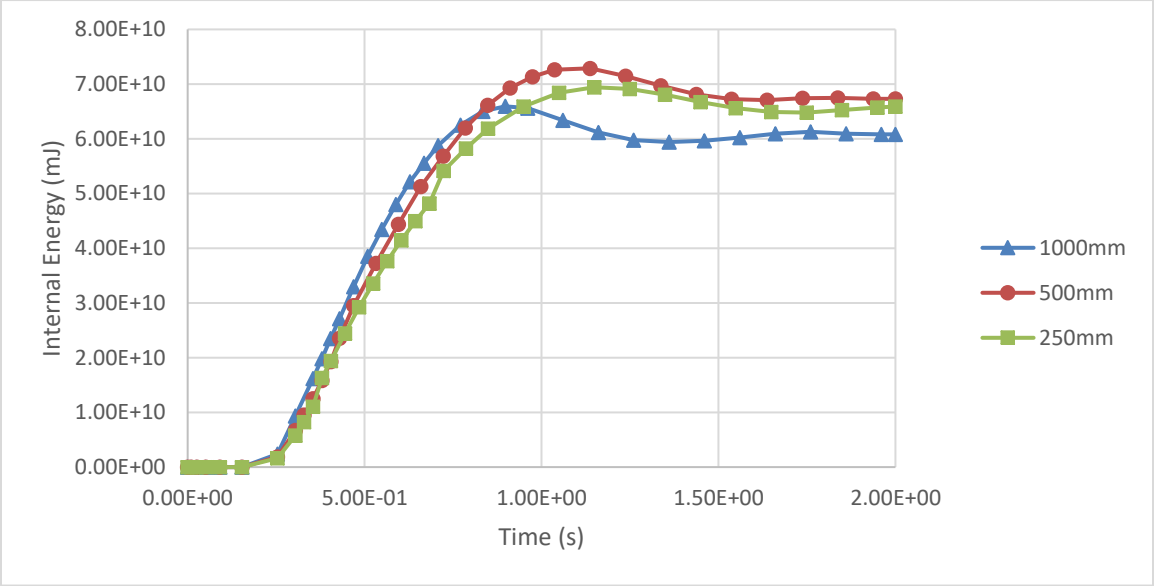

Figure 6-18: Variation of the average internal energy sampled at the location shown in Figure 6-14 as a function of time

The results illustrated in Figure 6-15 indicate that the 500 mm and the 250 mm models exhibit near identical behaviour in the elastic region of the stress curve. Following yielding, the models should have similar behaviour in their post-yield regime with the stress in the 500 mm and the 250 mm models reducing to minimum values of 218 MPa

276 MPa, respectively. After 1.0 s (during the rebound regime of the cylinder), both curves exhibit similar behaviour until diverging at t=1.8s (well after onset of the collision event). While the 1000 mm exhibited a similar trend to the 500 mm and the 250 mm models prior to the material yielding, the stress magnitude reached only to a maximum of 309 MPa, where it should have reached 350 MPa as in all cases. After material experiences yielding, the material stress in the model suddenly dropped and then gradually increased to 338 MPa. This abnormal behaviour suggests that an element size of 500 mm would be the minimum capable of simulating reasonable results in the collision area during a full scale STOPC using the defined parameters, and due to the similarity in behaviour of the 500 mm and 250 mm models, the models are approaching to the converged solution.

Figure 6-16 shows that the radial displacement values at the selected collision node produced by all models are in very close aggreeance until t=1.0s, at which stage they begin to diverge. The 1000 mm model produces the greatest divergence from the 250 mm model at t=2.0s, and the 500 mm model displaced roughly three times the magnitude produced by the 250 mm model. This shows that while the 250 mm and 500 mm models may show similar stress patterns during the collision event, the 250 mm model absorbs more energy in the collision area than the 500 mm model. A contributing factor to this difference is the artificial increase in stiffness resulting from using a coarse mesh.

Figure 6-18 shows that the total internal energy exhibited by the 500 mm model is very similar to the 250 mm model, with a maximum energy difference of 6.1% at t=0.85s. The

maximum difference in internal energy of the system between the 1000 mm model and the 250 mm model occurs at t=1.26 seconds.

From the comparisons above, it can be concluded that a model with similar parameters (which is investigated in the following section), a mesh size of 500 mm or 250 mm is adequate to accurately simulate the VM stress patterns resulting from a STOPC. However, in order to increase accuracy in simulating the resultant energy of the system and deformation, it is recommended that a finer mesh density be used. The finest mesh that could be investigated in this section was 250 mm due to computational constraints of the problem, which represent an element size 10x the thickness in the area of interest (10t). It is evident from these analyses that the mesh had converged during the collision event for the VM stress pattern, radial y-displacement in collision area, and the total kinetic energy of the system, but did not produce converged displacement results of the system in the post collision regime.

As the results of this section had only partially converged given the mesh density, the full scale STOPC model presented in Section 6.5 will be created using a varying density mesh with a relatively coarse mesh outside the direct collision area, and with general element size of t to 2t within and surrounding the collision area. Using such a mesh density for the full scale analysis should ensure results with a reasonable accuracy.

6.5 INVESTIGATION OF NOISE AFTER COLLISION FOR VM STRESSES OF EXPLICIT COLLISION ANALYSES

Due to the level of spurious oscillations found in the explicit collision analyses once the material had stressed beyond its yield strength (as seen in the VM stress graphs presented in Section 6.6.8), additional explicit analyses were performed to determine whether an increase in the time step would have an effect on the somewhat stochastic numerical results. Therefore, the stiffened cylinder model presented in section 6.3 was analyzed explicitly using ELFORM2 with time increments of 0.1s, 0.01s, 0.001s while keeping all parameters as presented in Section 6.3. The VM stresses for this study are presented in Figure 6-19.

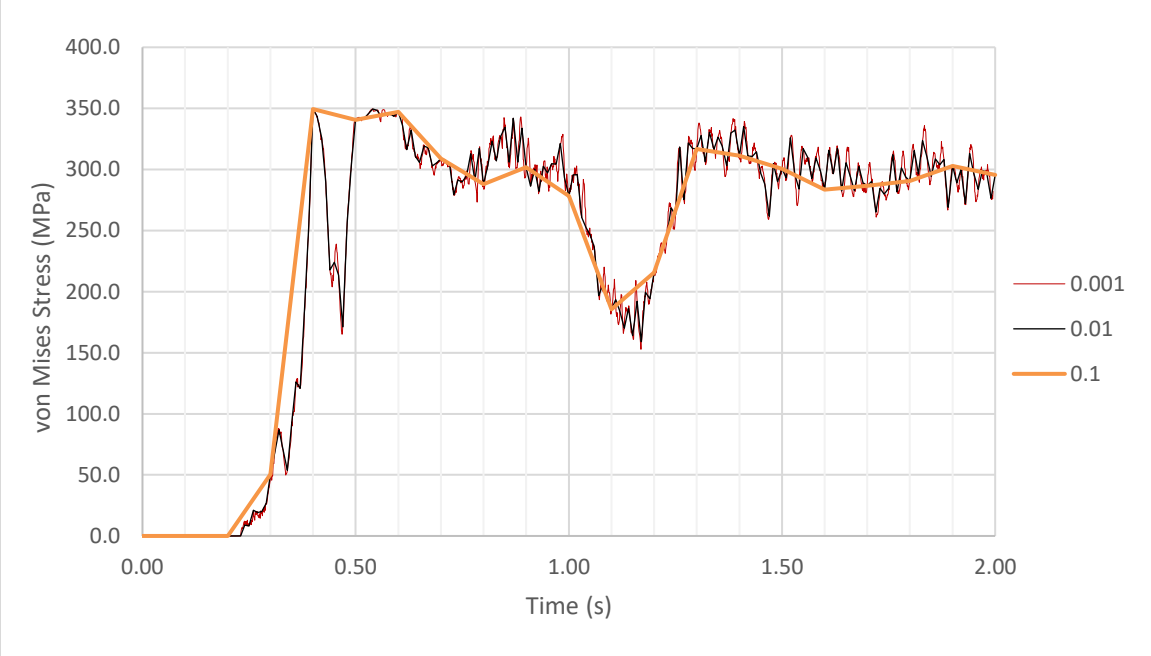

Figure 6-19: Variation of von Mises stress as a function of time in element 72554 obtained by the various time steps used in the collision analysis

As shown in Figure 6-19, the VM stresses for ELFORM 2 are very similar regardless of time step used in the fully explicit analyses. Bathe had also shown this behaviour when

analysing the numerical noise resulting in the analyses of an impact event of a bar [79]. From Figure 6-19, it can be concluded that decreasing the time step will not cause reduction of post-collision spurious oscillations in a STOPC assessment.

6.6 Full scale STOPC assessment of an Offshore Exploration Vessel and Vertical Monopole

6.6.1 Model Parameters and Mesh Density

The benchmark marine vessel used for the full scale STOPC analyses is an offshore research vessel with total length 83150 mm, transverse frame spacing 800 mm, and a total of 105252 elements and 79889 nodes. The model was produced entirely using Hypermesh FEA and is shown in Figure 6-20:

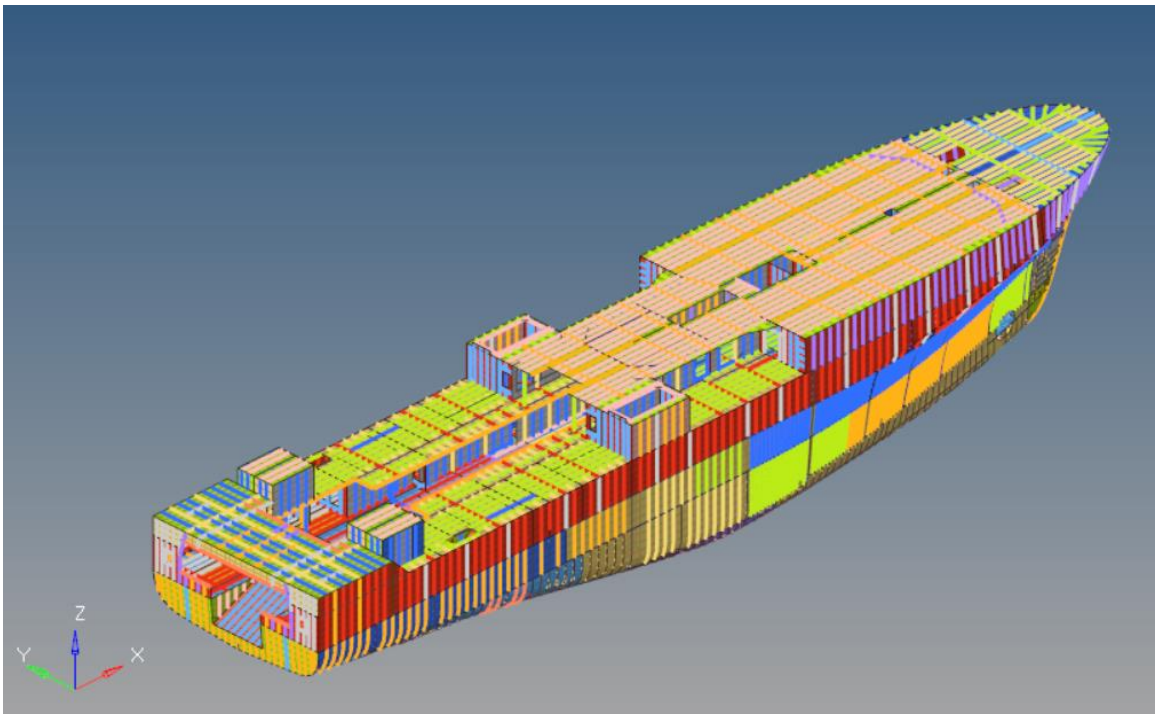

Figure 6-20: Coarse model of the benchmark offshore research vessel used for analyses

The benchmark model used has been modelled using an element size of roughly 800 mm in the coarse region. The average hull thickness in the collision area is 22 mm, while the average deck thickness is generally 6 mm-8 mm across all decks. Web stiffeners generally have thicknesses of 8 -10 mm. All bulb flat stiffeners throughout the model have been simplified as angles using DNV angle equivalent approximation rules. All girders have been modelled as 2D shell elements. Minor hull stiffeners and girder flanges outside the collision area have been modelled using 1D beam elements. A typical deck underside outside the collision area is as shown in **27** and Figure 6-22:

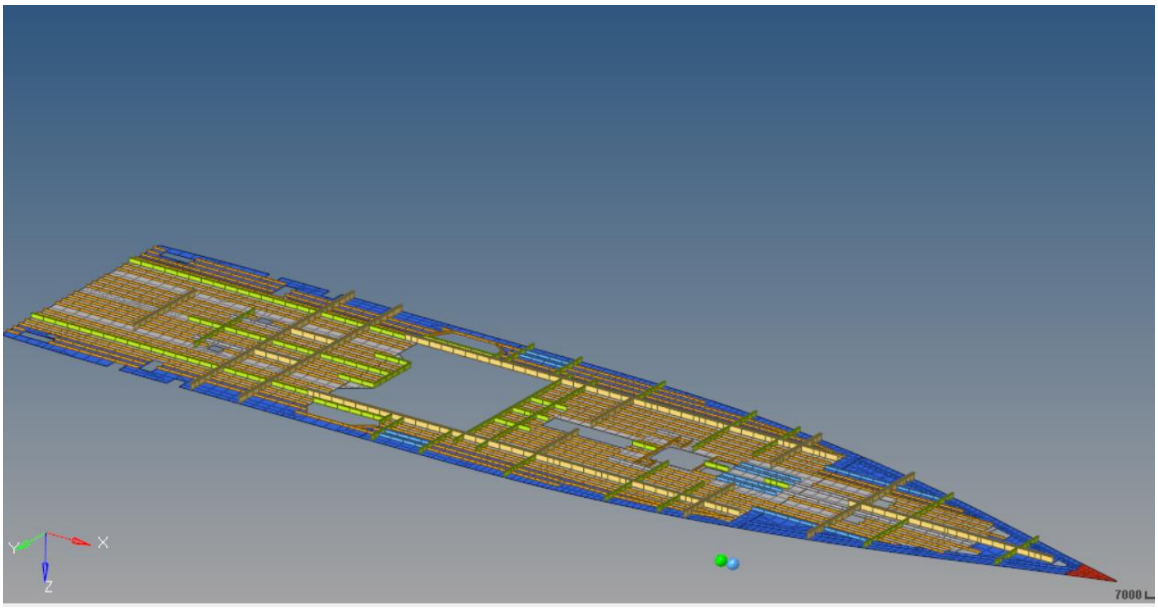

Figure 6-21: Typical deck underside of offshore research vessel (global reverse isometric view)

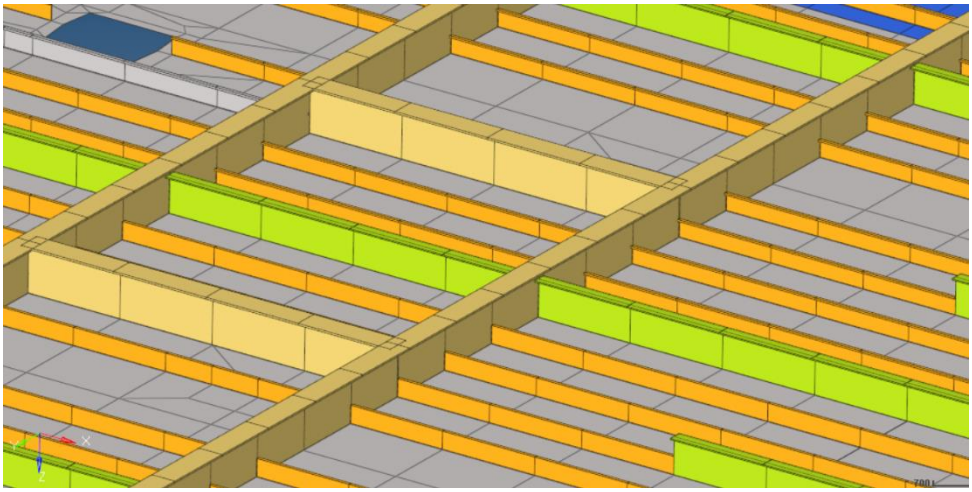

Figure 6-22: Typical deck underside of offshore research vessel (magnified, reverse isometric view)

Vessel plate elements within the collision area have been refined to average dimensions of 25-50 mm. The area with this level of refinement spans 11 m in the longitudinal direction, 3.8 m in the transverse direction, and the entire height of the vessel. The refined region is shown as white within a full shaded isometric view of the vessel within Figure 6-23, and is shown in detail in Figure 6-24:

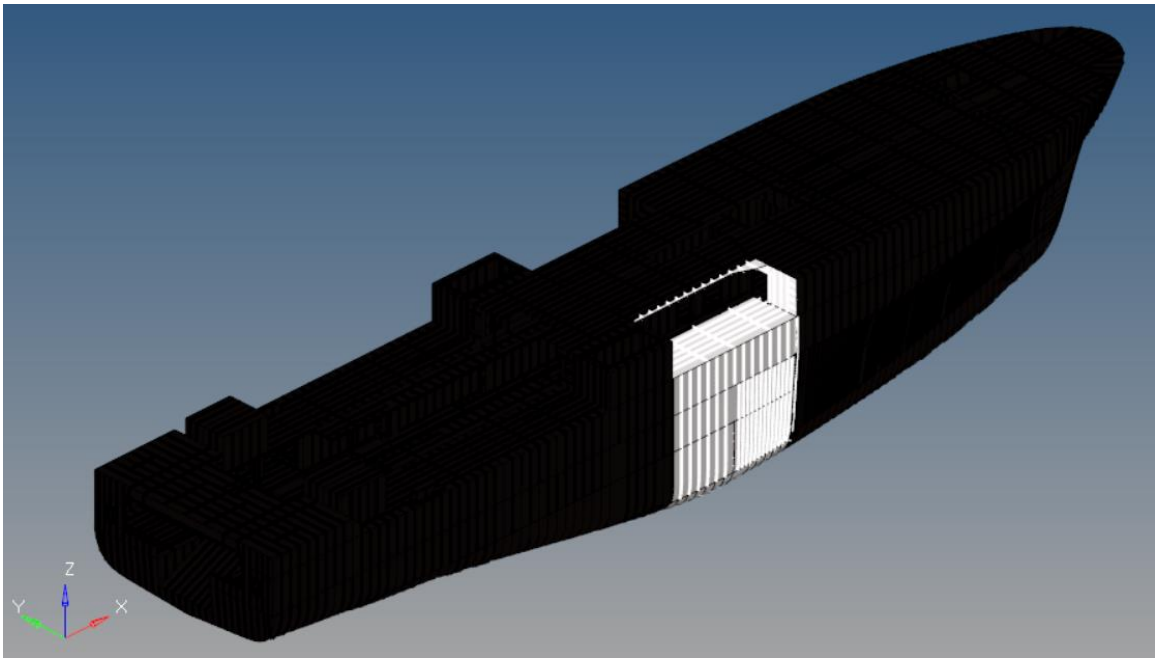

Figure 6-23: Refined region of the offshore research vessel model

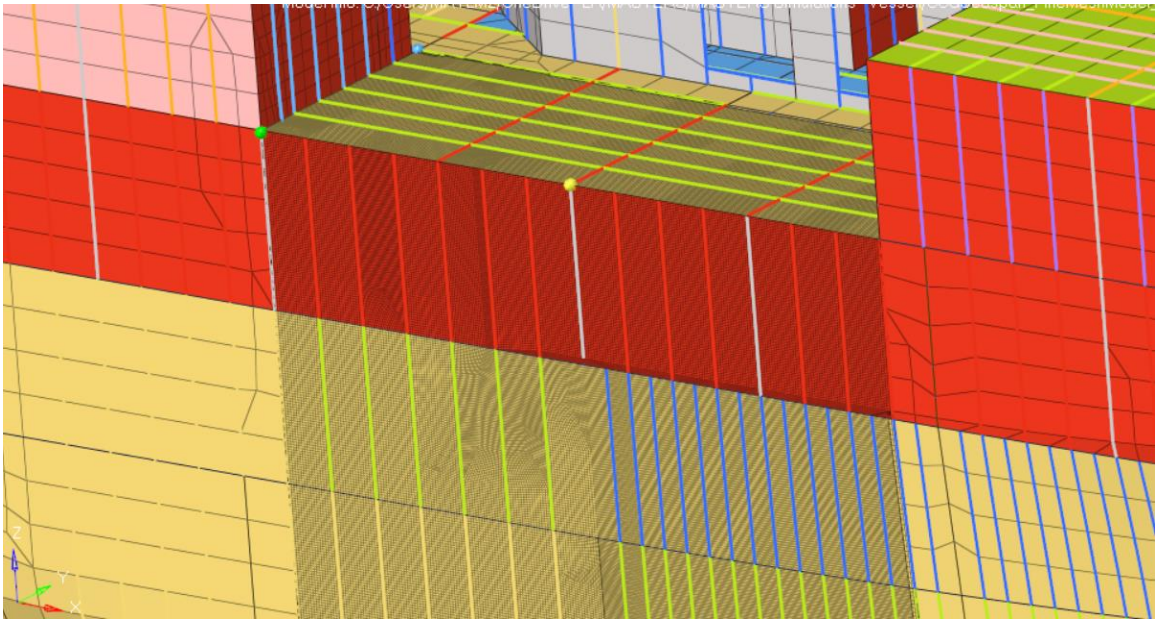

Figure 6-24: Magnified view of the refined region of the offshore research vessel

Similar to the stiffened cylinder model, adaptive mesh refinement algorithms were not used during these analyses, as this would cause difficulty in directly comparing element formulations across models. Within the collision region of the model represented in

Figure 6-24, all stiffeners, girders, and beams have been modelled using 2D shell elements. In addition, brackets and sniped stiffener connections have been included to ensure proper shear and moment transfer.

The vertical monopole column diameter of 7.0 m has been selected for broadside collision through all analyses with wall thickness 100 mm. This diameter has been selected based on NORSOK provided local indentation curves, as it is within the bounds of cylinder diameters shown in Figure 4-17. The wall thickness through these simulations will not, however, come into effect as the vertical column has been modelled using rigid 2D elements.

6.6.2 Simulation Parameters

The offshore research vessel was assumed to be approaching the monopole Starboard side at a velocity of -7.1 m/s (in the direction of the radial depth of the monopole). This velocity was chosen using NORSOK standards of maximum broadside collision speed of a marine vessel with a stationary object in the North Sea. While mass has been included, vertical acceleration due to gravity was not considered for simplicity purposes. Automatic implicit to explicit switching was used to maintain the accuracy provided by explicit analysis while allowing timesteps which were not involved in the collision to be simulated implicitly.

6.6.3 Boundary Conditions:

Similar to the stiffened cylinder collision assessment discussed in Section 6.3, no boundary conditions were used to constrain the marine vessel as the entire vessel was modeled. Pinned constraints were used at all nodes at the top and bottom of the monopole section shown in Figure 6-3.

6.6.4 Element and Material Formulations

Similar to the stiffened cylinder STOPC analyses completed in the previous section, element formulations {1,2,6,7,8,10,11,16,25,26} have been explored using the simple linear elastic material (MAT 1). It was found that due to the complexity of the model, MAT 1 was not sufficient as its use caused several errors. Consequently, the piecewise linear plasticity material (MAT24) was used to model the vessels material with a stress-strain curve that allows the inclusion of strain rate effect and strain hardening, with parameters as shown in Table 6-2. This selection resulted in a greater stability when running the model and resolved several convergence issues that arose when using MAT 1.

Table 6-2: Summary of MAT24 parameters used to represent vessel

Parameter	Value
Modulus of Elasticity (MPa)	350×10^{5}
Density (ton/mm^3)	7.89×10^{-9}
Poisson Ratio	0.3
Yield Stress (MPa)	355
Tangent Modulus (MPa)	207

While steel grades of AH36, Grade A, and Grade B steel are typically used in marine vessel construction, the entire vessel has been assumed to contain AH36 steel for simplicity purposes, with a yield strength of 355 MPa throughout the vessel.

The vertical monopole has been modelled using rigid 2D shell elements to maximize energy transfer within the marine vessel and consequent deformation. All 1D elements throughout the model (beams/ stiffeners, stringers in the coarse mesh area, and pillars) were modelled using ELFORM 1, which requires an integration beam formulation as well as a section beam formulation. While this method of modeling beams is more labor intensive due to the requirement of two cards vs one (example: beam ELFORM 3), it was necessary to use it over the less demanding beam formulations such as ELFORM 3, so that it would be compatible with both implicit and explicit solvers. ELFORM 3 is a less intensive method for modeling 1D elements, but as the full scale STOPC analysis involved implicit/explicit switching, the use of ELFORM 1 beam was necessary.

6.6.5 Contact Control Cards

Due to the complexity of the full-scale vessel model, early iterations of the analyses showed excessive internal contact due to the level of deformation and internal geometry of the vessel. Consequently, two contact control cards were used to accurately simulate contact taking place throughout the analyses: one for contact between the vertical monopole and the vessel, and the second for self-contact of the deformed vessel.

The Mortar contact option within LS-DYNA is a very robust penalty-based segment to segment contact algorithm where the contact tractions are proportional to the penetrations of segments as well as their overlapped area. The contact between the vessel and the monopole was simulated using automatic mortar surface to surface contact, while self-contact of the vessel was simulated using automatic single surface mortar contact.

6.6.6 Solver Control Cards

*CONTROL_IMPLICIT_AUTO with automatic time step control, optimum equilibrium iteration count of 100 per time step, allowable iteration window of 1.0e-6, minimum time step of 0.2 seconds, maximum time step of 3 seconds and a specified Kcycle failure of 10,000 was used for the full scale vessel collision analysis. The time step bounds were selected for implicit analysis to prevent a non-converging solution, and to output an error message if the analysis was not moving forward at a reasonable rate. It is recommended that a minimum allowable timestep be used for all analyses, as it was found that if there are no limitations on this parameter, the timestep can continually reduce without converging on a solution. The definition of a minimum timestep would facilitate identification of a non-convergence issue if it is to occur at an earlier time, allowing the appropriate parameters to be adjusted and the implicit to explicit switch to be triggered.

The control card: "*CONTROL_IMPLICIT_DYNAMICS" was used with the IMASS of 1, which invoked a dynamic analysis using Newmark time integration . The Newmark time integration constants of 0.6 for Gamma and 0.38 for Beta were used. While these values are within the range prescribed by the LSTC theory manual [63], the specific

values used were recommended for general collision analyses by LSTC and may be further optimized.

After the collision event, there is no need to run the model explicitly if the intent of the analysis is to determine the total deformation or energy dissipation of the vessel. For this reason, *CONTROL_IMPLICIT_GENERAL with IMFLAG 5 (implicit with automatic switching and mandatory implicit finish) was used instead of IMFLAG 4 (automatic switching without mandatory implicit finish) for the full-scale collision analysis to reduce overall analysis time.

*CONTROL_IMPLICIT_SOLUTION with a divergence flag of 2 was used to allow for iterative correction of the FE model in areas where divergence would have otherwise been an issue. If there are any mesh quality issues in a given model (which, for a full-scale vessel model is very likely in the coarse areas), then the use of this flag is highly recommended.

6.6.7 Additional Control Cards

There are several hourglass control types within LS-DYNA, but as the full scale STOPC simulation involves the yielding portion of the stress-strain curve, hourglass control type 7 (IHQ 5) was used to allow any element with material remaining within the elastic region to return to its original shape after the collision event. This is realistic, as only the

material that has undergone inelastic deformation would not be returning to its original form.

A control accuracy card, which helps to improve accuracy of the results, was present throughout the analyses. The EQ4 formulation was used as it is applicable for both shell, thick shell and solid elements. Several other control accuracy equations (such as eq -4 and eq-2) were not used as they are not applicable to triangular shells (which were present throughout the model outside the collision area.

6.6.8 Results

The VM stress and Y-displacement values have been plotted in the area of interest for the full-scale collision analysis. Implicit-explicit switching was used as it was found to be the most efficient solver selection for the simulation of collision between two structures, as discussed in section 6.3.5. The only element formulation capable of running a full scale STOPC of the chosen complexity to completion without error using implicit/explicit switching was ELFORM 16/-16. Upon investigation of the LS-DYNA error files resulting from the various analyses, this was found to be due to elements in violation of heuristic shape criterion and issues arising from highly deformed elements during the collision assessment. Consequently, if implicit-explicit switching is to be used, it is highly recommended that ELFORM -16 be selected for full scale collision assessment. Consequently, the results for element formulation -16 have been presented in the plots of this section. The total run time required for this analysis was found to be 31,438 seconds.

To compare the computational times of running ELFORM -16 with implicit / explicit switching and running the analysis explicitly using other recommended element formulations, four additional analyses were performed explicitly as discussed in section 6.6.9.

Plots showing the Y-displacement of the vessel with reference to the vertical monopole are presented in Figure 6-25 to Figure 6-27. The elements and nodes selected for stress and displacement plotting are as shown in Figure 6-28 and Figure 6-29. Figure 6-30 to Figure 6-34 show the VM stresses experienced by the vessel as a result of the collision at various times. Figure 6-35 to Figure 6-39 show plots of the displacement of the vessel as a function of time.

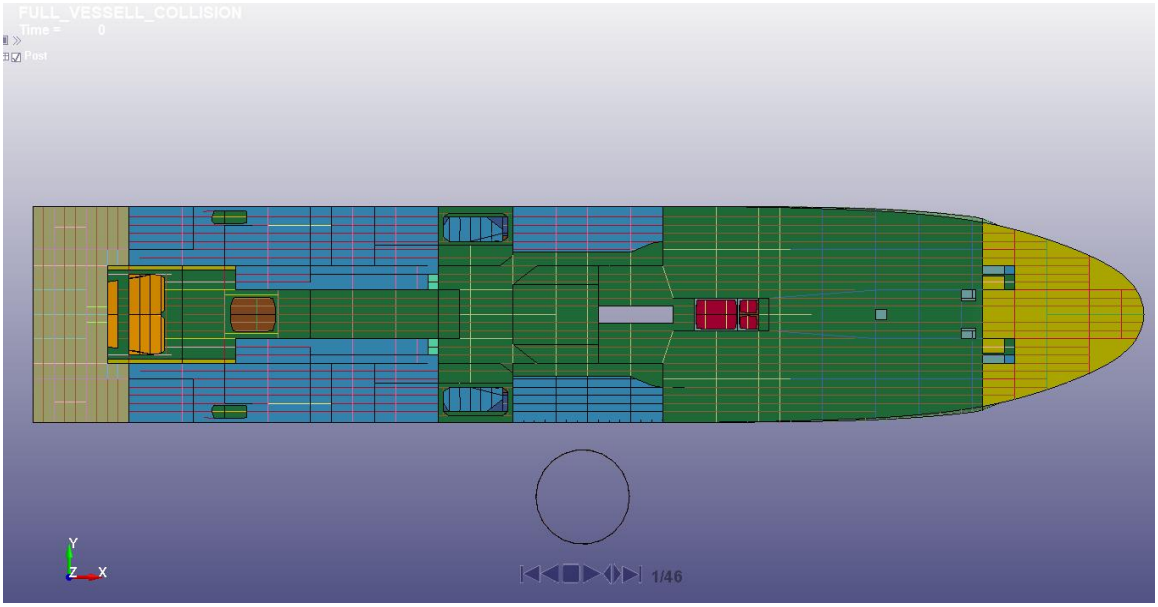

Figure 6-25: Vessel at t=0

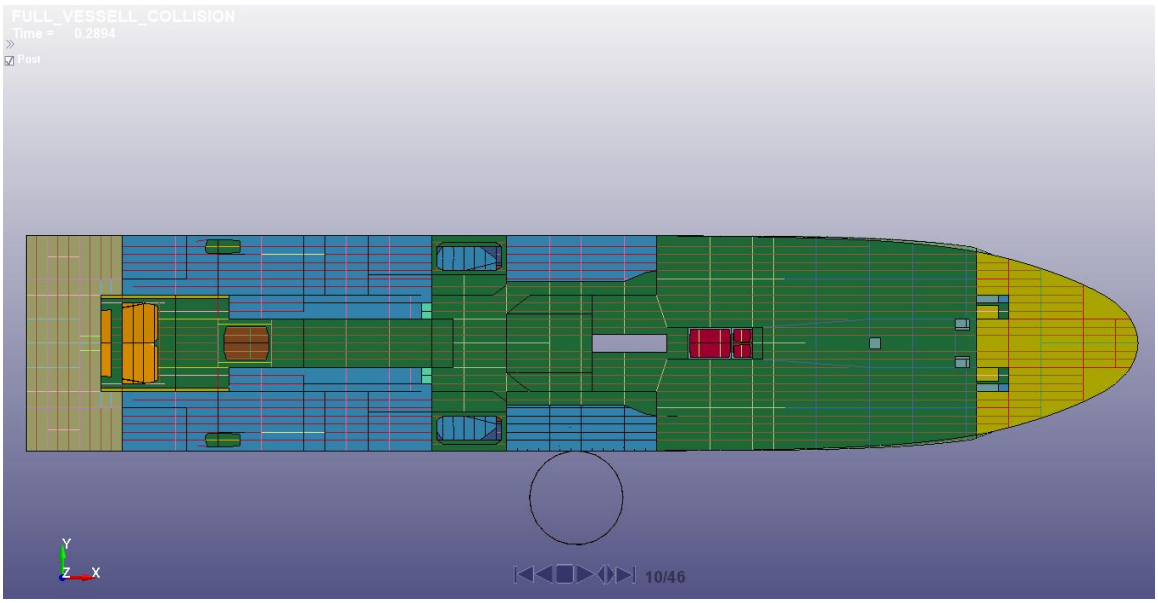

Figure 6-26: Vessel at t = 0.29s

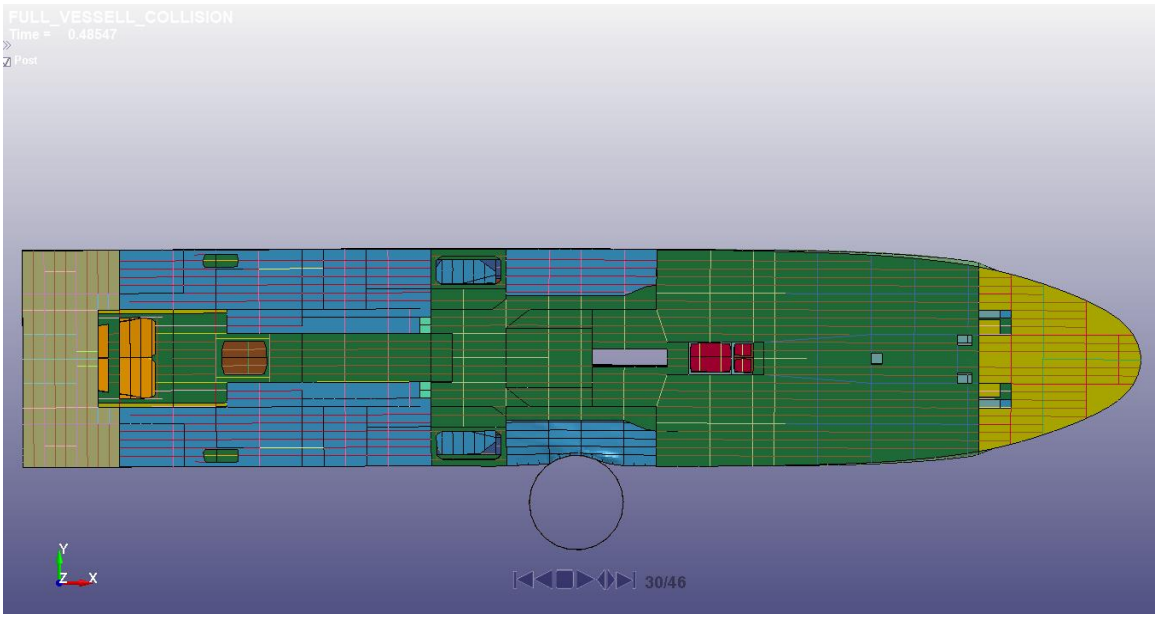

Figure 6-27: Deformed vessel at t=0.485s

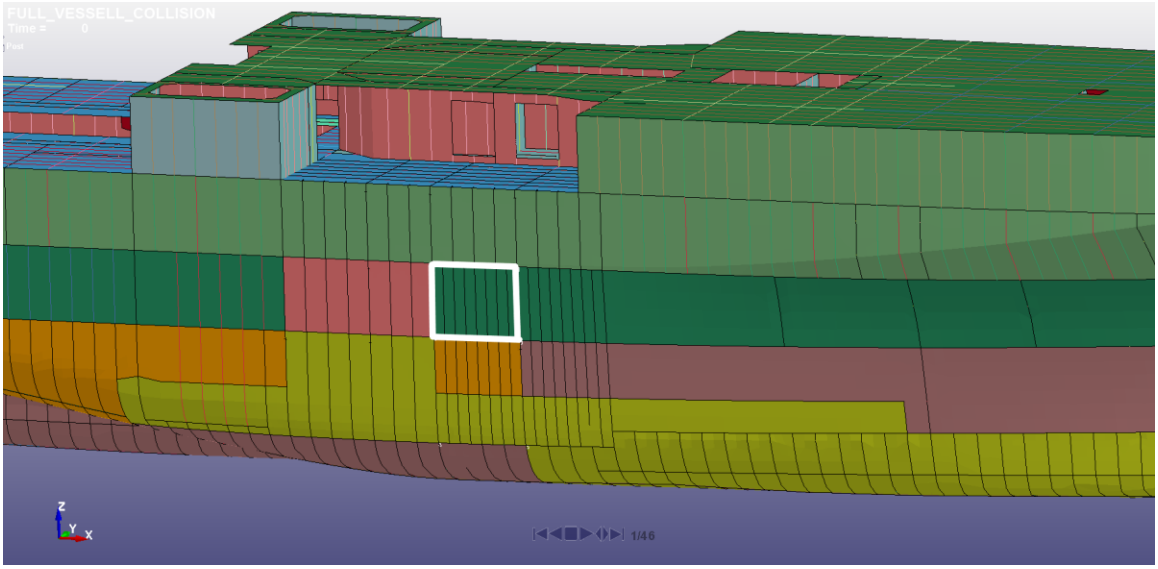

Figure 6-28: Hull elements selected for stress plotting (elements outlined by white)

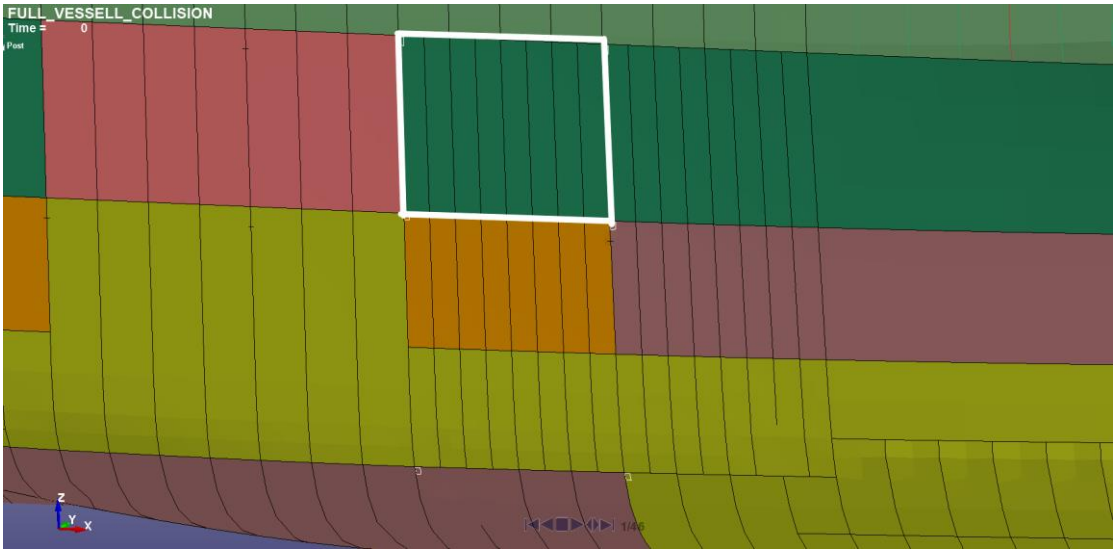

Figure 6-29: Elements selected for stress plotting, magnified view (elements outlined in white)

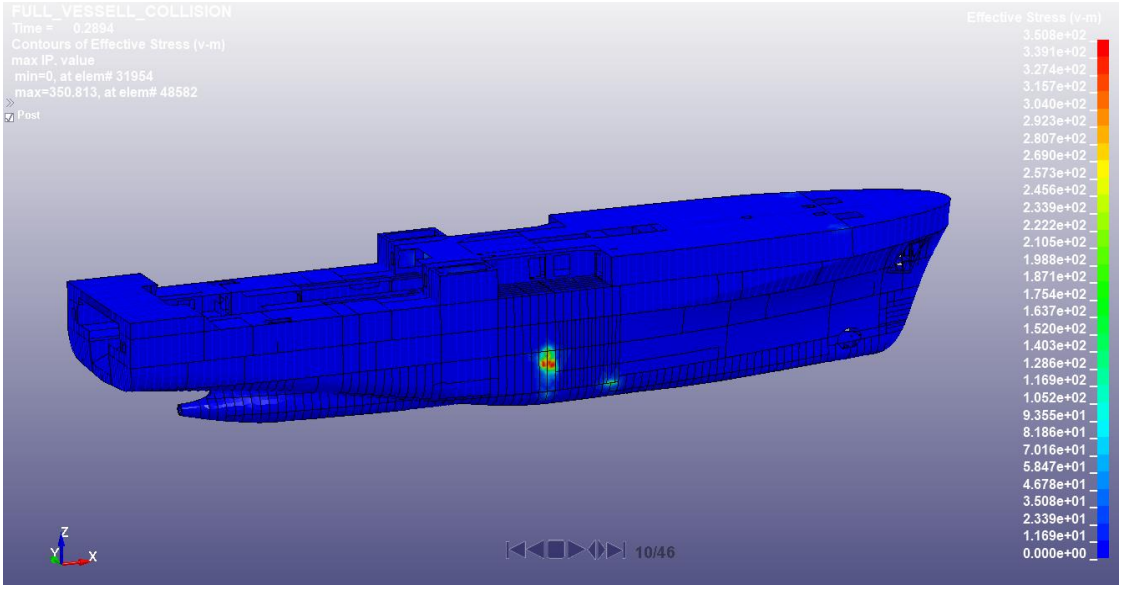

Figure 6-30: Distribution of VM Stress plot at t=0.2894s, full scale vessel collision, ELFORM -16, monopole hidden

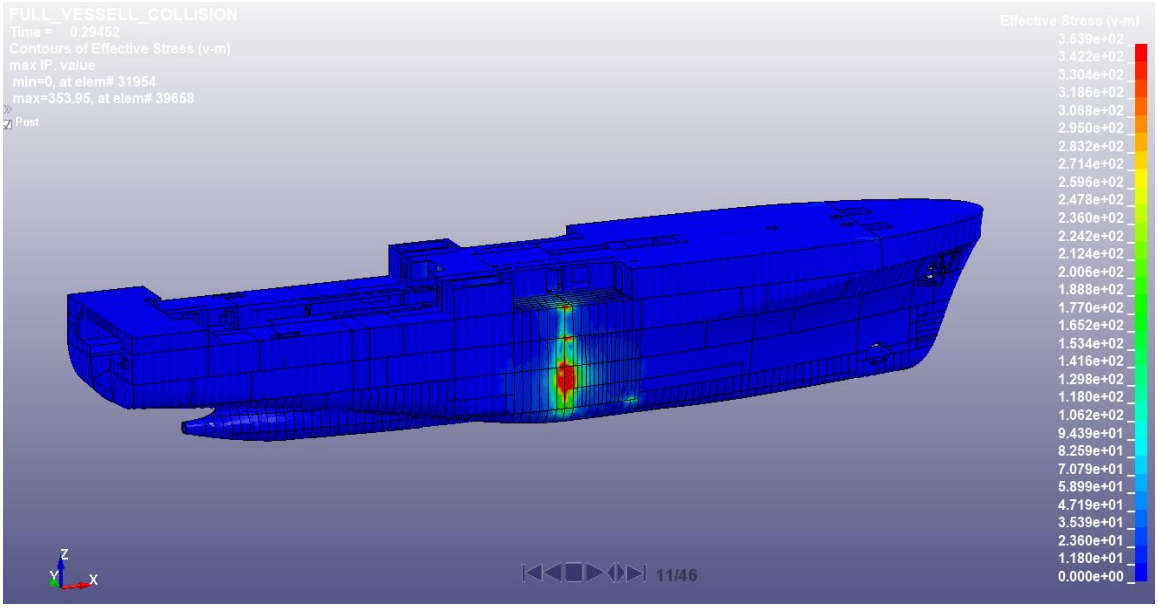

Figure 6-31: Distribution of VM Stress plot at t=0.2946s, full scale vessel collision, ELFORM -16, monopole hidden

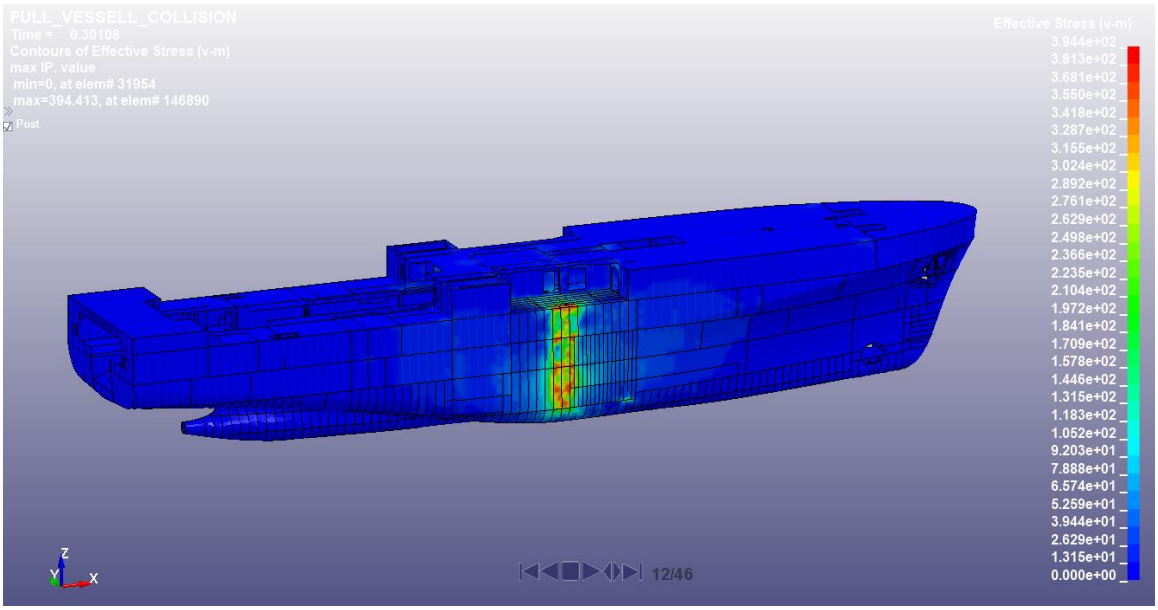

Figure 6-32: Distribution of VM Stress plot at t=0.3011s, full scale vessel collision, ELFORM -16, monopole hidden

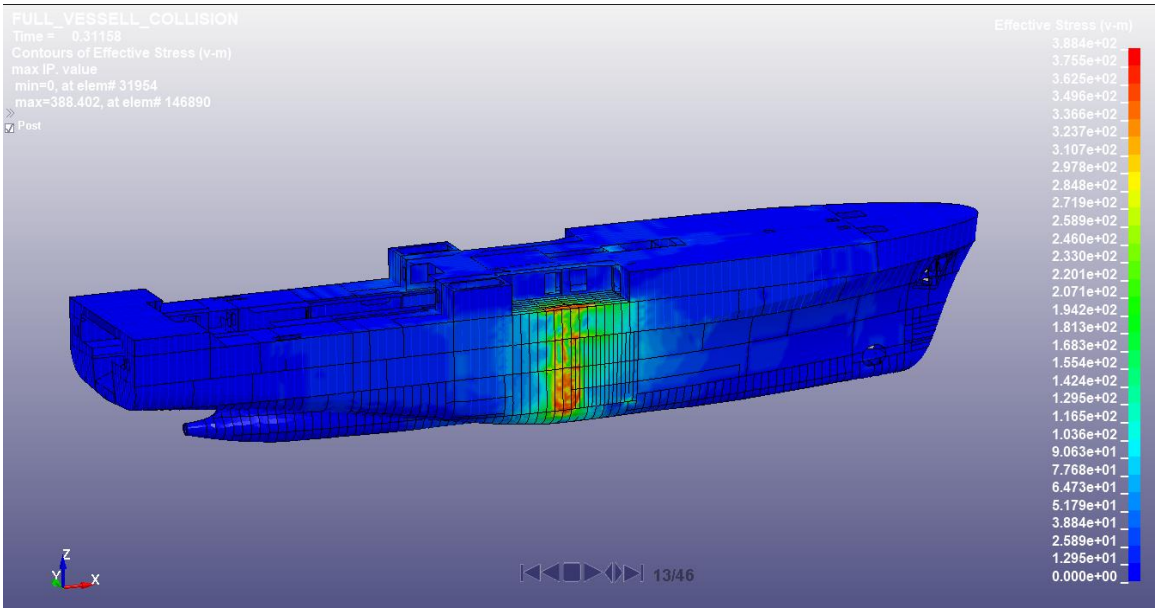

Figure 6-33: Distribution of VM Stress plot at t=0.3116s, full scale vessel collision, ELFORM -16, monopole hidden

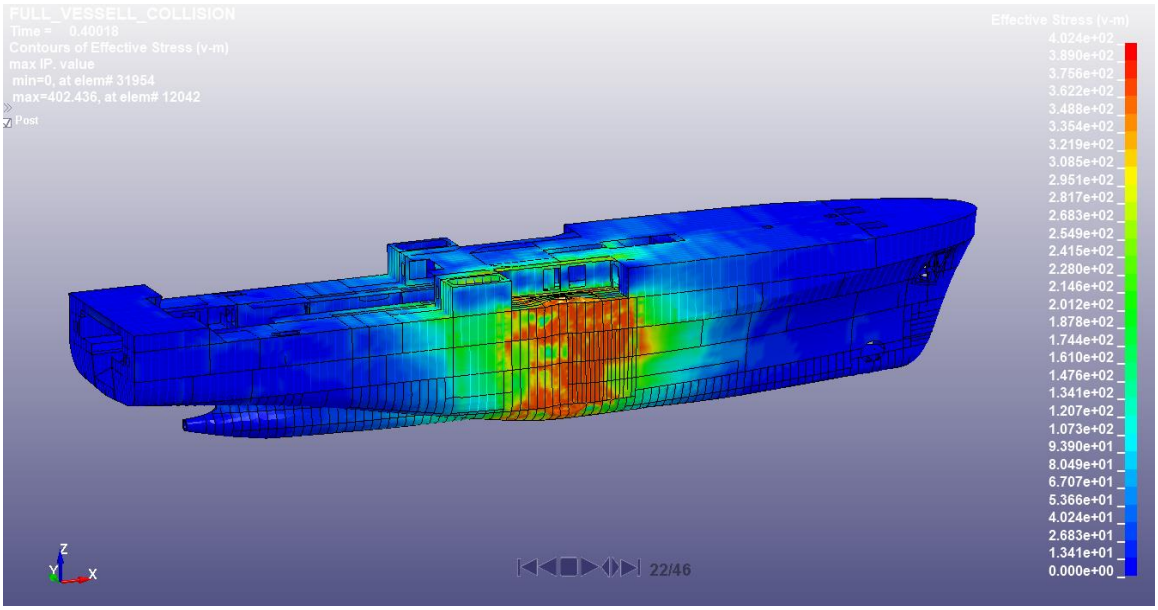

Figure 6-34: Distribution of VM Stress plot at t=0.4002s, full scale vessel collision, ELFORM -16, monopole hidden

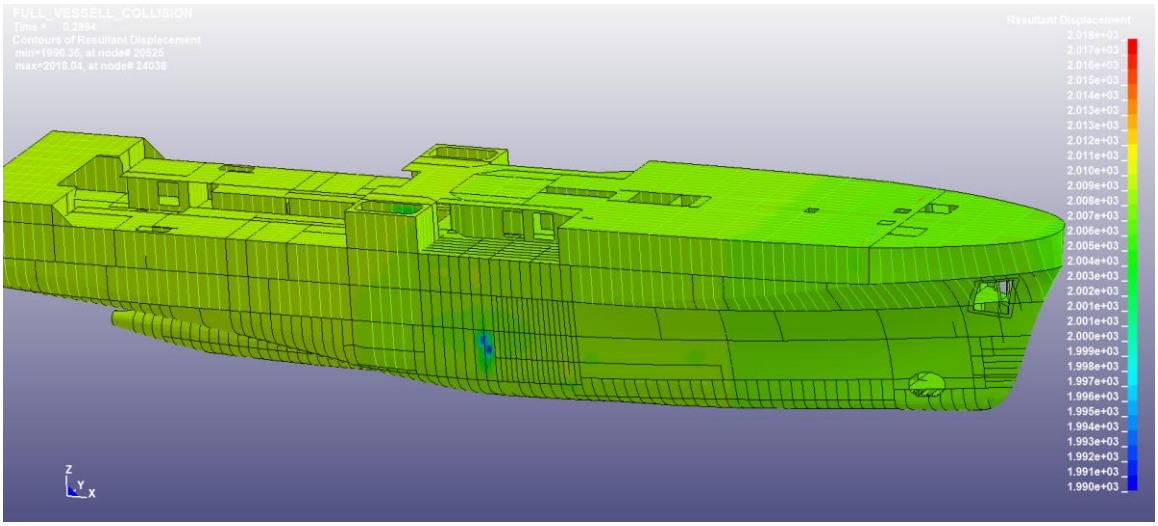

Figure 6-35: Resultant Displacement plot at t=0.2894s, full scale vessel collision, ELFORM -16, monopole hidden

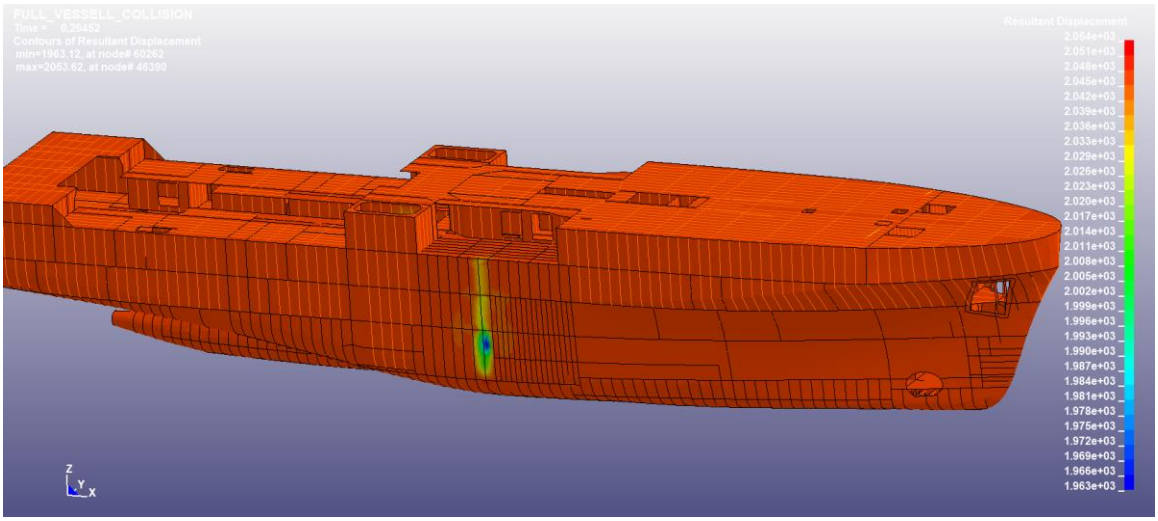

Figure 6-36: Resultant Displacement plot at t=0.2945s, full scale vessel collision, ELFORM -16, monopole hidden

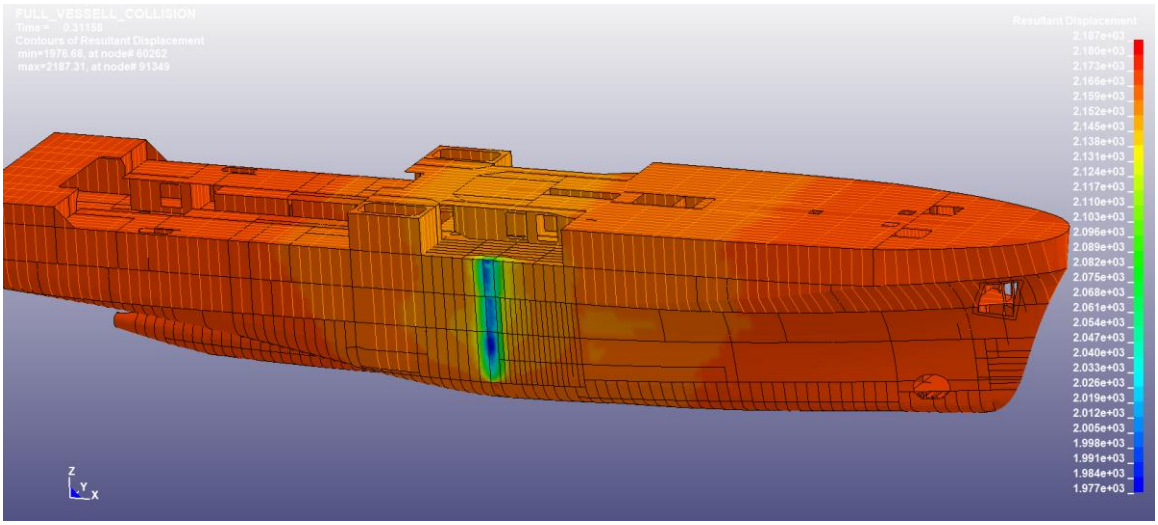

Figure 6-37: Resultant Displacement plot at t=0.3116s, full scale vessel collision, ELFORM -16, monopole hidden

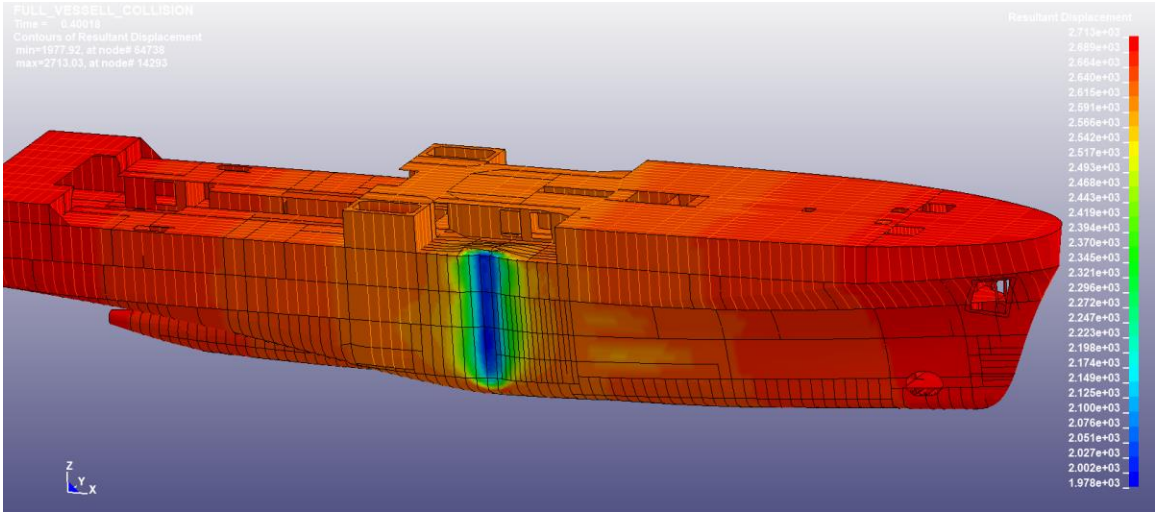

Figure 6-38: Resultant Displacement plot at t=0.4002s, full scale vessel collision, ELFORM -16, monopole hidden

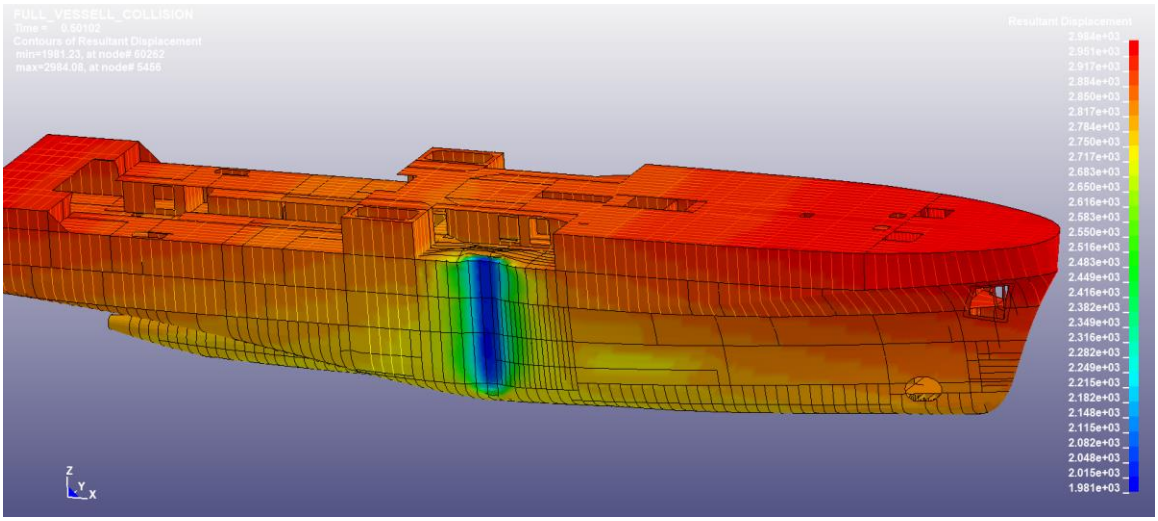

Figure 6-39: Resultant Displacement plot at t=0.5010s, full scale vessel collision, ELFORM -16, monopole hidden

6.6.9 Comparison of CPU Run Times

Five additional analyses were performed to compare the CPU times in the full scale STOPC analyses performed completely explicitly, and those run with implicit / explicit switching. The CPU times are summarized in Table 6-3. Unlike the previous analyses

presented within this thesis that were performed on the PC, these analyses were run on a 120 CPU core Intel Xeon Cluster configured on LINUX with the assistance of LSTC Support (Cincinnati, Ohio office). This is largely because the estimated time to run the full scale STOPC simulations using ELFORM 2 (the most efficient shell formulation) solved fully explicitly using an 8 CPU HP EliteBook 8570w was estimated to be roughly 5092 hours by LS-DYNA. This analysis was not completed due to the computational time required. The estimated time is nonetheless far greater than the roughly 9 hours of CPU time required to analyze the same vessel on the EliteBook when shell ELFORM -16 was used along with the implicit/explicit switching option.

Table 6-3: Summary of the analysis schemes performed on LSTC 120 CPU core Intel Xeon Cluster configured on LINUX

ELFORM	Analysis Type
1	Fully Explicit
2	Fully Explicit
-16	Fully Explicit
16	Implicit / Explicit Switching
25	Fully Explicit

As shown in Table 6-3, models constructed with two of the more efficient 2D element formulations (ie. Belytschko-Tsay ELFORM 2 and Hughes Liu ELFORM 1) were run explicitly to compare the overall run time with the implicit/explicitly run (ELFORM -16). In addition, a model with ELFORM 16 was run explicitly to determine the total run time if solver switching was not used. A model constructed with ELFORM 25 was also run explicitly to determine the total run time of a full-scale vessel analysis when through-thickness stretch was taken into consideration. Representative elements were taken along

the hull of the vessel within the collision region, as shown in Figure 6-28. The variation of VM stress of one of these elements (19851) as a function of time is presented in Figure 6-40:

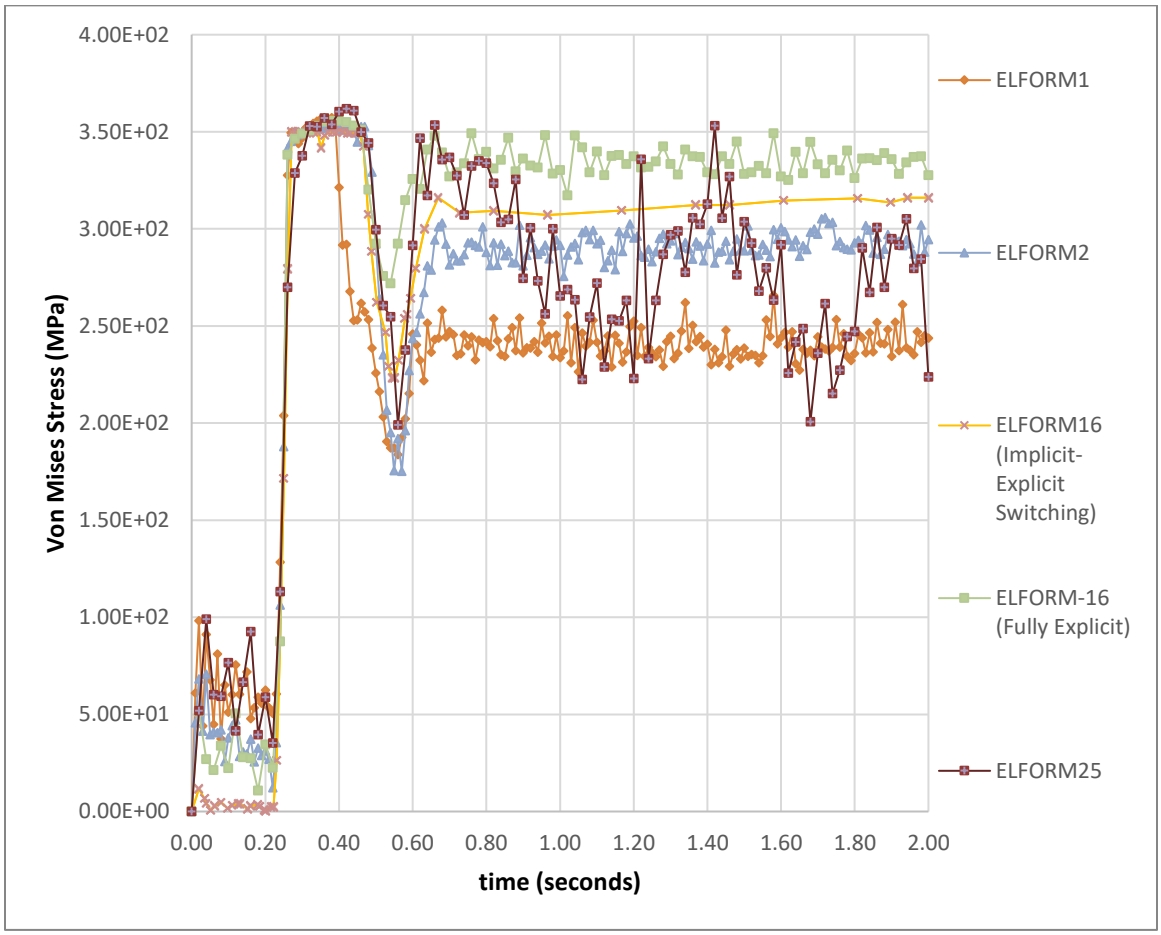

Figure 6-40: Variation of the VM stress of Element 19851 as a function of time in the full scale STOPC analysis

As seen in Figure 6-40, the results produced by all element formulations aside from ELORM 1 are in relatively good agreeance up to yield, but not post-yield. Prior to the collision event, there was a high level of noise in the results of all explicit analyses, several times greater than that produced by ELFORM 16 with implicit / explicit switching. In addition, the level of noise in the results after the onset of the collision

event is far greater with fully explicit formulations. A fully explicit simulation necessitates a consistent time step throughout the collision event and after the collision. A major advantage of the implicit / explicit switching formulation over a fully explicit formulation is the automatic reduction in time of explicit time steps during the collision event. The similarity between the VM stress results of ELFORM 16 run fully explicitly during the first 0.75s of the analysis, and ELFORM 16 run with implicit/explicit switching is shown in Figure 6-41.

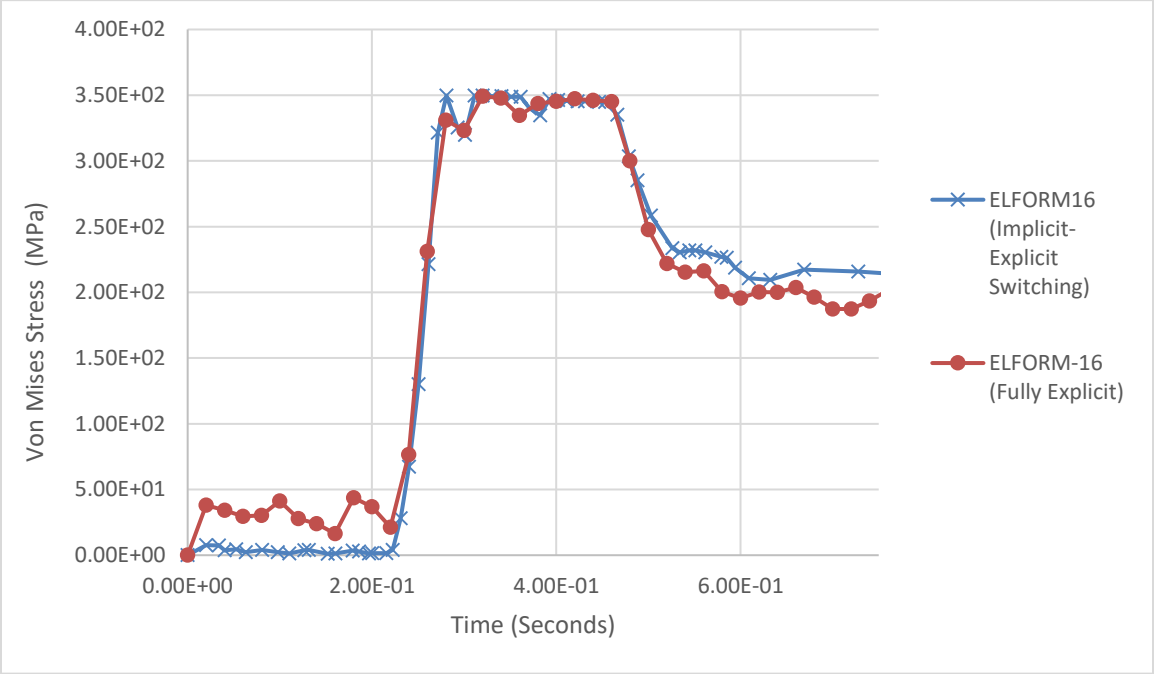

Figure 6-41: Variation of VM stress results as a function of time for full scale STOPC analyses performed with ELFORM 16, element 104588

As shown in Figure 6-41, the full scale STOPC analyses performed explicitly with implicit switching, and fully explicitly yield similar behavior during the event. While the VM stress results of these two simulations are very similar, the overall run time on the LSTC cluster for the analysis run explicitly was four times greater than the analysis run

with implicit / explicit switching using the same element formulation, as presented in Figure 6-45.

The resultant nodal displacement in the collision area as a function of time is presented in Figure 6-42.

the internal energy of the colliding structure, and the kinetic energy of the colliding structure as functions of time are presented in Figure 6-43 and Figure 6-44, respectively.

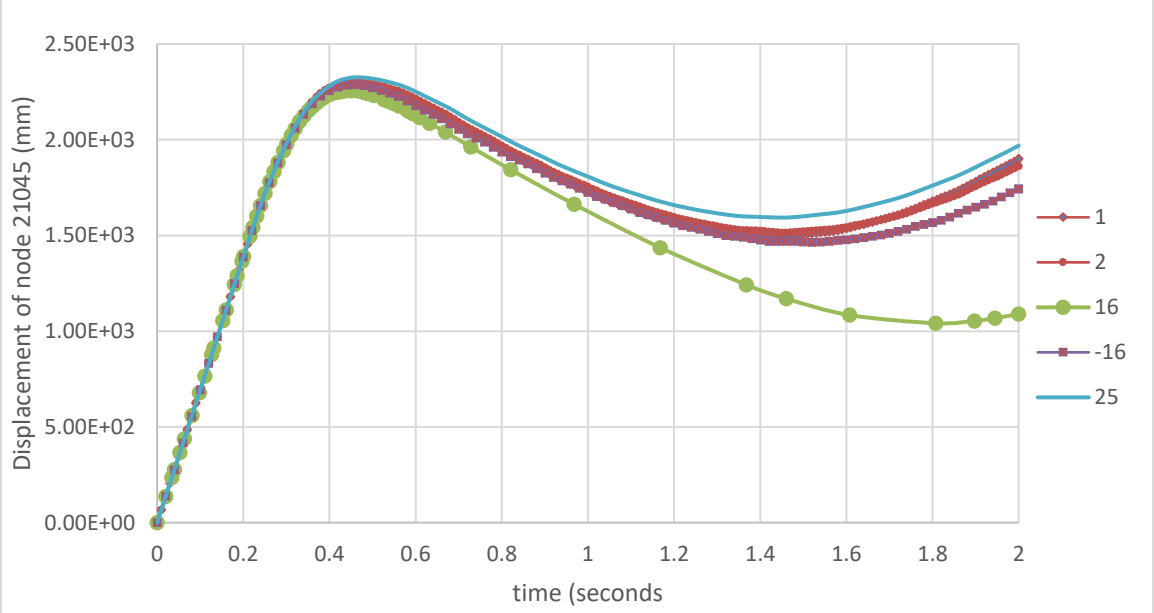

Figure 6-42: Relative Displacement of node 19851 as a function of time for full scale STOPC analysis

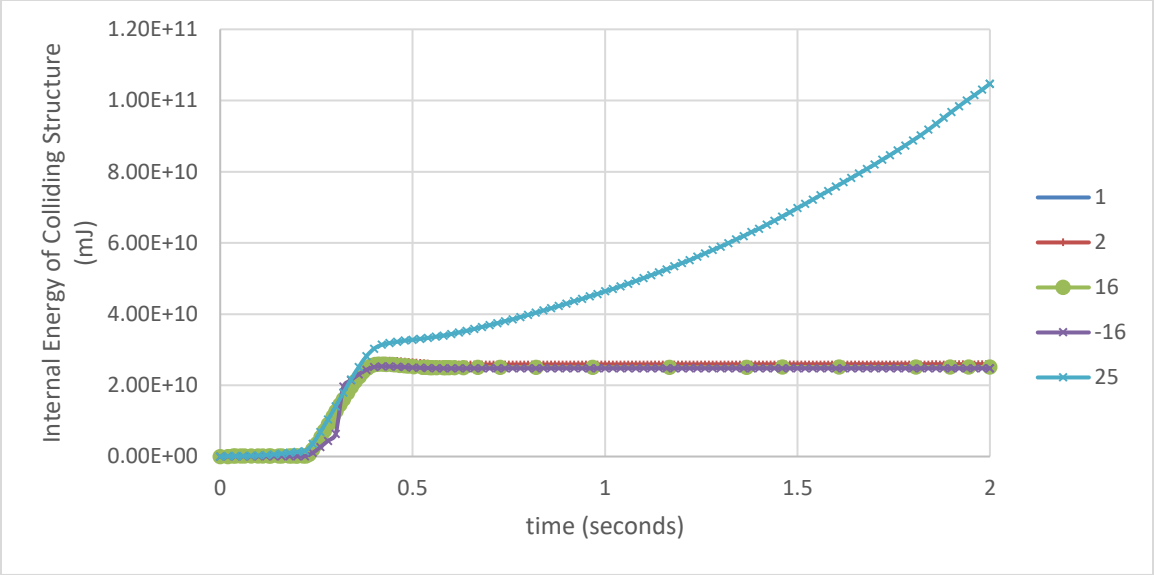

Figure 6-43: Internal energy of colliding structure as a function of time for full scale STOPC analysis

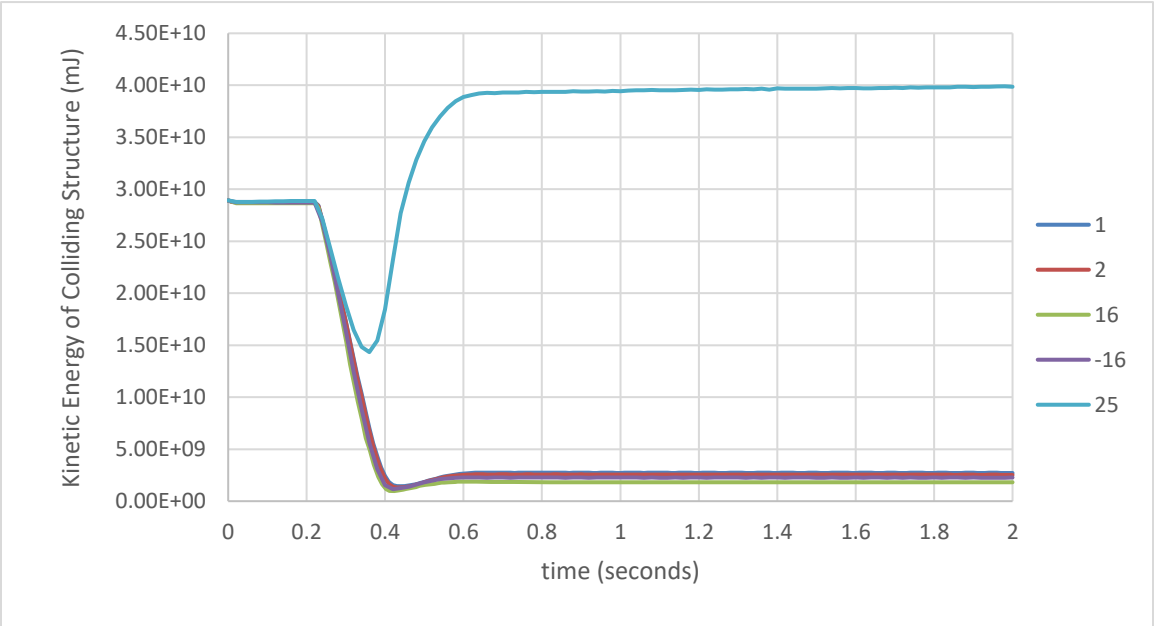

Figure 6-44: Kinetic energy of colliding structure as a function of time for full scale STOPC analysis

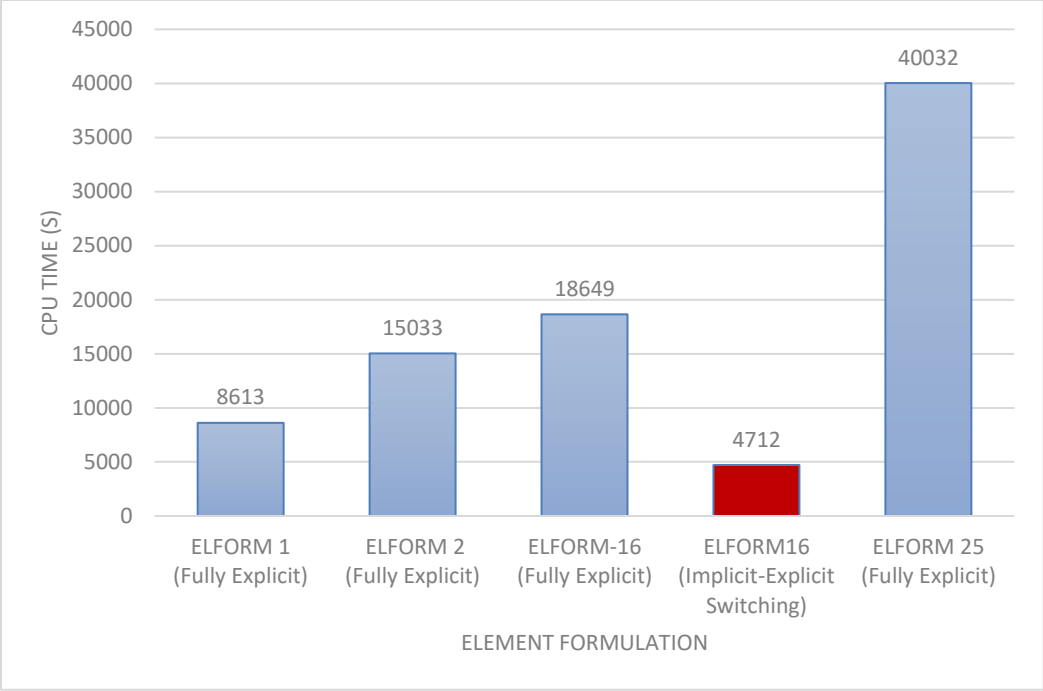

Figure 6-45: Comparison of CPU times for various fully explicit STOPC simulations (ELFORM 1, 2, -16, and 25) and full scale STOPC simulation ran with implicit/explicit switching (ELFORM 16)

As shown in Figure 6-42, there is a significant difference in the displacement of the colliding vessel after the STOPC event produced by the implicit and explicit analyses. The models have less than 3.0% difference in magnitude between the results produced by the upper and lower limits prior to t=0.4s. At t=0.5s the difference between the limits of the curves grows to roughly 10.2%, and reaches 74% by t=2.0s. This suggests that the rebound of the marine vessel resulting from a STOPC analysis is highly dependent on whether the problem is solved implicitly or explicitly.

Figure 6-43 and Figure 6-44 reveal ELFORM 25 to be a very poor candidate for STOPC analysis due to the overestimation of energies associated with the system. This may be due to the assumptions and additional terms associated with thickness stretch present

within the element formulation. Both the implicit and explicit solvers results showed near coincident behavior for both internal and kinetic energy history results.

It should also be noted that conducting a STOPC analysis fully explicitly on a personal computing system is largely inefficient and highly discouraged due to the high CPU consumption for models of this scale. This disadvantage of fully explicit collision analysis is not as significant when the problem is run on a 120 core LINUX cluster. Figure 6-45 indicates that running the analysis with implicit / explicit switching is still by far the most efficient method of running a full scale STOPC assessment. Running the STOPC analysis with implicit-explicit switching was found to be four times more efficient than the same simulation run explicitly. In addition, running the simulation with ELFORM -16 and implicit / explicit switching, the analysis took 54% the time of the same analysis run fully explicitly using the most efficient formulation; (i.e. ELFORM 1) at 8613 seconds.

7. SUMMARY AND CONCLUSION

7.1 SUMMARY OF WORK PERFORMED IN THIS THESIS

The following is a brief summary of the work performed in this thesis:

- The history and progression of Ship To Offshore Platform Collision Analysis was investigated, with specific focus on studies performed by Jorgen Amdahl and associates.
- Available standards for collision assessment were reviewed and compared to determine which one would provide guidelines for the analysis.
- The fundamentals of Ship Impact and Collision were discussed.
- The response of jacket type structures was briefly discussed. This included methods alternative to finite element tools and techniques.
- Modeling software, analytical software, explicit vs implicit solvers, and the various methods of modeling material during collision were investigated and discussed to determine how to best simulate and analyze a full scale ship to offshore platform collision analysis.
- Element formulations available within LS-DYNA were investigated and discussed to determine which would be applicable to a full scale STOPC assessment using implicit-explicit switching.
- A stiffened cylinder model was constructed. This model was created to compare the performance of various shell elements available for a STOPC collision prior to performing the full scale assessment with the much more complex full marine vessel.

- Ten collision assessments using the implicit-explicit switching option of LS-DYNA were performed using the stiffened cylinder model. This was done to determine which element formulations available for implicit-explicit switching would be suitable for a full scale STOPC assessment.
- A mesh sensitivity analysis was performed using the cylinder model. This was done to determine the required mesh density for the full scale STOPC analyses.
- Three additional fully explicit analyses were performed using the cylinder model. This was done to determine whether reducing the timestep in an explicit analysis would have an effect on post collision numerical noise of STOPC assessment.
- A full-scale marine vessel was modelled in detail. The more refined meshing was used to model the collision region of the vessel. Beams and stiffeners within the collision region were modelled using 2D shells, where throughout the coarse region of the model they were modelled using 1D elements.
- A full scale STOPC collision with implicit-explicit switching was also simulated. ELFORM -16 was the only element formulation within LS-DYNA capable of handling the complexity involved with the yielding and deformation of the full scale marine vessel without LS-DYNA crashing.
- In addition, four additional full scale fully explicit STOPC analyses were performed. This was done to compare the total CPU times to that of a model which used ELFORM -16 and implicit-explicit switching.

7.2 Concluding Remarks

There are several 2D shell formulations available within commercially available software, capable of including a variety of element effects such as warping, through-thickness stress and moment transfer. While it is well documented that running these analyses explicitly is recommended due to non-conditional stability aspect of the solution algorithm if large deformation is anticipated, these simulations are run most efficiently with implicit-explicit switching to allow the timesteps outside of the collision event to be computed explicitly. For simplistic models with high element and mesh quality, most 2D element formulations within LS-DYNA provide converged solutions using the implicit-explicit switching solver. However, as the colliding structure becomes more complex, several element formulations of LS-DYNA (such as 1, 2, and 25) would necessitate a fully explicit analysis. The von Mises stress results were found to be nearly identical for a full scale STOPC simulation using ELFORM -16 run with implicit/explicit switching option versus the same analysis run fully explicitly. As the documentation supporting fully explicit analysis procedures using LS-DYNA for full scale STOPC assessments are well established and documented, it is recommended that due to the similarity of results, STOPC be performed with ELFORM -16 and implicit-explicit switching.

ELFORM -16 was the only element formulation available for both implicit and explicit analysis with a converged solution when running the analysis using the implicit-explicit switching. The use of implicit-explicit switching reduced the total run time of the analysis by a factor of 4, which is 1.8x faster than the most efficient fully explicit solution obtained in this study. While the results generated throughout this analysis strongly

indicate the use of the of ELFORM -16 with implicit/explicit switching, the overall accuracy of these results can not be verified due to the lack of STOPC deformation data available.

It is recommended that for a full scale STOPC, hourglass controls, mortar contact, self contact, and strain hardening be used regardless of the element type and formulation chosen.

7.3 RECOMMENDATIONS FOR FUTURE ANALYSES

1. Full-scale STOPC assessment with refinement algorithm (P refinement, H refinement, or R refinement) in area of interest should be performed to compare the results to determine whether refinement in collision region as been adequate to capture the induced stresses. This will save on modeling time, but may impact accuracy of results.

2. Analyses using alternative material formulations should be conducted with the aim of accurately representing the response of the vessel materials.

3. Analyses with solid elements in region of interest (i.e., the collision region) should be performed to determine whether there are any advantages associated with their use over 2D elements.

4. Analyses should be performed with higher energy dissipation to determine the limits of various element applicability.

5. The focus of this thesis has been broadside collision only. These element comparisons should be performed for head-on collisions with ships containing bulbous bow structure to maximize deformation and further test the limits of the elements available within LSDYNA for STOPC assessments. |

6. The effect of simplifying the model outside the collision region should be further investigated. This may increase STOPC assessment efficiency by reducing overall modeling time. Moreover, the limits of such simplification should be assessed.

REFERENCES

[1] H. A. Oltedal, "Ship-Platform Collisions in the North Sea," in *the proceedings of the Annual European Safety and Reliability Conference (ESREL)*, Helsinki, Finland, 2012.

[2] J. Daley, "Mumbai High North Platform Disaster," in *the proceedings of the 2013 Coastal and Ocean Engineering Undergraduate Student Forum, COASTAL-2013*, St. John's, Newfoundland.

[3] O. Furnes and J. Amdahl, "Ship Collisions with Offshore Platforms," in *the proceedings of Intermaritec '80*, Hamburg, Germany, 1980.

[4] A. AbuBakar, R. Dow, A. G. Tigkas, M. S. Samuelides and K. J. Spyrou, "Investigation of an Actual Collision Incident between a Tanker and a Bulk Carrier," in *the proceedings of the 11th International Symposium on Practical Design of Ships and Other Floating Structures*, Rio de Janeiro, Brazil, 2010.

[5] O. Kitamura, "FEM Approach to the Simulation of Collision and Grounding Damage," *Marine Structures,* vol. 15, no. 4-5, pp. 403-428, 2002.

[6] J. Amdahl and J. Atle, "High-Energy Ship Sollision with Jacket Legs," in *the Eleventh International Offshore and Polar Engineering Conference*, Stavanger, Norway, 2001.

[7] T. H. Soreide, T. Moan, J. Amdahl and J. Taby, "Analaysis of Ship/Platform Impacts," in *the proceedings of the International Conference on Behaviour of Offshore Structures*, Trondheim, Norway, 1982.

[8] J. Amdahl, "Energy Absorption in Ship-Platform Impacts (Report No. UR-83-34)," Norwegian Institute of Technology, Trondheim, Sweden, 1983.

[9] J. Amdahl and E. Eberg, "Ship Collision with Offshore Structures," in *the proceedings of the 2nd European Conference in Structural Dynamics (EURODYN'93)*, Trondheim, Norway, 1993.

[10] J. Amdahl, "Consequences of Ship Collisions, Seminar on Collide II Project Risk Assessment," Norwegian Institute of Technology, RINA, London, UK, 1991.

[11] J. Amdahl and M. Storheim, "Accidental Ice Management - Platform vs. Ice Breaking Supply Vessel Collision," in *the proceedings of The Twenty-third International Offshore and Polar Engineering Conference*, Anchorage, Alaska, 2013.

[12] J. Amdahl and M. Storheim, "Design of Offshore Structures Against Accidental Ship Collisions," *Marine Structures,* vol. 37, pp. 135-172, 2014.

[13] R. Törnqvist, "Design of Crashworthy Ship Structures," Doctoral Thesis, Department of Mechanical Engineering, Tehnical University of Denmark, Copenhagen, Denmark, 2003.

[14] DET NORSKE VERITAS (DNV), "Design Against Accidental Loads - Recommended Practice," DNV GL DNV-RP-C204, Oslo, Norway, 2010.

[15] TANKEROperator Magazine, "DNV GL to unveil rules this year," 30 January 2015. [Online]. Available: http://www.tankeroperator.com/news/dnv-gl-to-unveil-rules-this-year/6356.aspx. [Accessed 16 June 2019].

[16] American Bureau of Shipping (ABS), "ABS Rules & Guides Archives," 2019. [Online]. Available: https://ww2.eagle.org/en/rules-and-resources/rules-and-guides/archives.html. [Accessed 29 November 2019].

[17] MSL Engineering Limited, "Collision Resistance of Ship Shaped Structures to Side Impact (Standard No. OTO 053/2000)," Health and Safety Executive , Berkshire, United Kingdom, 2000.

[18] NORSOK, "N-003 Actions and Action Effects," Standards Norway, Strandveien, Norway, 2007.

[19] NORSOK, "N-004 Design of Steel Structures," Standards Norway, Lysaker, Norway, 2004.

[20] American Petroleum Institute (API), "22nd Edition of API RP 2A Recommended Practice for Planning, Designing and Constructing Fixed Offshore Platforms-Working Stress Design," in *the proceedings of the 2010 Offshore Technology Conference*, Houston, Texas, 2010.

[21] Lloyd's Register, Guidance Notes for Risk Based Analysis: Collisions, London, UK: Lloyd's Register Group Limited, 2014.

[22] M. Storheim and J. Amdahl, "Design of Offshore Structures Against Accidental Ship Collisions," *Marine Structures,* vol. 37, pp. 135-172, 2014.

[23] VERITEC, "Design Guidance for Structures Exposed to Ship Collisions, VERITEC (Report No. 88-3172)," Veritas Offshore Technology and Services 88-3172, Oslo, Norway, 1988.

[24] M. J. Petersen and P. T. Pedersen, "Collisions Between Ships and Offshore Platforms," in *the proceedings of the 13th Annual Offshore Technology Conference*, Houston, Texas, 1981.

[25] S. Zhang, "The Mechanics of Ship Collisions (ISBN 87-89502-05-1)," Department of Naval Architecture and Offshore Engineering, Technical University of Denmark, Copenhagen, Denmark, 1999.

[26] W. Visser, Ship Collision and Capacity of Brace Members of Fixed Steel Offshore Platforms, Delft, Netherlands: HSE Books, 2004.

[27] B. C. G. Jr., "Other Applications of Marine and Offshore Construction Technology," in *Construction of Marine and Offshore Structures, Third Edition*, Boca Raton, Florida, Taylor & Francis Group, 2007, pp. 557-566.

[28] J. Y. Kim, "Analysis of Bow Crushing in Ship Collision," MSc Thesis, Department of Ocean Engineering, Massachusetts Institute of Technology, Cambridge, Massachusetts, 2000.

[29] ATSB Transport Safety Report 339-MO-2018-002, "Collision between the container ship Beijing Bridge and fishing vessel Saxon Onward," Australian Transport Safety Bureau, Canberra, Australia, 2018.

[30] A. Bela, L. Buldgen and P. Rigo, "Numerical Crashworthiness Analysis of an Offshore Wind Turbine Monopile Impacted by a Ship," in *Analysis and Design of Marine Structures*, vol. 23, London, Taylor & Francis Group, 2015, pp. 661-670.

[31] P. T. Pedersen and J. J. Jensen, "Ship Impact Analysis for Bottom supported Offshore Structures," in *the proceedings of 2nd International Conference of Advances in Marine Structures*, Dunfermline, Scotland, 21-214 May 1991.

[32] P. T. Pedersen, "Review and Application of Ship Collision and Grounding Analysis Procedures," *Marine Structures,* vol. 23, no. 3, pp. 241-262, 2010.

[33] D. P. Servis and M. Samuelides, "Ship Collision Analysis using Finite Elements," in *the Proceedings of SAFER EURORO Spring Meeting*, Athens, Greece, 1999.

[34] M. Muller, S. Schirm, M. Teschner, B. Heidelberger and M. Gross, "Interaction of Fluids with Deformable Solids," *Journal of Visualization and Computer Animation,* vol. 15, pp. 159-171, 2004.

[35] A. Robinson-Mosher, T. Shinar, J. Gretarsson, J. Su and R. Fedkiw, "Two-way Coupling of Fluids to Rigid and Deformable Solids and Shells," *ACM Transactions on Graphics (TOG),* vol. 27, no. 3, 2008.

[36] F. Losasso, J. O. Talton, N. Kwatra and R. Fedkiw, "Two-way Coupled SPH and Particle Level Set Fluid Simulation," *IEEE Transactions on Visualization and Computer Graphics,* vol. 14, no. 4, pp. 797-804, 2008.

[37] W. F. Hosford, "An Overview of the History of Plasticity Theory," in *Fundamentals of Engineering Plasticity*, Cambridge, United Kingdom, Cambridge University Press, 2013, pp. 1-5.

[38] A. C. Bannister and S. J. Trail, "Structural Integrity Assessment Procedures for European Industry," British Steel PLC, Rotherham, United Kingdom, 1996.

[39] E. Romhanji, M. Popovic, D. Glisic, M. Stefanovic and M. Milovanovic, "On the Al-Mg Alloy Sheets for Automaotive Application: Problems and Solutions," *Journal of Metallurgy,* vol. 10, pp. 205-2016, 2004.

[40] J. H. Ryu, J. I. Kim, H. S. Kim, C.-S. Oh, H. K. D. H. Bhadeshia and D.-W. Suh, "Austenite stability and heterogenseous deformation in fine-grained transformation-induced plasticity assisted steel," *Scripta Materialia,* vol. 68, no. 12, pp. 933-936, 2013.

[41] H. N. Jones and C. R. Feng, "Thermal Activation of Flow Stress Transients in Mild Steel," *Materials Science and Engineering A,* vol. 309, pp. 92-96, 2001.

[42] J. Wei-liang, J. Song, S.-f. Gong and Y. Lu, "Evaluation of Damage to Offshore Platform Structures due to Collision of Large Barge," *Engineering Structures,* vol. 27, no. 9, pp. 1317-1326, 2005.

[43] J. Amdahl, R. Watan, Z. Hu and T. Holmas, "Broad Side Ship Collision with Jacket Legs - Examination of NORSOK N-004 Analysis Procedure," in *the proceedings of the International Conference on Ocean, Offshore and Arctic Engineering*, Rio de Janeiro, 2012.

[44] C. P. Ellinas and A. C. Walker, "Effects of Damage on Offshore Tubular Bracing Members," in *IABSE Colloquium, Ship Collision with Bridges and Offshore Structures*, Copenhagen, Denmark, 1983.

[45] G. Maenchen and S. Sack, The Tensor code, URCL-7316 Nuclear Explosions - Peaceful Applications, UC-35 TID-4500 (19th Ed.), vol. 3, University of California, Berkeley, California, 1964.

[46] M. L. Wilkins, "Calculation of Elastic-Plastic Flows," Laurance Laboratory, University of California, Berkeley, California, 1963.

[47] O. C. Zienklewicz and R. L. Taylor, The Finite Element Method: Solid Mechanics, Oxford, United Kingdom: Butterworth-Heinemann, 2000.

[48] S. Stupkiewicz, R. Denzer, A. Piccolroaz and D. Bigoni, "Implicit Yield Function Formulation for Granular and Rock-Like Materials," *Computational Mechanics,* vol. 54, no. 5, pp. 1163-1173, 2014.

[49] Altair Hyperworks, "http://www.altairhyperworks.ca/Product,7,HyperMesh.aspx," 2015. [Online]. [Accessed 07 September 2015].

[50] Bentley Systems, "Bentley Acquires SACS, Leading Software for Offshore Structure Analysis," Bentley Systems, 02 March 2011. [Online]. Available: https://www.businesswire.com/news/home/20110302006539/en/Bentley-Acquires-SACS-Leading-Software-Offshore-Structure. [Accessed 16 06 2019].

[51] Livermore Software Corperation (LSTC), LS-DYNA Keyword User's Manual, Volume 1, Livermore, California: Livermore Software Technology Coorperation (LSTC), 2009.

[52] Z. Liu, "Analytical and Numerical Analysis of Iceberg Collisions with Ship Structures," Doctoral Thesis, Departmnent of Marine Technology, Norwegian University of Science and Technlogy, Trondheim, Norway, 2011.

[53] A. Carlebur, "Full-scale collision tests," *Safety Science,* vol. 19, no. 2-3, pp. 171-178, 1995.

[54] Simulia, "http://www.3ds.com/products-services/simulia/products/abaqus/," Dassault Systemes. [Online]. [Accessed 07 September 2015].

[55] Bentley Systems, "http://www.bentley.com/fr-FR/Promo/SACS/Offshore+Structures+Design+Analysis+eSeminars.htm," Bentley Systems. [Online]. [Accessed 24 August 2015].

[56] J. P. Singh and S. Verma, "https://www.sciencedirect.com/topics/engineering/stress-strain-curve," 2019. [Online]. Available: https://www.sciencedirect.com/topics/engineering/stress-strain-curve. [Accessed 28 11 2019].

[57] E. Levold, L. Marchionni, A. Restelli and C. Molinari, "Strength and Deformation Capacity of Corroded Pipes," in *the proceedings of the ASME 2013 32nd International Conference on Ocean, Offshore and Arctic Engineering*, Nantes, France, 2013.

[58] A. Fouratier, A. Lucas, J. H. Bianchi, P. Vescovo, F. Dionisi and P. D. Putz, "Control of Sheet Surface Defects and Deep Drawings Properties in Final Strip Production Steps," European Commission, Luxembourg, Luxembourg, 2007.

[59] H. Qu, J. Huo, C. Xu and F. Fu, "Numerical Studies on Dynamic Behavior of Tubular T-joint Subjected to Impact Loading," *International Journal of Impact Engineering,* vol. 67, pp. 12-26, 2014.

[60] N. J. Hoff, IUTAM colloquium Creep in Structures, Berlin, Germany: Springer, 1962.

[61] H. Ziegler, "A modification of prager's hardening rule," Eidgenossische Technische Hochschule, Zurich, 1959.

[62] M. E. Kassner, P. Geantil, L. E. Levine and B. C. Larson, "Backstress, the Bauschinger Effect and Cyclic Deformation," *Materials Science Forum,* Vols. 604-605, pp. 39-51, 2009.

[63] Livermore Software Technology Corporation, "LS-DYNA Theory Manual Volume 10," Berkley, California, 2018.

[64] M. Dietenberger, M. Buyuk and C.-D. Kan, "Development of a High Strain-Rate Dependent Vehicle Model," in *LS-DYNA Anwenderforum*, Bamberg, Germany, 2005.

[65] H. Singh, "Mass Reduction for Light-Duty Vehicles for Models Years 2017-2025," Natinoal Highway Traffic Safety Administration, US Department of Transportation, Washington, DC, 2012.

[66] Livermore Software Technology Coorperation (LSTC), "Material Selector for LS-DYNA," Livermore Software Technology Coorperation (LSTC), 09 04 2019. [Online]. Available: http://www.lstc.com/dynamat/. [Accessed 16 06 2019].

[67] P. Dalhoff and F. Biehl, "Ship Collision, Risk Analysis - Emergency Systems - Collision Dynamics," Hamburg University of Technology, Hamburg, Germany, 2005.

[68] M. G. Hansen, S. Randrup-Thomsen, T. Askeland and M. Ask, "Bridge Crossings at Sognefjorden - Ship Collision Risk Studies," in *Collision and Grounding of Ships and Offshore Structures*, Taylor & Francis Group, London, United Kingdom, 2013, pp. 9-17.

[69] A. Haufe, K. Schweizerhof and P. Dubois, *Properties and Limits: Review of Shell Element Formulations,* Filderstadt, Germany, Filderstadt: LS-DYNA Developer Forum, 2013.

[70] G. P. Bazeley, Y. K. Cheung, B. M. Irons and O. C. Zienkiewicz, "Triangular Elements in Plate Bending - Conforming and non-conforming solutions," Air Force Flight Dynamics Laboratory Technical Report, Wright-Patterson AFB, Ohio, 1965.

[71] T. Belytschko and A. H. Marchertas, "Nonlinear Finite Element Formulation for Transient Analysis of Three Dimensional Thin Structures (Report No. ANL-8104)," Argonne National Laboratory Tehnical Report, Lemont, Illinois, 1974.

[72] Livermore Software Technology Corporation (LSTC), "LS-DYNA Keyword user's manual," Livermore Software Technology Corporation (LSTC), Livermore, California, 2017.

[73] T. Erhart, "Review of Solid Element Formulations in LS-DYNA," Livermore Software Technology Corporation (LSTC),, Livermore, California, 2011.

[74] BETA CAE Systems S. A., "Full Scale Ship Collision Simulation using ANSA & μEta," Beta CAE Systems SA, June 2015. [Online]. Available: https://www.ansa-usa.com/wp-content/uploads/2015/06/ship_collision_simulation.pdf. [Accessed 08 September 2017].

[75] A. Huerta, A. Rodrigues-Ferran and P. Diez, "Error Estimation and Adaptivity for Nonlinear FE Analysis," *International Journal of Applied Mathematics and Computer Science,* vol. 12, no. 1, p. 59–70, 2002.

[76] Z. Uthman and H. Askes, "R-adaptive and H-adaptive Mesh Optimisation Based on Error Assessment," in *the proceedings of the 13th ACME Conference: University of Sheffield*, Sheffield, United Kingdom, 2005.

[77] J. B. M. Saetre, "Collision between Platform Deck and Service Vessel Wheelhouse," Masters Thesis, Department of Marine Technology, Norwegian University of Science and Technology, Trondheim, Norway, 2013.

[78] K. Gieck and R. Gieck, Engineering Formulas, Germering, Germany: Gieck Verlag, 2006.

[79] K.-J. Bathe, "Advances in the Multiphysics Analysis of Structures," in *Topping BHV, editor. Chapter 1 in computational methods for engineering science*, e. B.Stirlingshire, Scotland, Saxe-Coburg Publications, 2012.

[80] Livermore Software Technology Coorperation (LSTC), LS-DYNA3D Theoretical Manual, Livermore: Livermore Software Technology Coorperation (LSTC), 1993.

[81] B. Skallerud and B. Haugen, "Collapse of Thin Shell Structures: Stress Resultant Plasticity Modelling within a Co-rotated ANDES Finite Element Formulation," *International Journal for Numerical Methods in Engineering,* vol. 46, no. 12, pp. 1961-1986, 1999.

[82] R. Hutanu, L. Clapham and R. B. Rogge, "Intergranular Strain and Texture in Steel Luders Bands," *Acta Materiala,* vol. 53, no. 12, pp. 3517-3524, 2005.

[83] N. Srinivasan, N. Raghu and B. Venkatraman, "Study on the Deformation Band Characteristics in Mild Steel using Digital Image Correlation," *Journal of Multidisciplinary Engineering Science and Technology (JMEST),* vol. 1, no. 5, pp. 400-403, 2014.

[84] J. Symonds, J. P. Vidosic, H. V. Hawkins and D. D. Dodge, "Chapter 5: Strength of Materials," in *Marks' Standard Handbook for Mechanical Engineering*, McGraw Hill, New York, New York, 2014, pp. 5.1 - 5.67.

[85] Livermore Software Technology Corporation, "LS-DYNA Theory Manual," Livermore Software Technology Corporation, Livermore, California, 2006.